CUTOFF MODELLING FOR EXCAVATION SEALING IN UNDERGROUND NUCLEAR WASTE REPOSITORIES

PUSHPENDRA SHARMA

A THESIS SUBMITTED TO THE FACULTY OF GRADUATE STUDIES

IN PARTIAL FULFILLMENT OF THE REQUIREMENTS FOR THE DEGREE OF

MASTER OF APPLIED SCIENCE

GRADUATE PROGRAM IN CIVIL ENGINEERING

YORK UNIVERSITY

TORONTO, ONTARIO

December, 2020

Abstract

When placement rooms in a deep geological repository are constructed, different excavation damage zones (EDZs) with connected fractures (inner excavation damage zone - EDZi) close to the excavation surface and disconnected fractures (outer excavation damage zone - EDZo) further away form. A cutoff is an excavation constructed perpendicular to the placement room axis that creates a cross-sectional enlargement of the excavation, which when filled with a sealing material such as bentonite, seals the EDZi to minimize radionuclides transport through this zone. This research developed a framework to help determine the dimension and shape of an optimum cutoff, examining a wide range of geological scenarios using continuum numerical modelling. In the first stage, dimensions of different EDZs induced due to the excavation of the placement room were determined. In the second stage, based on the dimensions of EDZi from the first stage, rectangular, triangular, and trapezoidal cutoffs with different dimensions under different geological settings were constructed. In the third stage, the effect of different variants such as shape and orientation of placement room, rock mass properties and anisotropy, and heat from the nuclear fuel on the extent of EDZi around the optimum cutoff was studied. The depth of EDZs was predicted based on the sign and magnitude of volumetric strain inside the plastic zone from the numerical model. The extent of EDZs increases with an increase in the ratio of maximum stress around the excavation to the strength of the rock mass. The trapezoidal shaped cutoff, with a minimum thickness to depth (aspect) ratio (0.2), was found to be the optimum in this study based on its ability to induce a minimum increase in the EDZi after the construction of the cutoff. The radial extent of EDZi for the optimum cutoff is smaller for the granite followed by limestone and mudstone. The radial extent of EDZi for the optimum cutoff is lower for the limestone and mudstone with the absence of bedding planes compared to when bedding planes are present. Furthermore, for the given stress situation in this study, the radial extent of EDZi for the optimum cutoff for the horizontal placement room and vertical room (shaft) is found approximately equal. The radial extent of EDZi for the optimum cutoff for a circular placement room is smaller than the rectangular placement room. Finally, a maximum temperature of 64 ^{o}C at the cutoff increases from the mechanical only model the radial extent of EDZi and EDZo by 72 cm and 61 cm, respectively. This study helps in understanding excavation damage zones and designing cutoff for underground excavations, especially in underground nuclear waste repositories.

Acknowledgements

I would first like to express my sincere gratitude to my supervisors Professor Matthew Perras, PEng, and Professor Jit Sharma, PEng for their continuous support and assistance without which I could not have completed this thesis. Their expertise and guidance were invaluable in formulating the research questions and methodology. Their valuable discussion and patient helped me to improve the technical results of the study very much. Their continuous feedback pushed me to sharpen my technical knowledge and interpersonal skills.

The research work presented in this thesis builds on previous EDZ and cutoff modelling research financially supported by the Natural Sciences and Engineering Research Council of Canada (NSERC) and the Nuclear Waste Management Organization of Canada (NWMO) of Professor Matthew Perras. Continued financial support for this research from NSERC is acknowledged. The insightful comments on the research from Dr. Hossein Kasani, Tom Lam at NWMO, Canada, and Professor Gabriel Walton at Colorado School of Mines, USA, greatly helped me to improve the work.

I would also like to thank Professor Magdalena Krol, PEng, Professor Kamelia Atefi-Monfared, PEng, and Ms. Sindy Mahal at the Dept. of Civil Engineering, for their valuable assistance throughout my studies. Professor Krol and Professor Atefi generously provided their time, support, and feedback throughout the preparation and review of the thesis. In addition, Professor Krol helped me to carry out the research by providing access to the software COMSOL. Ms. Mahal provided me the tools and guidance that I needed to choose the right direction and successfully complete my thesis.

In addition, I would like to thank my parents and siblings for their wise counsel and emotional support. Finally, I could not have completed this research without the support of my friends, Rodrigo, Jeffrey, Josephine, and Ubaid, who provided stimulating discussions as well as happy distractions to rest my mind outside of my work.

Tables of Contents

List of Tables

List of Figures

Chapter 1: Introduction

1.1 Background

Safe and secure storage and disposal of radioactive waste over a long period are essential to avoid any detrimental impact on humans and the environment around them (Csullog et al., 2002). In modern nuclear plants, 96% of the spent fuel is recycled back into uranium-based fuel and Mixed Oxide Fuel (MOX). The remaining 4% of the fission products must be isolated and confined in appropriate facilities for a sufficient period until their radioactivity decreases to an acceptable level (Orano, 2018). International Atomic Energy Agency (IAEA) classified the radioactive waste into three categories (IAEA, 1994):

1. High-level waste (HLW) - the highly radioactive liquid, containing mainly fission products and some actinides, which are separated during chemical reprocessing of irradiated fuel (aqueous fuel from the first solvent extraction cycle and those fuel streams combined with it). Or any other waste with radioactivity levels intense enough to generate significant quantities of radioactive heat. Or spent nuclear fuel, if it is declared as waste.
2. Intermediate-level waste (ILW) - waste which, because of its high radionuclide content, requires shielding but needs little or no provision for heat dissipation during its handling and transportation.
3. Low-level waste (LLW) - waste which, because of its low radionuclide content does not require shielding during normal handling and transportation.

Currently, countries around the world have or are planning for storage and segregation facilities for short-lived waste, and near-surface disposal for low-level and some of the intermediate-level waste. There is a general consensus among scientists and engineers that the long-term solution for solid nuclear waste disposal is deep geological repositories (DGR) (Efremenkov, 2003; Lidskog and Sundqvist, 2004; Durant, 2006; Kojo et al., 2010; Strandberg and Andrén, 2009; Carfora, 2012).

1.1.1 Deep Geological Repository (DGR)

As of 2020, there are no operational underground deep geological repositories (Findlay, 2010). Finland is in the advanced stage of construction of a DGR, which will be located at 400-450 m below the ground surface. According to the current plan, the repository would be sealed in 2120 (Vira, 2017). France is planning to dispose the nuclear waste in a 160 million-year-old clay formation at a depth of 500 m in a DGR at Bure. The clay serves as a long-term natural barrier for the waste (Voinis et al. 2016). In June 2009, the Swedish Nuclear Fuel and Waste Management Ltd. (SKB) decided to dispose the waste in a to be constructed DGR at Forsmark, Sweden. SKB plans to make the repository operational by 2030 (Kwon et al. 2016). Canada considers The Township of Ignace in northwestern Ontario, and the Municipality of South Bruce in southern Ontario as two potential sites for a HLW DGR (NWMO, 2019).

The basic concept of deep geological disposal is to locate a large, stable geological formation and use mining technology to construct rooms 500 to 1000 m below the ground surface where nuclear waste can be disposed. The goal is to permanently isolate the used nuclear fuel from the human environment. Some radioactive species have a half-life of more than 1 million years. Therefore, it is important to isolate them very tightly, for even small radionuclide leakage can be devastating for human lives given the half-life time scale (Vandenbosch and Vandenbosch, 2007). A 1983 review of the Swedish radioactive waste disposal program by the National Academy of Sciences found that country's estimate of several hundred thousand years - perhaps up to one million years - being necessary for waste isolation is "fully justified" (Yates, 1989). The long timescales of the radioactivity of some of the isotopes have led to the idea of deep disposal in repositories in a stable geological environment. In the DGR, isolation is provided by a combination of natural (geological environment) barrier and engineered barriers (such as the waste packaging and the engineered repository), which are supposed to prevent the reaching the radionuclides to humans and the environment. The most acceptable deep disposal concept will contain horizontally-mined rooms where nuclear waste packaged into containers would be placed. In most cases, the packaged containers are surrounded by material such as cement or clay (also known as backfill material) to provide another layer of the engineered barrier. The type of waste container, its material, its design, and the type of the backfill material will depend upon the type of nuclear fuel to be contained and

the geology of the available host rock. The contents of the repository would be retrievable in the short term, and if desired, in the long term as well.

SKB uses the KBS-3 (an abbreviation of kärnbränslesäkerhet, nuclear fuel safety) concept for the disposal which consists of three protective barriers namely, copper canisters, bentonite clay, and Swedish bedrock located in Forsmark (Kwon et al., 2016). In this concept, the nuclear fuel will be encapsulated in copper canisters and then will be placed in a system of tunnels at 500 m below the ground surface. There are two alternatives to the concept: first, KBS-3V in which the canisters are placed in individual vertical deposition holes; and second, KBS-3H, in which serval canisters are placed in horizontal drifts as shown in Fig. 1.1. The studies during 2002-2007 have demonstrated that the horizontal deposition alternative is technically feasible and fulfills the same long-term safety requirements as the reference design KBS-3V. In the KBS-3H design, multiple canisters containing the spent fuel are placed in parallel, approximately 300 m long, and slightly inclined deposition drifts. The copper canisters, each with a surrounding layer of bentonite clay is placed in perforated steel shells before deposition into the drift. The canister in combination with the bentonite clay is known as the supercontainer. The supercontainers are deposited coaxially in the drifts and supported on steel feet to leave an annular gap between the supercontainers and the drift wall. Bentonite distance blocks separate the supercontainers from one another along the drift. The void space along the circumference of the drift is filled with bentonite, which is designed to swell after coming in contact with water, thereby providing a tight seal.

Finnish spent nuclear waste disposal program is based on the SKB's KBS-3H design. The fuel will be disposed in the underground nuclear waste repository at a 400 m depth in Olkiluoto bedrock.

The French geological repository, Centre Industriel de Stockage Géologique (CIGEO) will be located in Meuse (Haute-Marne) around 500 m below the ground surface (Voinis et al. 2016). It will be located in a stable 130 m thick clay layer. The repository will be divided into two zones: one for intermediate-level and the other for high-level waste as shown in Fig. 1.2. After getting the license for the construction in 2019, Agence Nationale pour la Gestion des déchets radioactifs (ANDRA) is planning the first phase of the repository construction in 2022.

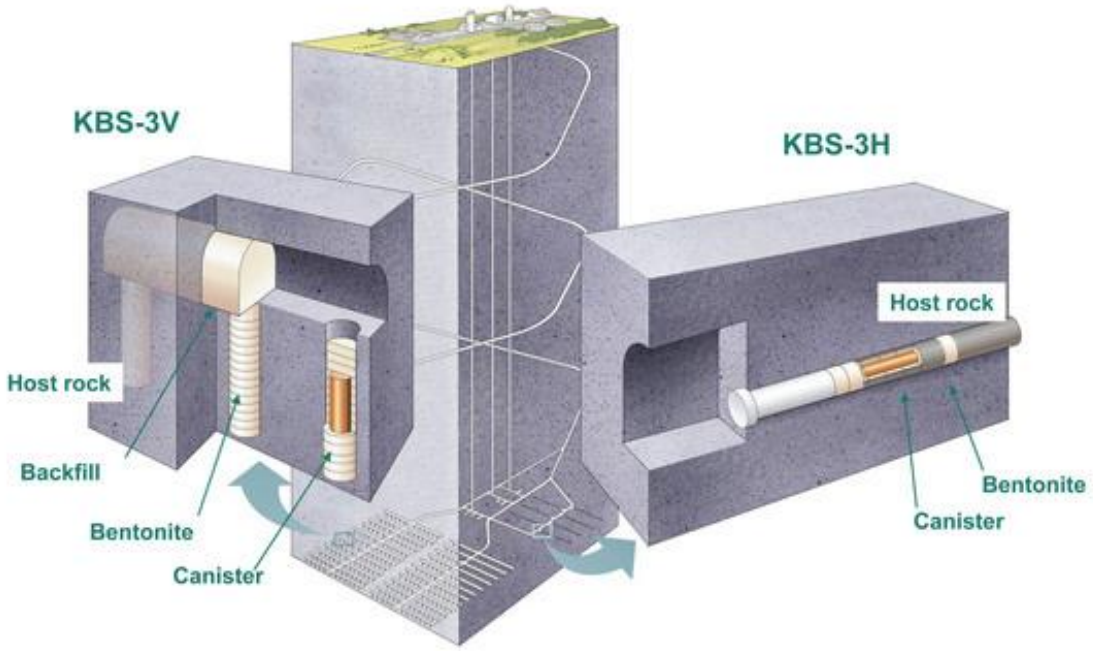

Fig. 1.1 The KBS-3V (left) and KBS-3H (right) alternatives of the KBS-3 spent fuel disposal method (Rinne, 2020).

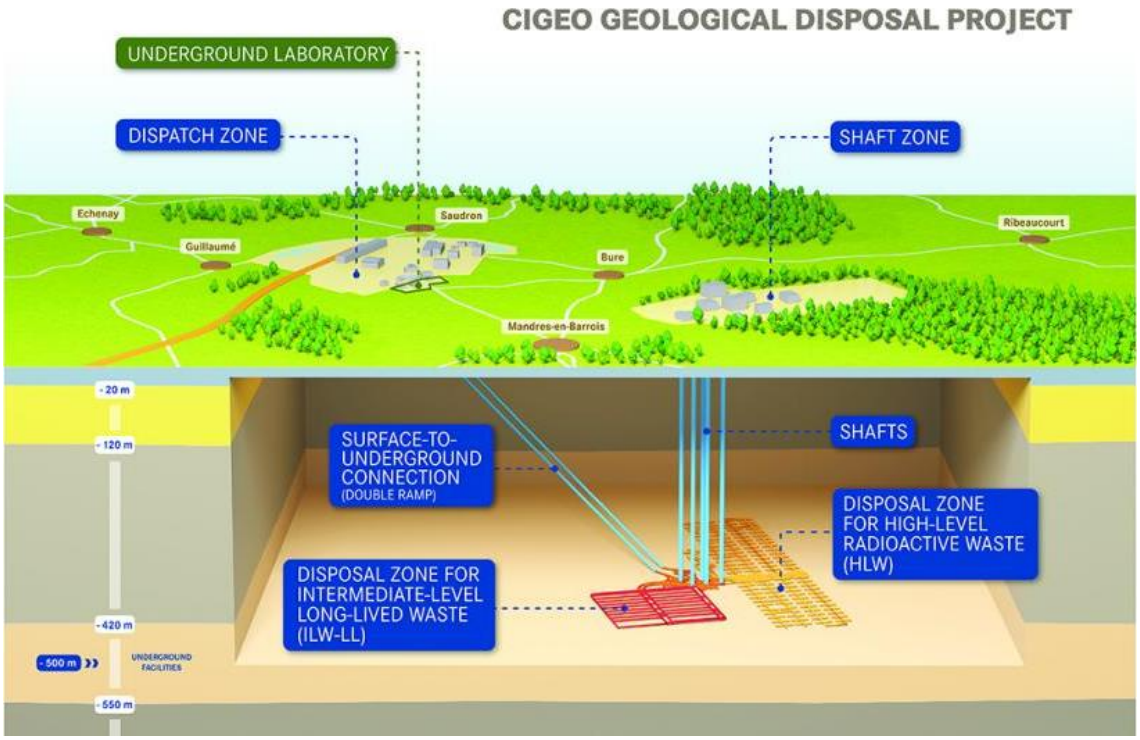

Fig. 1.2 Conceptual diagram of the French geological disposal facility, CIGEO (ANDRA, 2020).

As of June 30, 2019, Canada has an inventory of 2.9 million used nuclear fuel bundles (Noronha, 2016). At the end of the planned operation of Canada's existing nuclear reactors, the number of used fuel bundles could total about 5.5 million. Canada has chosen the adaptive phase management plan for the long-term management of its used nuclear fuel. This plan involves realistic, manageable phases with a possibility for the incorporation of new knowledge with time. One DGR will be large enough to contain all the used fuel inventory generated from the planned operation of Canada's nuclear reactors. The DGR will be constructed at a depth of 500 m, covering an area about 2 km by 3 km in crystalline or sedimentary rock by excavating the rock using controlled drilling and blasting operation. Rock boring machine can also be used depending on the final design and site conditions.

Since 2010, NWMO is working on the site selection process which involves nine steps, with opportunities to incorporate new knowledge along the way. Broadly the first three steps include initiating the siting process, carrying out initial screening, and preliminary assessment of suitability, while the remaining steps (steps 4 to 9) include the site confirmation, construction, and operations. The process is community-driven and it is designed to ensure that the site selected is safe, secure, and has an informed and willing host. At present, the Township of Ignace in northwestern Ontario, and the Municipality of South Bruce in southern Ontario are considered potential sites for the repository by NWMO (NWMO, 2018).

The proposed repository will contain a series of engineered and natural barriers to contain and isolate the used nuclear fuel from the human environment. The first component of engineered barrier is a durable container made of stainless steel with a copper coating to contain fuel bundles. The used fuel container has a 3 mm copper coating and will be 2.8 m long and 0.568 m in diameter. It also contains a steel basket within the carbon-steel pipe and a spherical cap at the top to isolate the used nuclear fuel. The container will prevent the radionuclides from escaping into the underground environment from the fuel bundles and withstand pressure from overlying rock and glaciers during a future ice age. The second component of the engineered barrier is bentonite clay which is used to encapsulate the container and as a backfill material inside the placement room (Fig. 1.4). The host rock mass surrounding the placement room will act as a natural barrier to provide a high level of long-term isolation and containment without much future maintenance.

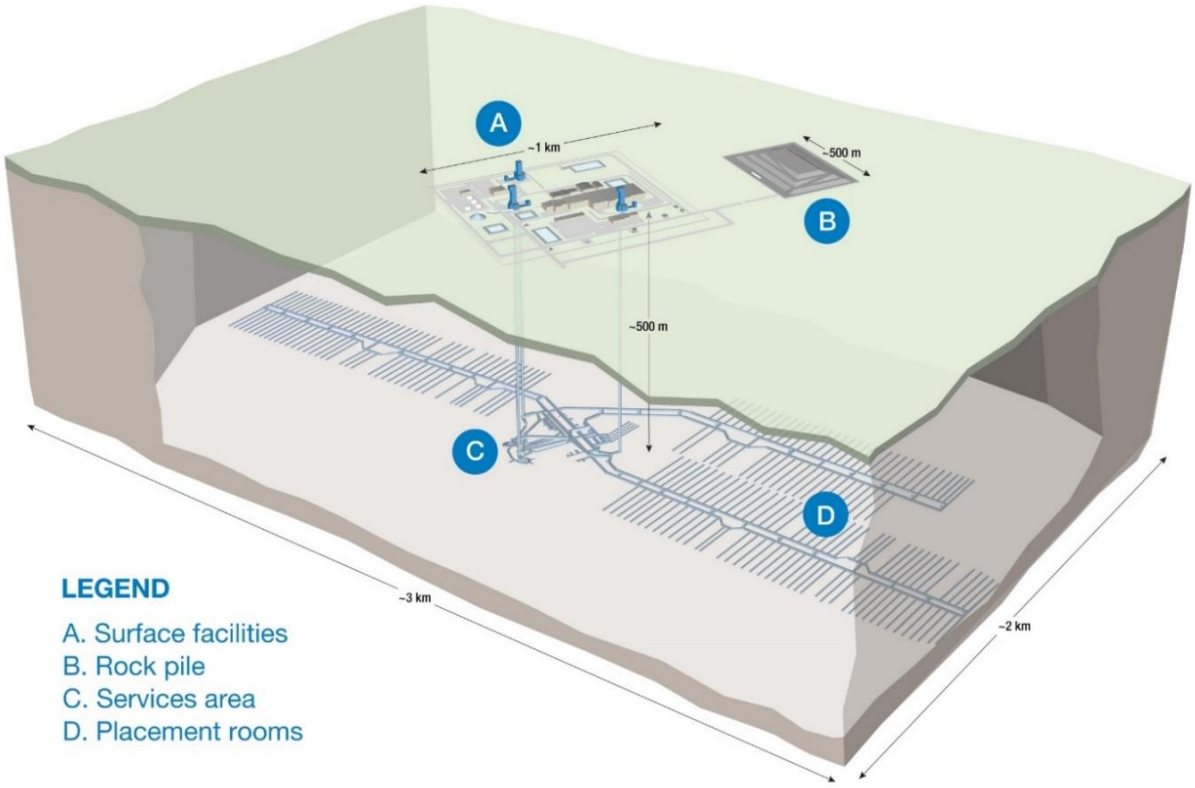

Fig. 1.3 Schematic showing conceptual Canadian underground repository (NWMO, 2018).

The spent nuclear fuel encapsulated into the canisters will be placed into the parallel rectangular rooms in multiple panels of the DGR as shown in Fig. 1.3 (NWMO, 2018). Each panel consists of 35 or 36 placement rooms with a center to center room spacing of 20 m. These rooms will be 3.2 m wide and 2.2 m high. Each room will contain two layers of buffer blocks containing the used fuel containers (Fig. 1.4). The bentonite buffer block will be placed horizontally, perpendicular to the room axis. The gap between host rock and buffer blocks will be filled with highly compacted bentonite while the gap between adjacent buffer blocks will be filled using dense backfill blocks. The rooms will be sealed using the cutoff seals combined with bentonite and concrete. These placement rooms will be connected to the main drift via crosscuts for material handling and transportation. When the placement rooms are constructed excavation damage zones (EDZs) are also created in the rock mass along the periphery of the excavation due to the construction process and redistribution of the in-situ stresses. In the case of a canister breach, radionuclides can transport through the connected fractures in the EDZs.

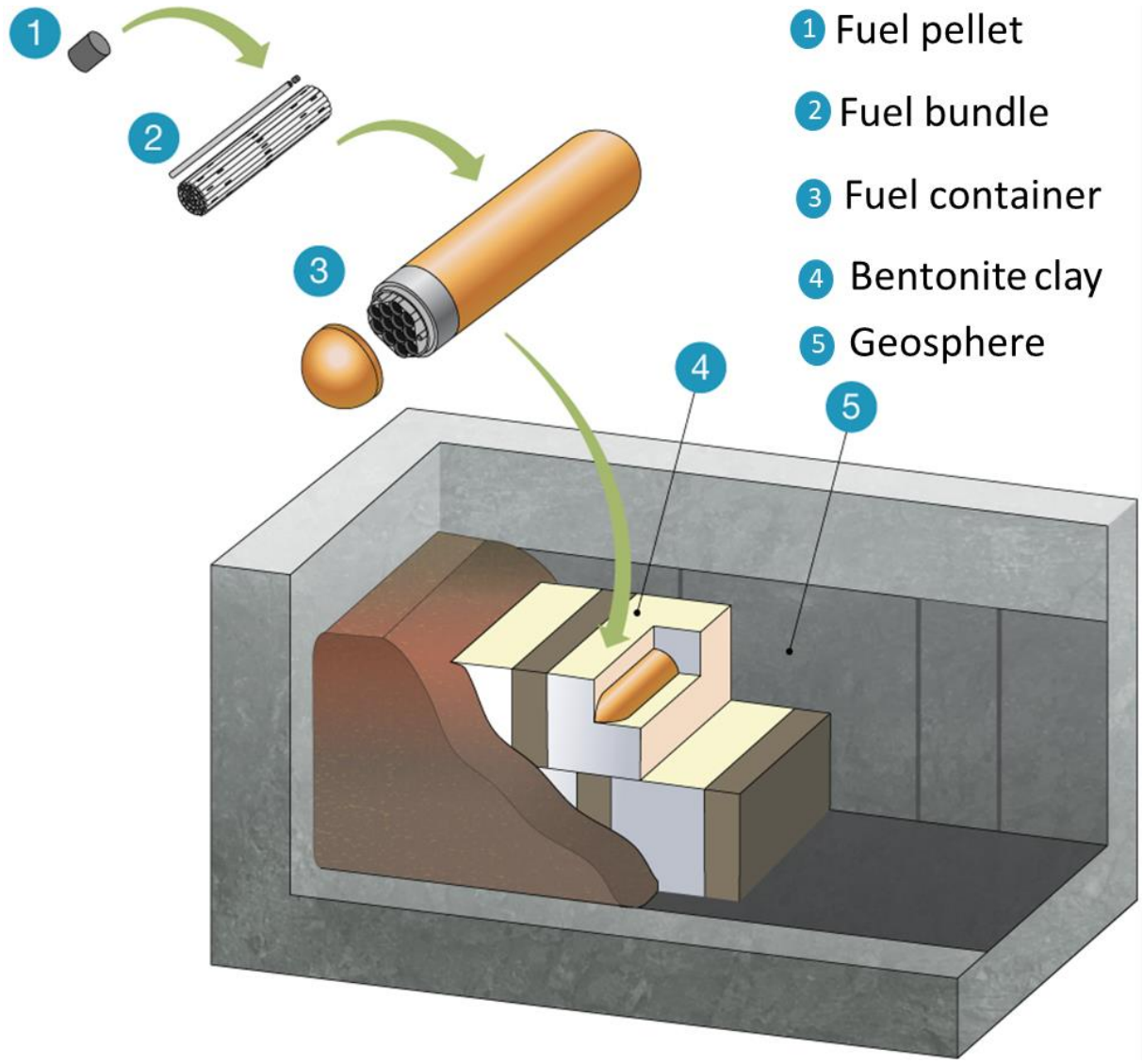

Fig. 1.4 Conceptual illustration of the multi-barrier system used to contain and isolate the used nuclear fuel (NWMO, 2018).

1.1.2 Excavation Damage Zones (EDZs)

During the construction of the underground excavations, damage occurs in the surrounding rock mass due to the construction process and redistribution of in-situ stresses. The permeability of the rock mass in EDZs significantly increases due to the damage caused by excavation. The increase in permeability poses a significant risk of potential transport of radionuclides through EDZs escaping from the geological barriers used for isolation. Therefore, it is important to determine the depth of EDZs for the effective design of placement rooms and engineered barriers.

In the past, researchers have classified the EDZs based on how the damage is induced and how it changes the permeability around the excavations. Siren et al. (2015) provided a comprehensive classification for stress-induced and construction-induced EDZs in crystalline rocks. The EDZs are composed of various damage zones with varying densities of fractures as shown in Fig. 1.5. The density of excavation induced fractures decreases moving away from the excavation surface. Harrison et al. (2000) divided the excavation response into two categories: initial inevitable excavation consequences and additional effects induced by the construction method.

The construction method induces the construction damage zone (CDZ) which can be reduced or eliminated by changing or adjusting the construction method. In contrast, the damage induced by the change in geometry, structure, and redistribution of in-situ stresses is inevitable. The zone where inter-connected macro-fractures are present is known as a highly damaged zone (HDZ). Moving outward, the zone with connected micro-fractures is referred to as the inner excavation damage zone (EDZi). After EDZi, the zone where connected to isolated micro-fractures are present is known as the outer excavation damage zone (EDZo). Beyond EDZo, the zone where only elastic redistribution in in-situ stresses occurs is known as the excavation influence zone (EIZ).

The outer limit of the EIZ is not critical for the excavation design as it is at a far distance from the excavation boundary; however, it is important to consider the interaction between EDZ and EIZ. In the field, the transition between these zones is gradual, and distinguishing between them from in-situ measurement can be difficult. Radionuclides can transport through the connected micro-fractures present in the EDZi, thereby escaping from the engineered and natural barriers. To disconnect and seal the connected fractures, a cutoff structure is constructed and filled with backfill material. A cutoff of thickness T and depth D is shown in Fig. 1.5.

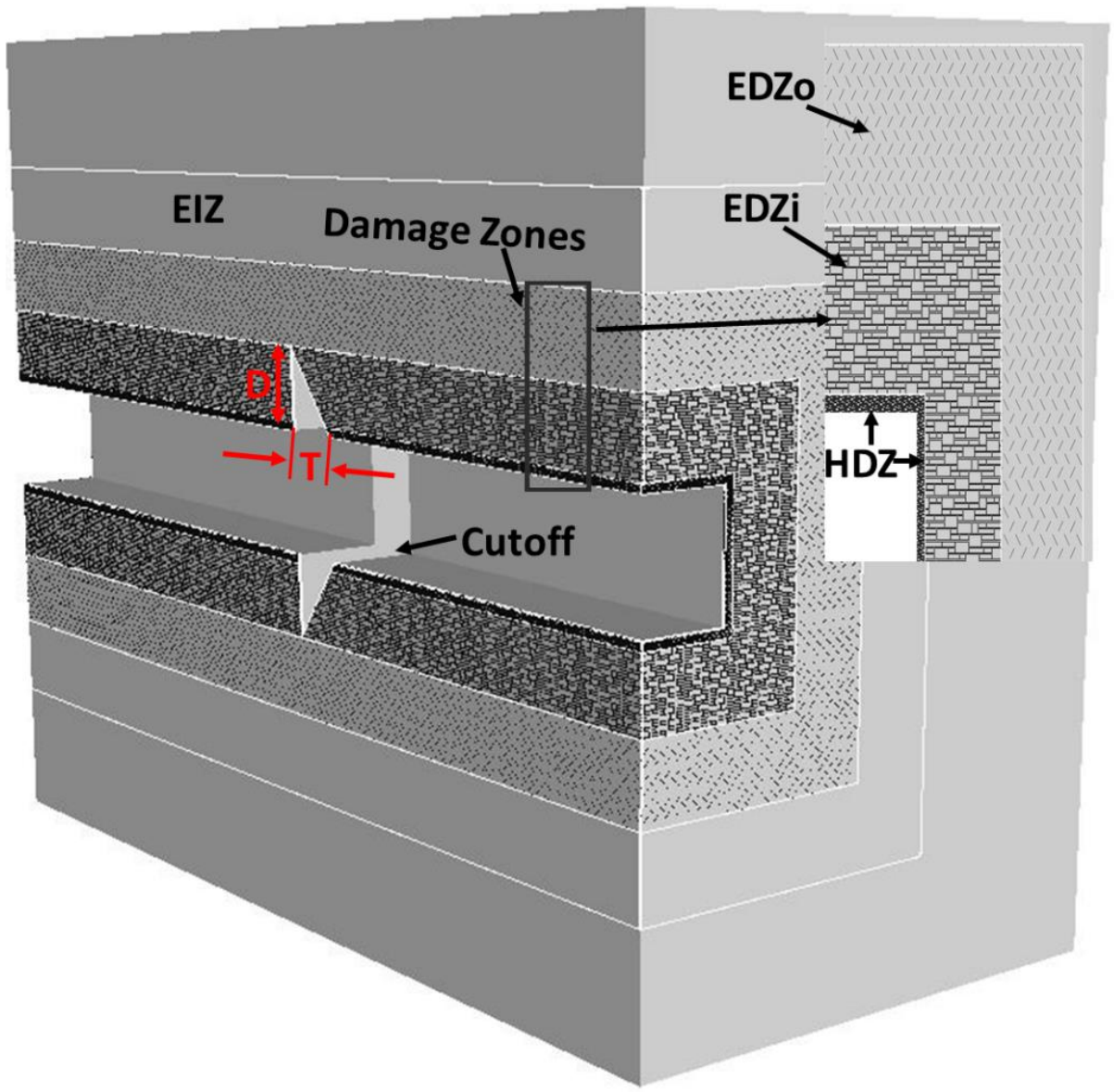

Fig. 1.5 The excavation damage zones and excavation influence zone. Where HDZ, EDZi, EDZo, and EIZ are highly damaged zone, inner excavation damage zone, outer excavation damage zone, and excavation influence zone, respectively. T and D are the thickness and depth of the cutoff.

1.1.3 Cutoff Seal

Room seals or cutoff seals are a type of engineered barrier placed at strategic locations in shafts, access drifts, and at the end of the fuel placement rooms to seal the repository (NWMO, 2018). A cutoff is an excavation constructed around the drift or shaft and filled with bentonite or other sealing material. The cutoff will be constructed perpendicular to the excavation axis to prevent the

potential migration of radionuclides and water flow through the EDZi parallel to the room axis. Note that in this study the term cutoff is used for the empty cutoff excavation while the term cutoff seal is used when the cutoff is filled with backfill material such as bentonite. According to SKB, the life cycle of a cutoff seal would be until the final closure of the repository and its purpose would be to cut off water flow and radionuclide transport along the placement room (Dixon et al., 2009).

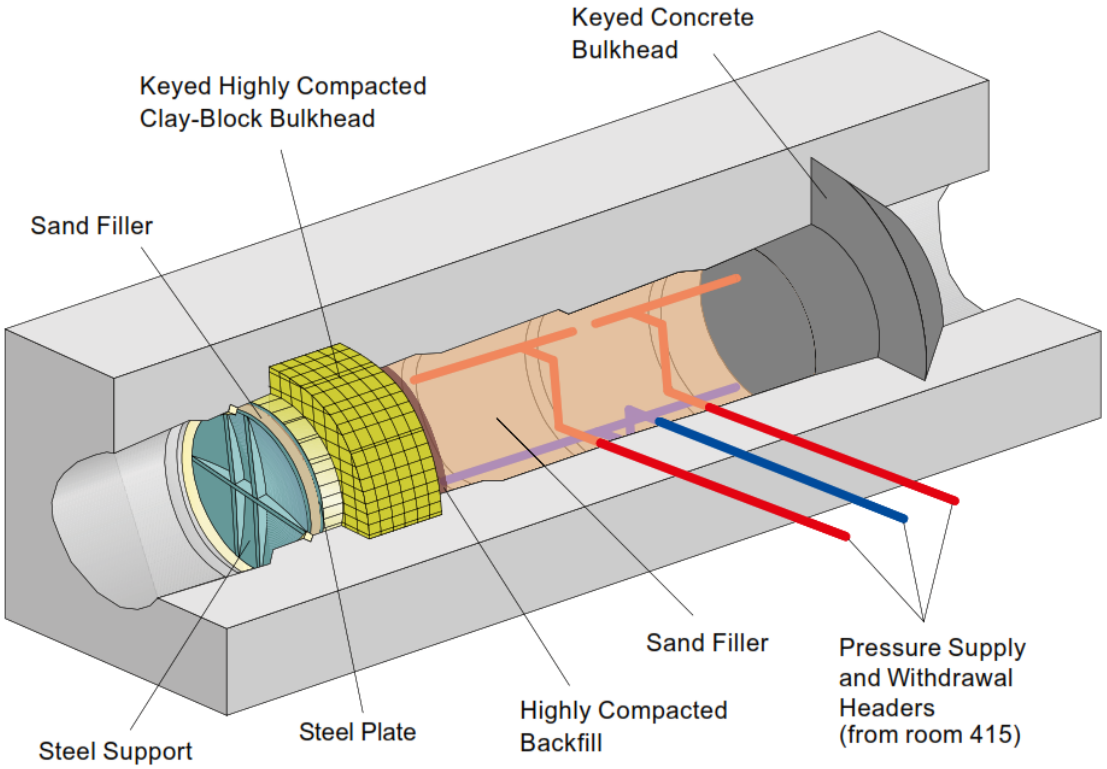

Fig. 1.6 The Tunnel Sealing Experiment for studying the performance of bentonite and concrete cutoff seals. (Chandler et al., 2002a, b).

The cutoff seal is expected to maintain its hydraulic and swelling capacity while remaining at a designed place and being subjected to water pressure and backfill material load. Most international concepts for drift or shaft cutoff seals include a concrete structure combined with a swelling clay material (Fig. 1.6). The cutoff is combined with highly compacted bentonite because of its high swelling potential and low permeability upon re-saturation to act as a stable engineered barrier under varying thermo-mechanical loads from the repository perturbations (Alonso et al., 2004). The concrete material used for the cutoff seal has a low pH (pH<11) (Holt and Koho, 2016) value

and high volumetric stability to effectively seal the opening. The low pH concrete is chosen because at high pH, the other component of the engineered barrier, bentonite is unstable (Holt and Koho, 2016). The seals will be installed in a way that they can be replaced or removed if necessary, during the pre-closure and pre-saturation period of the repository.

The cutoff seals are designed to endure the challenging hydrogeological environment where surrounding rock mass is fractured and hydraulically active resulting in a water pressure up to 5 to 7 MPa as well as the swelling pressure from adjacent sealing material. Hydraulically active rock can be present because of the EDZs and the presence of pre-existing fissures, joints, or cracks in the vicinity of the cutoff seal. High water inflow features are only effective during the pre-closure and pre-saturation period of the repository because once the repository is closed, water gradients will decrease and will become in equilibrium with the regional groundwater table.

The cutoff seal must be designed for a long period of time (up to 1 million years) as it will not be accessible after the repository closure (1000 years). Therefore, it is very important to design the effective shape, the size, and the location of the cutoff seals.

1.2 The Problem Statement

The performance of the cutoff seal is measured from its role to cut-off water flow to and along the room and to physically resist pressure that may be generated inside the room. Different nuclear waste management organizations around the world, interested in deep disposal of nuclear waste have carried out a number of tunnel cutoff seal tests (Pusch et al., 1987; Gunnarsson et al., 2002; Chandler et al., 2002a; Chandler et al., 2002b; Barnichon and Deleruyelle, 2009; Enzell and Malm, 2019) to understand the mechanical behaviour of cutoff seal. These tests are site-specific, and experiences from these projects can not be transferred to understand the performance and EDZs for cutoffs in varying geological settings for different DGRs. Therefore, numerical modelling can be an important tool to understand the EDZs for the cutoffs located in different geological settings.

While few researchers such as Perras et al. (2015) and Yuan et al. (2017) have numerically simulated the mechanical behaviour of a particular shape and dimension of the cutoff located in a specific rock type. In this thesis, numerical modelling is used to develop a generic methodology to

understand the EDZi and EDZo for different shapes and dimensions of cutoffs under a wide range of geological settings. Also, there is a scarcity of studies for EDZi and EDZo prediction for the cutoffs under thermal loads from nuclear fuel in the underground nuclear waste repository environment. Therefore, in this study, numerical modelling is used to understand EDZi and EDZo for the cutoff under different thermo-mechanical conditions in an underground nuclear waste repository.

1.3 Research Objectives

While field tests have been carried out to understand the performance and EDZs for the cutoffs, these tests are site-specific and the performance and EDZs for the cutoffs can vary depending on the repository site to site. Numerical modelling can be used to understand the EDZi and EDZo around the cutoff under varying thermal and mechanical conditions for a repository. In order to evaluate EDZi and EDZo for cutoffs using numerical modelling, this thesis focuses on the following objectives.

1. To evaluate dimensions of different EDZs around a conceptual placement room in an underground nuclear waste repository with various geological properties and conditions.
2. To model different shapes and dimensions of cutoffs designed to seal the EDZs from objective 1 and determine the optimum shapes and dimensions for different geological scenarios.
3. To study the effect of different variants such as shape and orientation of placement room, rock mass anisotropy, rock mass properties, and heat from the spent nuclear fuel on the change of the EDZi and EDZo around the optimum cutoff.

In order to achieve the above objectives, the following tasks have been undertaken:

1. Determine the dimensions of different EDZs around a conceptual placement room with and without the cutoff using a continuum numerical model (FLAC3D) under different geological settings.
2. Optimize the dimension and shape of threecutoff seal geometries by minimizing the increase in the pre-existing EDZi after constructing the cutoff.

3. Analyze the effect of different variants such as shape and orientation of the placement room, rock mass anisotropy, and rock mass properties on the change of the EDZi and EDZo around the optimum cutoff.
4. Determine the maximum possible temperature at the cutoff due to the heat from spent nuclear fuel during the repository life cycle using a finite element thermal model at the scale of the placement room.
5. Analyze the effect of heat from nuclear fuel on the change of the EDZi and EDZo around the optimum cutoff using a finite difference thermo-mechanical model.

1.4 Layout of the Thesis

Chapter 1 (this chapter) provides historic and state-of-the-art background information on nuclear waste disposal and develops a case for undertaking the research described in this thesis by providing a problem statement and outlining a set of objectives. Definitions of important terms, such as DGR, excavation damage zones around excavations, different types of barriers used in nuclear waste repositories, and description of cutoff seals, are also provided in this chapter.

Chapter 2 consists of an extensive review of past research on the analysis and design of cutoff seals in both underground nuclear waste repositories and underground mines. The design concepts for room seals from various countries around the world are presented. Experimental and numerical modelling studies for cutoff design are discussed and knowledge gaps identified. The specific objectives of the research are also discussed in detail in this chapter.

Chapter 3 describes the methodology that has been used to study the mechanical behaviour of the cutoff using a three-dimensional (3D) numerical model. Three shapes of cutoffs, triangular, trapezoid, and rectangular for circular and rectangular rooms, located in granite, limestone, and mudstone are numerically simulated. The rooms in the repository are considered at different depths to analyze the model behaviour for a range of in-situ stresses. This chapter also describes a parametric study that was used to optimize the cutoff shape and dimensions. The methodology to study the thermo-mechanical behaviour of the cutoff at the placement room scale was outlined in this chapter.

Chapter 4 presents the results from the numerical modelling conducted to understand the mechanical behaviour of cutoff located in a certain type of rock and in-situ stress conditions. Different Excavation damage zones (EDZs) due to the construction of the room and cutoffs are predicted. A parametric study was carried to optimize the shape and dimension of the cutoff that leads to a minimum increase in the pre-existing EDZi due to the construction of the cutoff. This chapter also describes the results on the effects of different variants such as shape and orientation of placement room, rock mass anisotropy, and properties on the change of the EDZi and EDZo around the optimum cutoff.

Chapter 5 describes the effect of heat from spent nuclear fuel on the optimum cutoff. To analyze the effect of heat, a 3D thermo-mechanical model has been used. The results of the study show the effect of heat on the optimum cutoff using a near field model and a placement room scale model.

Chapter 6 analyzes and discusses the numerical modelling results by comparing them with empirical and analytical solutions. The findings are discussed in the context of repository design. The limitations of the research and important assumptions made in the study are also discussed in this chapter. The effect of important parameters and their sensitivity on the numerical modelling results, for example, mesh size, are also discussed in this chapter.

Chapter 7 summarises the objectives, the methodology, and the findings of the research and provides key conclusions that can be drawn from it. It also outlines the scope of future research based on the limitations of the methods and available information.

Chapter 2: Literature Review

2.1 Introduction

This chapter contains a review of the studies conducted to determine the extent of the EDZs for underground openings in brittle rocks. Empirical studies based on field observation and numerical studies to determine the depths of EDZs are described.

Researchers have used numerical modelling tools to study the extent and evolution of EDZs with time for site-specific case studies. A concise overview of the different numerical approaches is provided in this chapter.

A detailed overview of the proposed concepts for the cutoff seals in the underground nuclear waste repositories around the world is presented. Different countries, such as Sweden, Belgium, Canada, Germany, Finland, Netherlands, and Switzerland, have carried out tunnel and shaft sealing field experiments to understand the performance and EDZs for cutoff seals. A detailed overview of the field performance of these cutoff seals and important parameters affecting the performance of cutoff seals are discussed here.

2.2 EDZs Studies

Studies have been conducted to understand the formation and evolution of EDZs with time (Blümling et al., 2007), depth of EDZs (Bäckblom, 2008), and changes in the permeability in EDZs (Ababou et al., 2011). These studies were conducted in crystalline rocks (Bäckblom, 2008), argillaceous rocks (Lanyon, 2011), and salt rocks (Hou, 2003). These three rock types are most commonly considered to act as a natural barrier for the deep geological repositories (Tsang et al., 2005).

Empirical studies have been carried out to predict the extent of different EDZs based on in-situ stress conditions. Perras and Diederichs (2016) collected the EDZs and in-situ stress data for underground excavations around the world. The in-situ measurement for the dimensions of EDZs collected by Perras and Diederichs (2016) are presented in Fig. 2.1. The x-axis of the plot represents the ratio of maximum tangential stress along the boundary of the excavation and crack

initiation stress while the y-axis of the plot represents the extent of EDZs normalized by the size of the excavation. The empirical depth of failure proposed by Diederichs (2007) has been shown to successfully predict the depth of brittle spalling around the tunnels (Carter et al., 2008). The theoretical basis of the failure in the hard rock mass, such as granite, dense sandstone, and andesite was discussed in detail by Diederichs (2007). It was observed that failure in hard rocks initiates at stresses approximately 0.3 to 0.5 times of the uniaxial compressive strength. Perras and Diederichs (2016) showed that the empirical model predicted the depth of failure well when σ_{max} to CI ratio was below 2 while it did not predict well above the latter ratio. This was due to the non-linear increase in the failure depth with σ_{max} to CI ratio as opposed to linear increase as assumed in the linear empirical model.

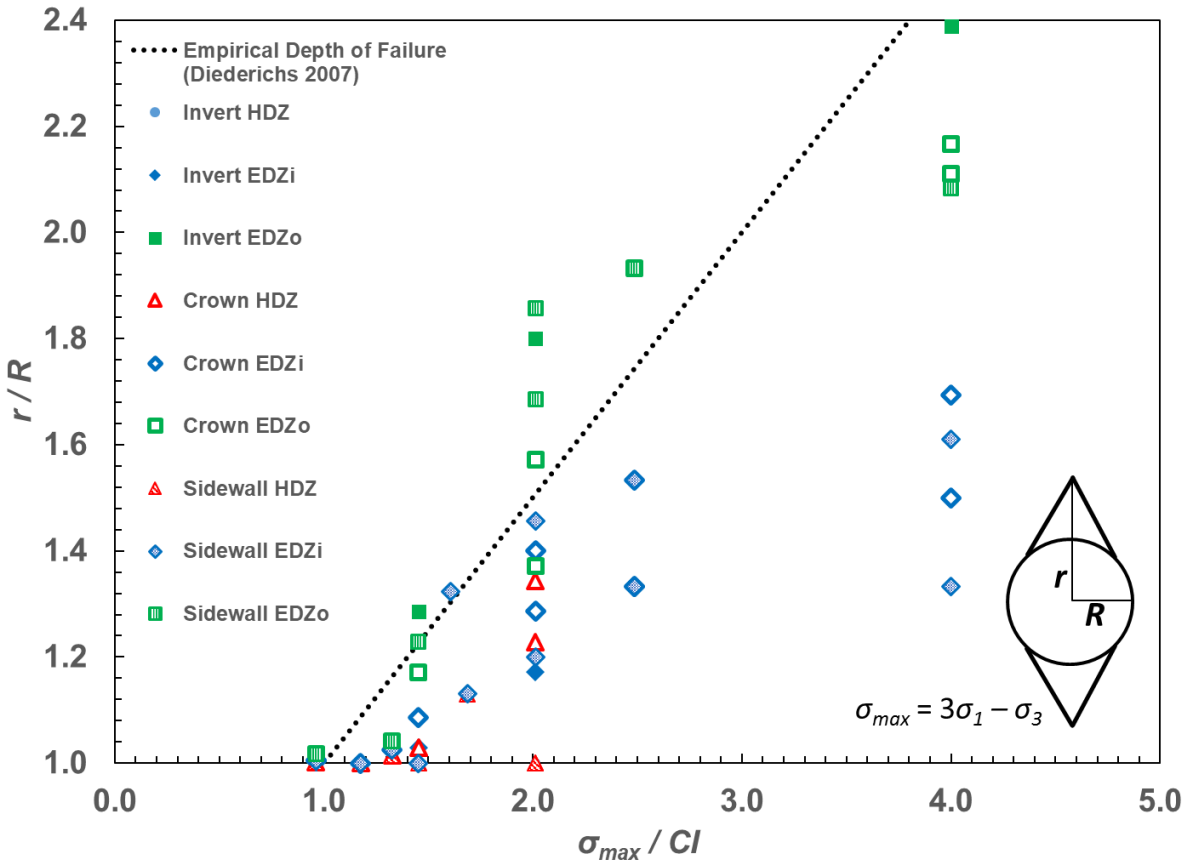

Fig. 2.1 In-situ measurements of the EDZ depths from the literature (Perras and Diederichs, 2016) compared with the empirical depth of spalling failure by Diederichs (2007).

Numerical modelling studies were carried out to understand the extent and evolution with time of EDZs for site-specific case studies. Continuum (Hou, 2003; Rutqvist et al., 2009), discontinuum (Fabian et al., 2007; Hudson et al., 2009), and hybrid modelling (Zhu and Bruhns, 2008; Lisjak et al., 2015; Lisjak et al., 2016) approaches were used to determine the EDZs. These studies were conducted on specific sites and lack generality and flexibility to use for other case studies where the geological setting of the rock mass considerably differs. Perras and Diederichs (2016) developed a more general approach to determine the dimensions of EDZs around circular excavations using the brittle failure rock mechanics.

The tunnel sealing experiment (TSX) was constructed inside a room of the Canadian underground research laboratory (URL) located 420 m below the ground surface to study the EDZs around tunnels in granitic rock (Martino and Chandler, 2004). The Canadian Nuclear Safety Commission (CNSC) used FRACON, a continuum numerical simulator to simulate the damage around the room (Rutqvist et al., 2009). The team used the Mises-Schleicher and Drucker-Prager unified (MSDPu) failure criterion proposed by Aubertin et al. (2000) and Li et al. (2005). The input parameters for the criterion was inferred from the laboratory tri-axial tests and field observations.

The input parameters for the MSDPu criteria were σ_c, σ_t, $\emptyset$, I_c, a_3, b where σ_c, σ_t, $\emptyset$, and b were uniaxial compressive strength, tensile strength, friction angle, and shape parameter, respectively while I_c, and a_3 were material parameters that can be determined from the lab experiments. More details on the formulation of the MSDPu criterion and some basic applications can be found in the article, Shirazi et al. (2006). The input parameters for the MSDPu yield function were derived from fitting the stress curve to Hoek-Brown failure criteria to simulate the rock mass behaviour. Using the parameters determined from the lab experiments and Hoek-Brown failure criteria, the determined damage zone (zone in the plastic state) around the tunnel was found equal to the observed EDZi in the field experiment (Rutqvist et al., 2009). The parameters for the Hoek-Brown failure criteria were determined from the tri-axial lab tests.

A study funded by the Swedish Nuclear Power Inspectorate and conducted at the Lawrence Berkeley National Laboratory (LBNL–SKI) used ROCMAS, a continuum numerical simulator to simulate the excavation-induced EDZs (Rutqvist et al., 2009). Mohr-Coulomb failure criterion was

used to simulate the failure process of rock mass and an empirical equation was used in combination with the failure criteria to simulate the excavation-induced permeability changes. The equivalent cohesion and friction angle to be used in the Mohr-Coulomb failure criterion were derived by fitting the failure curve to the Hoek-Brown failure criterion. The equivalent cohesion and friction angle were determined from the Hoek-Brown failure criterion in order to use the inbuilt Mohr-Coulomb criteria in ROCMAS. Using such parameters, the modelling results showed that there was limited yielding at the crown of the room, which was in agreement with the increased observed field macroscopic fracturing at the top of the TSX room.

The natural rock mass is heterogeneous due to the presence of fractures and joints. Discontinuum numerical simulators can simulate the discontinuity in jointed rock mass explicitly as opposed to converting it to an equivalent continuum by adjusting material properties. They can simulate the large-strain behaviour of damaged rock mass in the post-peak region accurately. The distinct element code by Itasca can simulate the rock damage by representing rock as particle assemblies and checking the breakage of bonds between these particles under stress (Itasca, 2003). However, such models are limited in size due to the large numbers of particles needed to simulate even a comparatively small volume of the rock mass. But it is also evident that only part of the rock mass is needed to simulate using the discontinuum approach as most of the other parts will not behave in large-strain and post-peak failure region. For example, for predicting EDZs, only the area near the tunnel circumference is needed to simulate using the discontinuum models. Based on this observation, Itasca also developed a coupled, three-dimensional, continuum/discontinuum modelling approach (Fabian et al., 2007).

The new model was called Adaptive Continuum/Discontinuum Code (AC/DC) which was based on the use of a periodic discontinuum ‘base brick’ for which more or less simplified continuum equivalents were derived. Based on the amount of strain in each part of the model, the AC/DC code can dynamically decide the appropriate type to be used for that part of the model. This approach was used to predict EDZs for an underground excavation laboratory at the Bure site of French nuclear waste agency, ANDRA. The EDZs were predicted after 2 years of excavation construction in the model. The results of the study showed an increase in micro-cracks over the given period of time. The numbers of connected micro-cracks were decreased after placing the

liner. However, the liner did not stop the generation of new micro-cracks with time. After 1 month the depth for connected micro-cracks was found to be 40 cm. Localization of micro-cracks was observed along the minor principal stress direction, the number of cracks increased with time, producing a well-connected fractured medium.

Dadashzadeh (2020) used the 2D Voronoi modelling technique using Universal Distinct Element Code (UDEC) (Itasca, 2014) to characterize the EDZs evolution by explicitly simulating the grain scale fracture propagation at the excavation scale. The simulation was carried out for a circular excavation located in the Cobourg limestone and granitic rocks. The EDZs were delineated based on the fracture density and their evolution around the tunnel. It was observed that plastic strain value may not be a good indicator to determine the highly damaged zone (HDZ), however, the strain gradient can still be used to determine the HDZ depth. Furthermore, the extent of EDZi can be determined using the volumetric strain values.

Lisjak et al. (2015) used the hybrid finite-discrete element method (FDEM) (Mahabadi et al., 2012) to simulate the EDZs for a circular excavation located in clay at the Mont Terri Rock Laboratory, located in Saint-Ursanne, Switzerland. The FDEM combines continuum mechanics principles with discrete element algorithms to simulate multiple interacting, deformable, and fracturable solids. The numerical values of EDZs for a micro-tunnel from the numerical models were compared with the field observations. The effect of backfill swelling pressure on EDZs was simulated by applying a compressive mechanical load perpendicular to the micro-tunnel surface. The circular tunnel and the surrounding zone of interest were discretized using linear elastic triangular finite elements and between each pair of triangular elements, 4-noded interface elements were inserted to capture the progressive failure of rock using a fracturing criterion. The progressive failure of the rock was captured using the cohesive-zone approach. The results confirmed the field observation that due shearing of the weak bedding planes was triggered around an unsupported excavation. It was shown that the compressive mechanical loading was ineffective in the sealing of EDZs because of the self-propping (arching) of fractures that formed during the rock mass damage process.

Perras and Diederich (2016) used a more general approach, termed as Damage Initiation and Spalling Limit (DISL) (Diederichs, 2007), to determine the dimensions of EDZs around circular

excavations. They used the combined weakening-hardening approach for the brittle rocks. The approach was based on the conceptual model of brittle spalling represented by cohesion loss and friction mobilization (Hajiabdolmajid et al., 2002; Diederichs et al., 2004). The approach was applicable for massive and moderately jointed rock mass where the joints do not significantly affect the stress-driven behaviour. The method captures confinement dependency of the brittle spalling process by defining the "damage initiation" threshold (elevated cohesion, low friction) transitioning to a "spalling limit" defined by the elevated friction and a cohesion loss.

To simulate this process, the cohesion loss was represented by the loss in the value of s while friction mobilization was represented by an increase in m in Hoek-Brown failure criterion. Here m and s were material constants that can be determined from the triaxial tests. This process shows that as confinement increases, away from the excavation surface, strain hardening is simulated after initial damage while at lower confinements brittle weakening is simulated. It was observed that positive (dilatant) numerical volumetric strain correlated with measured regions of connected micro-fractures around underground excavations; therefore, the zones within the plastic region with positive volumetric strain represented EDZi. The remaining zone in the plastic region was considered to be the EDZo, which contains zones that have undergone volumetric contraction.

Radionuclides can transport through the connected micro-fractures present in the EDZi, escaping the engineered and natural barriers. To disconnect and seal the connected fractures, a cutoff structure was constructed and filled with backfill material.

2.3 Cutoff Seal

Room seals or cutoff seals are a type of engineered barrier placed at strategic locations, for example in shafts, access adits and at the end of the fuel placement rooms, to seal the repository. A cutoff is an excavation constructed around the drift or shaft, which can be filled with bentonite or other sealing material. It is constructed perpendicular to the excavation axis to prevent the potential migration of radionuclide and water flow through the EDZs, parallel to the room axis. According to the SKB, the life cycle of a cutoff seal would be until the final closure of the repository and its purpose would be to cut off the water flow and radionuclide transport along the tunnel (Dixon et al., 2009).

2.3.1 Cutoff Seal in Mining and Other Industries

Open geological excavations can be detrimental to the environment. For example, inadequately-sealed mine adits may allow unacceptable discharge of acid mine drainage. Sealing strategies in mines vary depending on the purpose of sealing. One purpose is to seal the abandoned parts of the mine workings so that mining can be continued uninterrupted elsewhere. By sealing these openings, water inflow is reduced to rates that can be handled using the dewatering pumps at sumps. Kirkwood and Wu (1995) and Barcena et al. (2005) discussed the philosophy and approach to seal the construction in coal mines while Fuenkajorn and Daemen (1995) and Auld (1996) discussed more generic issues related to sealing performance and sealing approach.

Barcena et al. (2005) described the need for hydro-geological assessment to identify homogeneous rock mass without any structural features such as fault, fissures, friable or soft materials in the surrounding zone of the cutoff seal, with the length of the undisturbed zone being 3 times the length of the cutoff seal. Reinforcement of the cutoff seal and anchoring it into rock without causing stress conditions that favor flow along or close to cutoff seal was also recommended. Akgun and Daemen (1999) analyzed the design aspects of friction seals for abandoned underground mines. The stability of these seals was determined based on the shear and tensile strength of the contact between rock and cutoff seal in a borehole. They noted that the friction seals with a length to radius ratio of at least 8 should be considered reliable for the stability of the seals. Auld (1996) explained tunnel sealing applications and considerations in detail. He identified 4 types of seals (Fig. 2.2) and 8 factors to be considered in the design of seals. The important factors to consider while designing a cutoff seal are 1. The type of cutoff seal; 2. Nature of excavation; 3. Cutoff seal location; 4. Shape of the cutoff seal; 5. Hydraulic head condition; 6. Local rock and stress condition; 7. Strength and stress conditions in cutoff seal; and, 8. Cutoff seal construction method.

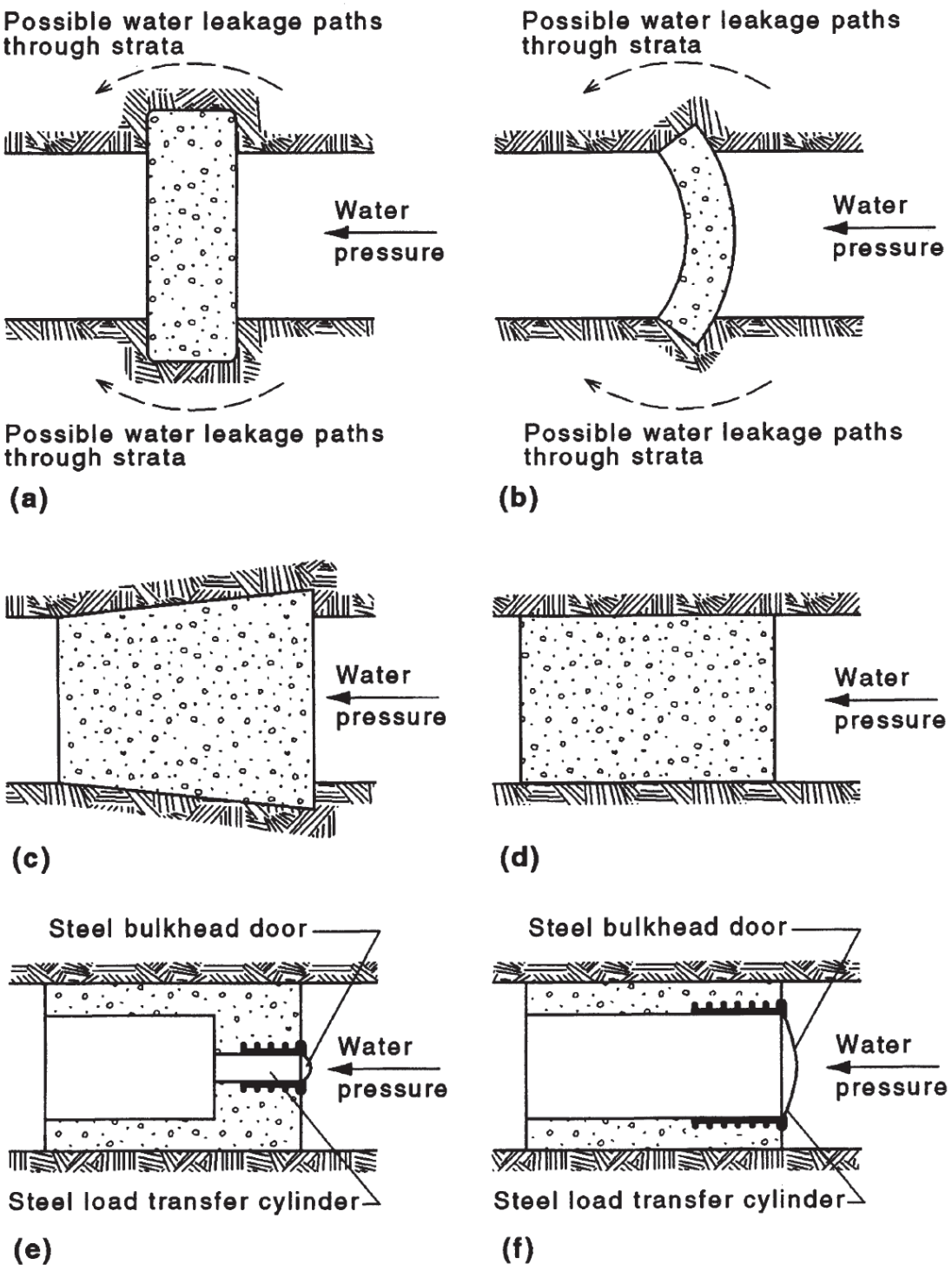

Fig. 2.2 Generic cutoff seal shapes (Auld, 1996). (a) Reinforced concrete slab; (b) Unreinforced concrete arch; (c) Unreinforced concrete tapered cutoff seal; (d) Unreinforced concrete parallel cutoff seal; (e) Unreinforced concrete cylindrical parallel cutoff seal, with human access; (f) unreinforced concrete cylindrical parallel cutoff seal, with roadway access.

Littlejohn and Swart (2006) noted that residual water tightness for the seals built-in one application in the mining industry was 1 to 3×10^{-7} m/s, which was much higher than the requirements of typical cutoff seal needed in underground nuclear waste repositories. Littlejohn and Swart (2006) also noted that these seals have a higher leakage rate; however, they did not experience any structural failure. Several research papers can be found on the design of seals for South African underground gold mines, for example, Brawner et al. (2005), Bruce et al. (2006), Littlejohn and Swart (2006), Robert M (2006). These papers outlined the design of a cutoff seal under a high hydraulic head (up to 28 MPa). Harteis et al. (2008) developed guidelines for permitting, constructing, and monitoring water seals in underground coal mines in the United States. Water seals have long been used to assure the safety of miners using water retention in mines (Djahanguiri and Abel, 1997; Pacovský, 1999). Masumoto et al. (2007) presented a technique for clay grouting to seal the excavation damage zone surrounding a water cutoff seal.

In high head hydro-electric facilities the rate of water supply to penstocks and turbines is controlled using seals. The seals are installed at the entrance to penstocks in unlined tunnels to control the water supply (Bergh-Christensen, 1989; Auld, 1996). The seals are made of concrete and have perforation at the center to control the rate of water supply by mechanically opening and closing it. These seals are designed to withstand water pressure up to 900 m head unlike the seals in the repository which are expected to have some water-bearing feature.

Underground natural gas storage caverns are used to store and stockpile critical hydrocarbon supplies closer to the market. These facilities are generally located in abandoned underground mines which can sustain substantial pressure e.g. 12.5 MPa (Pacovský, 1999) at which the natural gas is stored. As a part of the conversion of the Wilhelmine-Carlsgliick Mine, Germany for crude oil storage, seals were placed in the two shafts at the base of the tubbing section (Klemme,1979). The trapezoid-shaped concrete cutoff seal was anchored into an excavation made along the shaft lining. Pacovský (1999) explained the design aspects of a cutoff seal located 950 m below the ground surface in the granite rock mass. The cutoff seal was constructed using fiber-reinforced shotcrete to increase stability. Two of these seals are still in working condition without any significant structural damage (Hydrocarbons Technology, 2020).

In December 2001, UBC-CERM3 installed a mine cutoff seal in a mine drift for mine water management (Meech et al., 2006). The cutoff seal was designed to seal the facility for 1000 years and was given the name “The Millennium Seal Project”. This cutoff seal can be considered to have common features with the repository cutoff seal because of its lifecycle and ability to seal the water inflow. It was constructed with concrete in combination with a clay-based seal in downstream. The clay-based cutoff seal was designed to retard any seepage of water around the concrete seal. Water seeped through the concrete was collected mechanically and the cutoff seal was designed to have a seepage rate at least equal to or less than the surrounding rock.

The main purpose of sealing in mining and other industries is to prevent the water flow in excavations as described in this section. These seals may not be suitable for underground nuclear repositories due to strict requirements on the movement of water and radionuclides across the seals. For nuclear waste repositories, the main purpose of the cutoff seal is to seal the excavation with a permeability equal to or less than the permeability of the in-situ rock mass (Dixon et al., 2009).

2.3.2 Cutoff Seal in Deep Geological Repositories

Room, tunnel, and shaft sealing field experimentation had been carried out by different countries, for example, Sweden, Belgium, Canada, Germany, Finland, Netherlands, and Switzerland. Swedish Nuclear Fuel and Waste Management Company (SKB), developed two large research facilities at STRIPA Mine (1980-1992) and Aspo Hard Rock Laboratory (1995-2015) to understand the sealing process in repositories (Fairhurst et al., 1993). The STRIPA mine project was the first underground research facility for engineering demonstration of cutoff seal performance in granitic rock. The STRIPA mine was an abandoned iron ore mine that provided access to the adjacent granitic rock (Fairhurst et al., 1993).

Gray (1993) and Gnirk (1993) summarised all the important findings from this project. The first experiment known as the Tunnel Sealing Experiment was constructed in a 35 m long tunnel using a controlled drill and blast method to limit the excavation damage zone (EDZ). The cutoff seal consisted of a 2.2 m long concrete bulkhead seal and a 0.5 m long gaskets (O-rings) of highly compacted bentonite (Fig. 2.3) (Gray, 1993). The hydraulic conditions in the rock surrounding the tunnel were that a hydraulic pressure of 1 to 1.5 MPa was present within 3 to 5 m of the excavation

surfaces. The rock surrounding the cutoff seal was not homogeneous and contained structural features such as joints and fractures intersecting the excavation at and around the cutoff seal location. The main purpose of the experiment was to analyze the performance of HCB gaskets (Gray, 1993). The operational phase for this experiment was 21 months and hydraulic pressure in the chamber was cycled several times during the operation phase (Gray, 1993). It was observed that seepage occurred through the jointed rock along with the concrete rock interface. The flow rate was found to be 75 L/hr at a hydraulic pressure of 35 MPa and it could have been 1000 L/hr without HCB gaskets (Pusch et al., 1987b). This experiment showed the importance of HCB's self-grouting process to isolate the seepage along the excavation face and concrete cutoff seal face.

SKB also carried a Shaft Sealing Test inside a 14 m long tapered shaft (Fig. 2.4) at STRIPA Mine (Pusch et al., 1987a and Gray, 1993). Two tests were carried out, one with only concrete cutoff seal and the second with concrete cutoff seal and keyed HCB. In the first case, a seepage rate of 8-9 L/h was noticed at a hydraulic pressure of 100 kPa. Most of the seepage occurred through the geological features that spanned the concrete and were exposed to excavation walls (Pusch et al., 1987a). The second test was conducted at the same location as the concrete test, however this time with a concrete cutoff seal and keyed HCB. The seepage rate of 0.3 L/hr was noticed at a hydraulic pressure of 100 kPa. The bentonite cutoff seals expanded into the geological features and reduced the seepage rate. The shaft sealing test showed the effectiveness of bentonite in reducing the flow of water along the walls of the shaft.

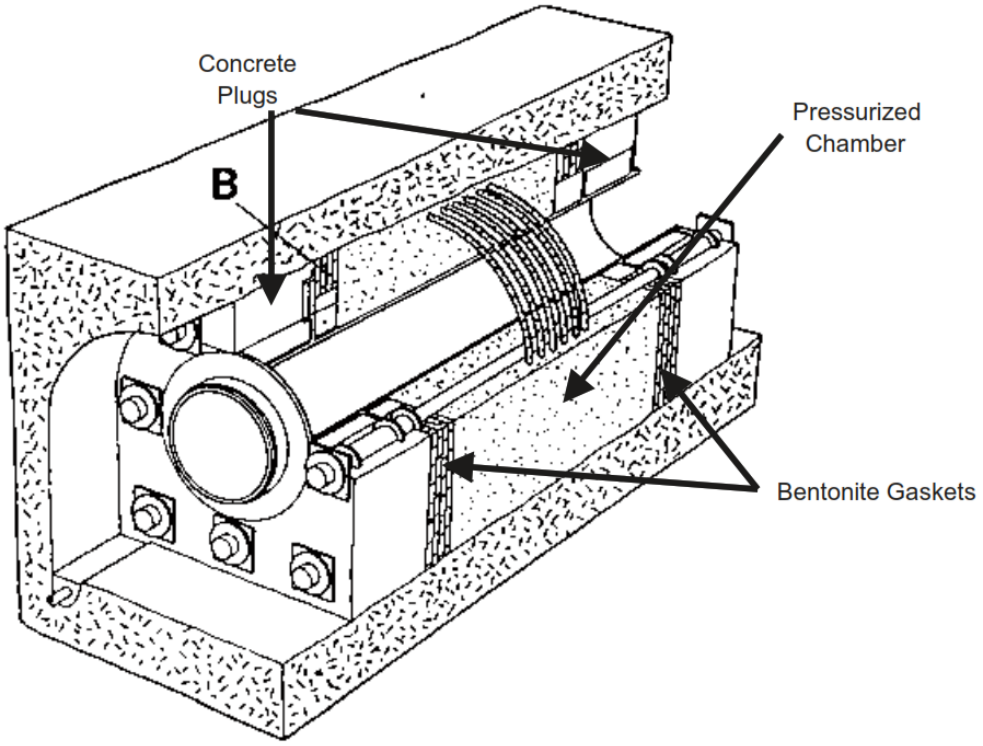

Fig. 2.3 Layout of the Tunnel Sealing Experiment after Pusch et al. (1987)b.

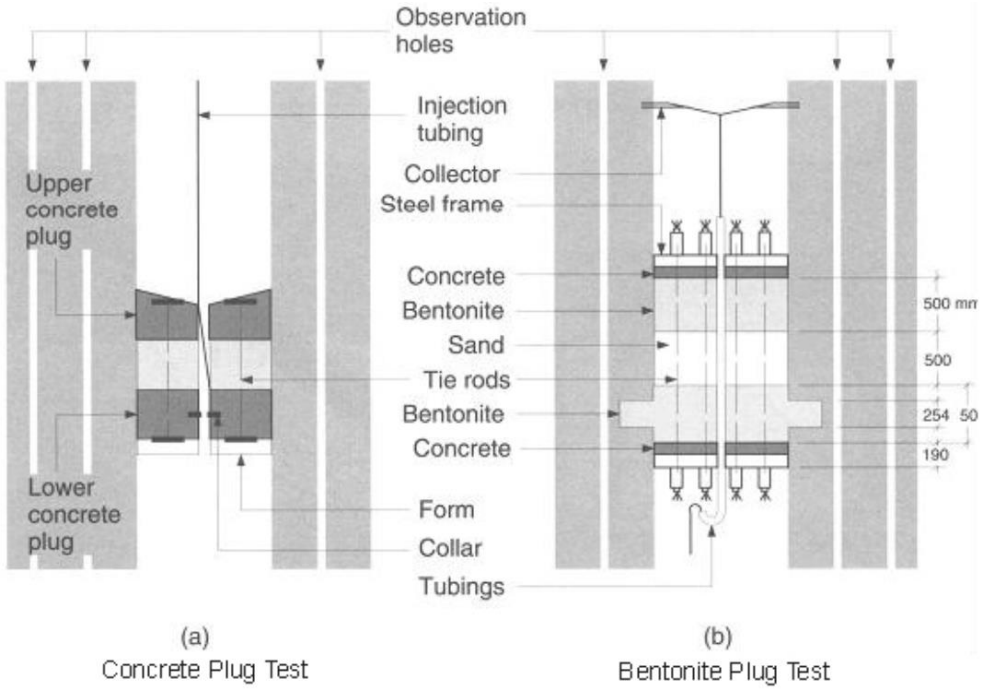

Fig. 2.4 Schematics of the arrangement of the concrete and HCB Shaft Sealing Tests (Dixon et al., 2009).

SKB also developed the Aspo Underground Research Laboratory for developing and testing technologies that will be used in the underground nuclear waste repository. The Backfill and Seal test (BPT) was carried out 420 m below the ground surface (Gunnarsson et al., 2002). This test consisted of the installation of a 28 m long cutoff seal system that was divided into three sections (Fig. 2.5). The innermost section was backfilled with bentonite material of different compositions. The second section was backfilled with crushed rock and bentonite pellets. The third section consisted of a concrete structure to provide the necessary support to backfill material and hence allowing it to develop its swelling potential. The concrete cutoff seal also had the purpose of retarding the seepage of water from the excavation and concrete interface. It was observed that at a hydraulic head of 530 kPa the seepage rate was 0.75 L/min.

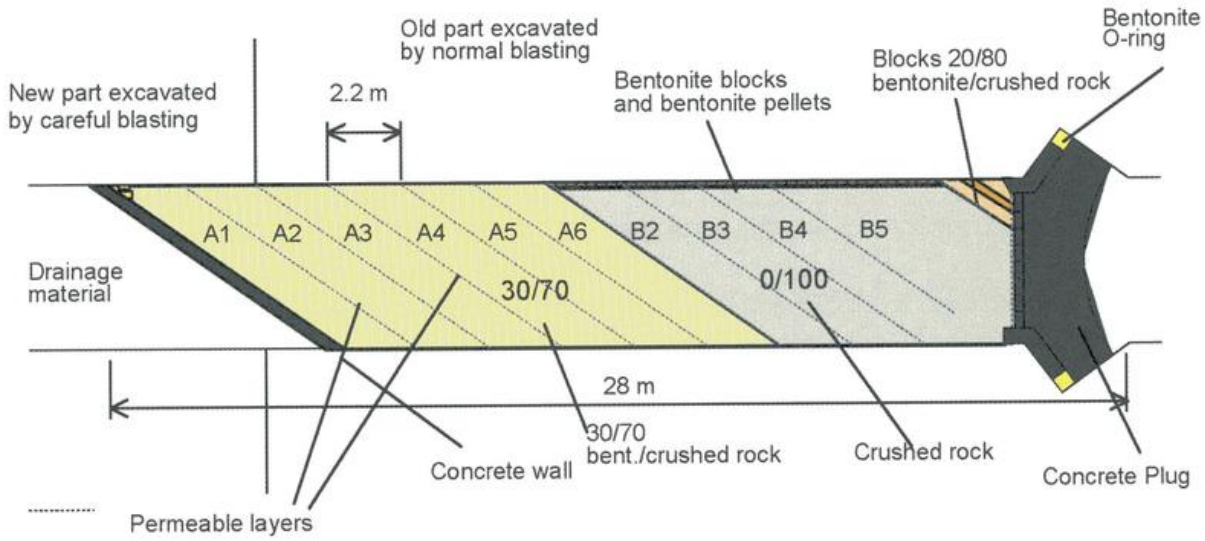

Fig. 2.5 The conceptual diagram of the Backfill and Seal Test. (Gunnarsson et al., 2002)

SKB also carried out a Prototype Repository (PR) test to simulate the full-scale deposition tunnel (Lydmark, 2010). For this test, 6 vertical emplacement holes were drilled in the floor of the tunnel and installed with electrical heaters of the same size to simulate heat generated from nuclear fuel (Fig. 2.6). The deposition tunnel consisted of two sections: in one section 4 heaters were installed, while in the second section 2 heaters were installed (Fig. 2.6). The two sections were separated by a cast concrete cutoff seal and one other seal was installed at the end of the tunnel. This experiment provided an opportunity to study the thermo-mechanical response of the cutoff seal in the repository. Beyond the cutoff seal, the tunnel was backfilled using 30% MX-80 bentonite and 70%

crushed rock aggregate, compacted in-situ. It was noted that due to the connection between the closed PR tunnel and nearby two perpendicular tunnels (I, J+) and one parallel tunnel (G), water pressure in the PR tunnel was reduced to 300-500 kPa. This condition could be present during the placement condition in the actual repository. A seepage rate of 2 L/min was observed for the PR tunnel at a hydraulic pressure of 500 kPa while seepage rates of 5 L/min and 3.5 L/min were observed at tunnel G and I, respectively.

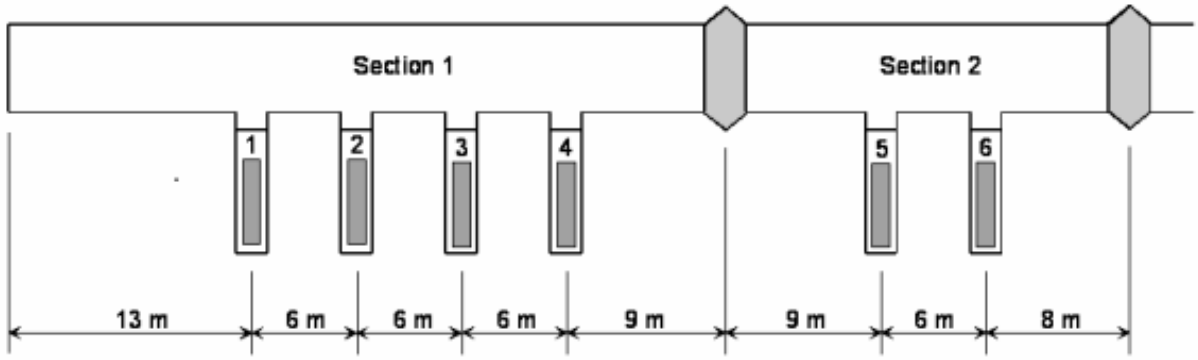

Fig. 2.6 The conceptual illustration of Prototype Repository Test for the cutoff seal (Lydmark, 2010).

The Dome Seal (DOMPLU) experiment was undertaken by SKB and Posiva at the Aspo Hard Rock Laboratory (Aspo HRL) in Sweden (Enzell and Malm, 2019). The objective of this experiment was to understand the strength, shrinkage, creep, and binding properties of rock and its interaction with concrete without any reinforcement of the concrete. It was conducted inside a 4.2-m-high and 4.2-m-wide horseshoe-shaped tunnel (Fig. 2.7). The design consisted of an unreinforced concrete dome with a watertight cutoff seal, a filter layer, and a backfill transition zone located upstream of the concrete cutoff seal. The filter layer was included to avoid high water pressure on the concrete dome before it reaches its full strength. The concrete dome was excavated using the wire sawing technique to minimize the extent of EDZs. The cutoff seal system was subjected to 4MPa at its upstream end. Initially, the pressure was designed to be 7MPa; however, a leakage through a rock joint occurred after 7MPa. Therefore, it was decided to monitor the cutoff seal leakage at 4MPa. The measured leakage rate across the cutoff seal was very low, which showed that the contact grouting seal provided a watertight cutoff seal. The bentonite cutoff seal was swelled and compressed the gravel filter, and the pellet filled the slot inside the LECA wall.

The full-scale test showed that the uniform saturation of bentonite did not progress rapidly to act as a watertight cutoff seal in the initial phases of the experiment.

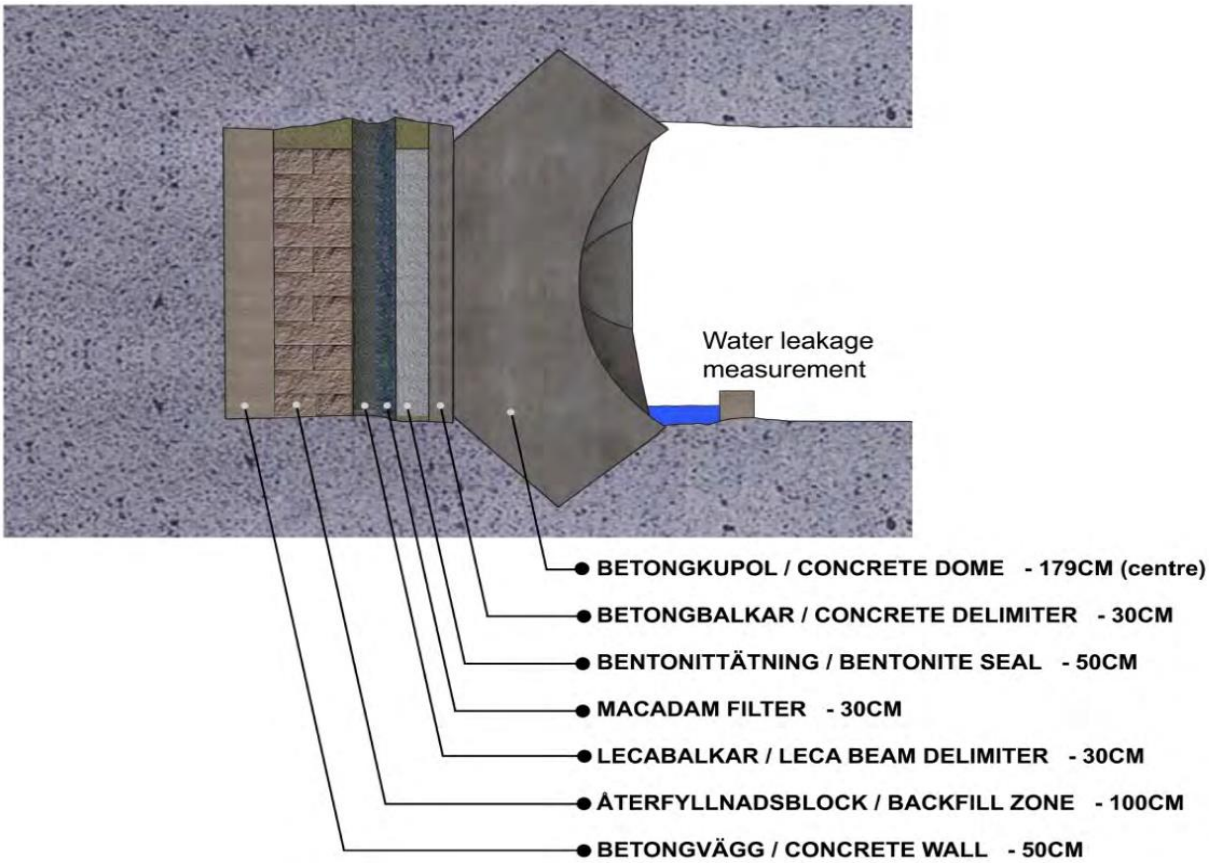

Fig. 2.7 Schematic section of the DOMPLU full-scale test carried out Asp HRL (Enzell and Malm, 2019).

Posiva's SEAL (POPLU) experiment was undertaken by Posiva, SKB, VTT, and BTECH at the ONKALO Underground Rock Characterisation Facility (URCF) in Finland, which was also the proposed site for the future Finnish Nuclear Waste Repository (Holt and Koho, 2016). The reference design for the POPLU experiment was the same as that of DOMPLU experiment as described previously. However, POPLU has a wedge-shaped cut-off slot that has been notched into the EDZ (Fig. 2.8). The slot was filled with a wedge-shaped low-pH (lower than 11) stainless steel-reinforced concrete structure. The slot was constructed using the wedging and grinding method instead of the wire sawing method. The wedge-shaped concrete structure was attached to a filter layer in front of the concrete tunnel back wall (Fig. 2.8). The concrete wedge was also equipped with bentonite circular strips and grouting tubes at the rock-concrete interface to ensure

water tightness. Steel reinforcement was used to counteract the shrinkage of bentonite and keep it attached to the rock tunnel. Analytical and numerical simulations were used to better understand the static and dynamic stress evolution, and water flow in different components of the cutoff seal. The results showed that the addition of bentonite behind the concrete wedge would increase the water tightness of the cutoff seal. The numerical results showed that the water outflow from the concrete wedge was reduced by a factor of 17 to 1380 when using a bentonite cutoff seal. The modelling results also showed that no leakage would be expected after using the bentonite fillings to seal the potential defects at the circumferential concrete-rock mass interface. From the mechanical integrity point of view, a maximum displacement of 3 mm was expected on the side of the concrete wedge facing the pressurization and the surrounding rock mass in contact with it while a slightly higher displacement of rock could be expected in the proximity of fractures. The study concluded that the concrete wedge can be expected to deform more than the rock in response to pressurization and the concrete wedge deformation may be asymmetric due to the heterogeneous nature of the surrounding rock mass.

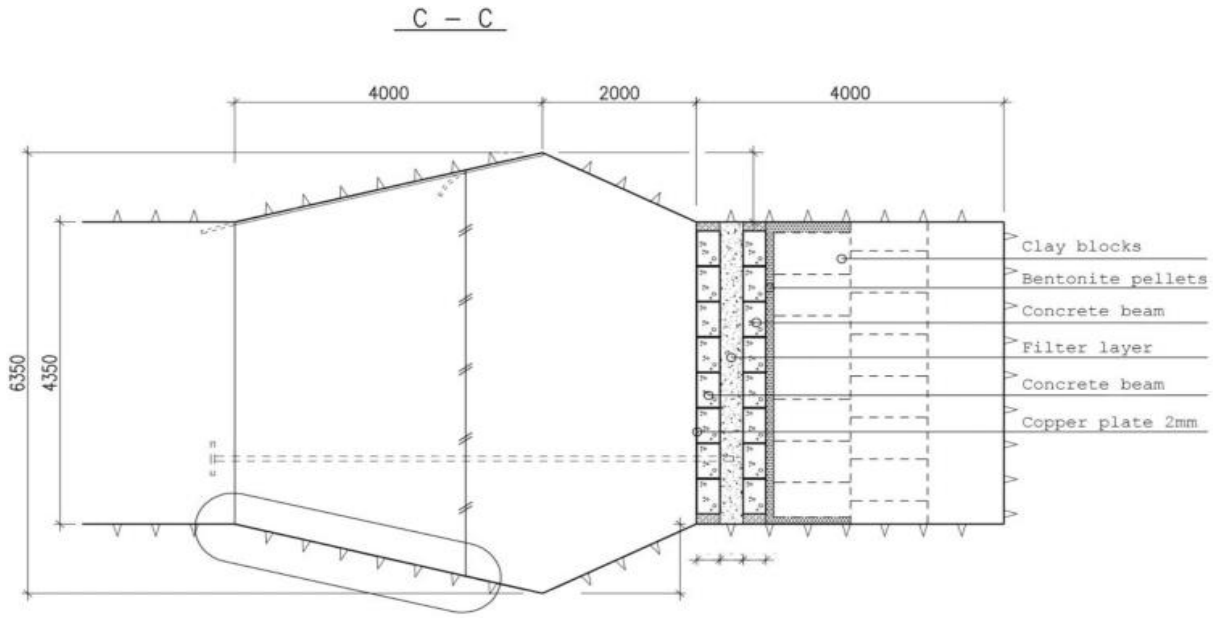

Fig. 2.8 Posiva's design for the POPLU (wedge cutoff seal) experiment, with iterative filter and cutoff seal layers shown at right (Holt and Koho, 2016).

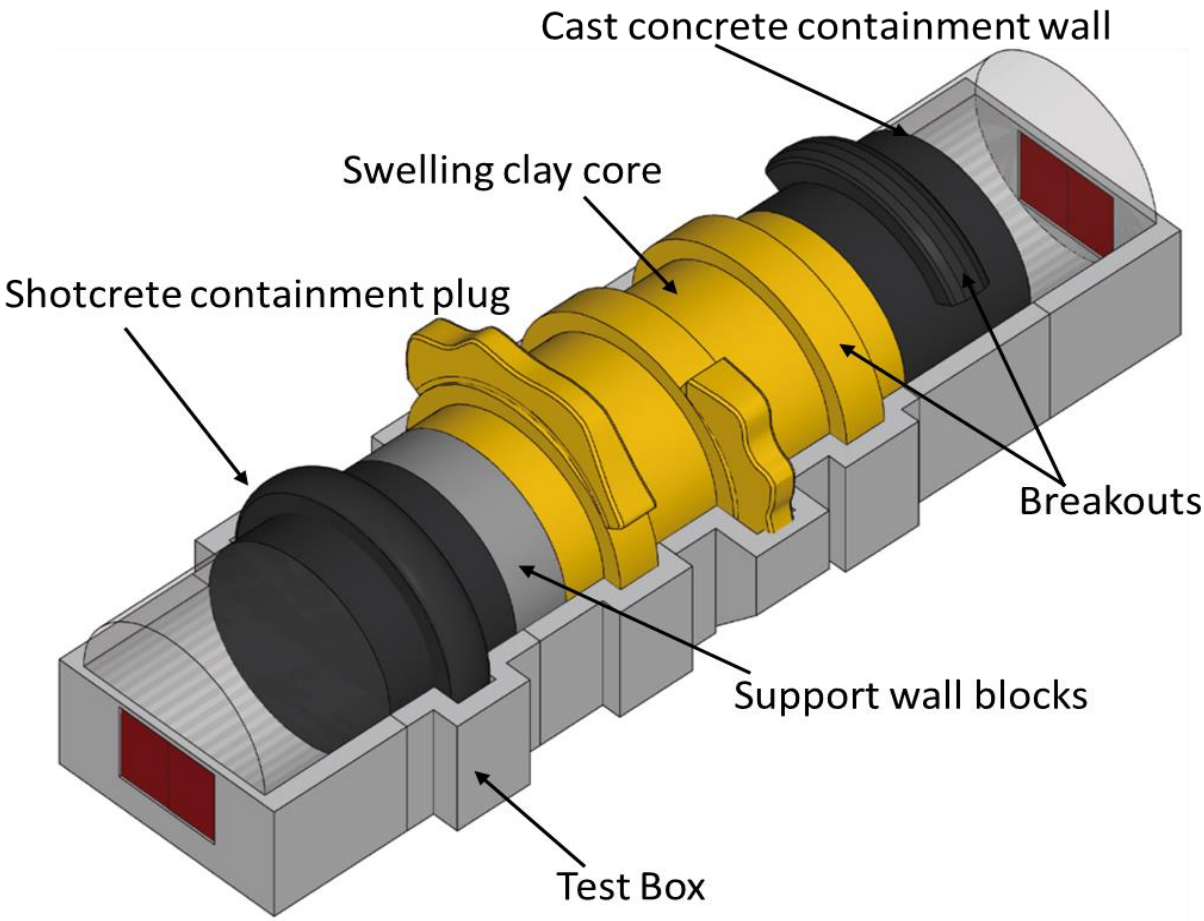

Fig. 2.9 Conceptual design illustration for the ANDRA FSS test, France (Noiret et al., 2013).

The French underground research laboratory (URL) at Bure carried out the Full-Scale Experiment (FSS) to demonstrate the industrial capacity to satisfactorily emplace large volumes of concrete and bentonite material for the cutoff seal (Noiret et al., 2013). The cutoff seal was composed of a swelling clay core with two low pH concrete containment seals, one at each end (Fig. 2.9). The remaining part of the tunnel will be backfilled using the excavated material. Thin groves were excavated at strategic locations along the tunnel liner and filled with bentonite, providing an EDZ cutoff. The main difference between the FSS experiment and the actual cutoff seal in the repository was the length of the cutoff seal. The length of the cutoff seal in the actual repository condition would be longer than in the experimental condition. The experiment was designed to address material requirements using mixtures of bentonites pellets and powdered swelling clay core for the efficient filling of the core volume. Low-pH (pH<11) concrete was used to limit the interaction between the concrete and clay core for preserving the core properties.

The experiment was important to understand the self-compacting concrete's (SCC) retardant dose to the ambient temperature and the need to control bentonite pellet breakage during the emplacement of bentonite mixture.

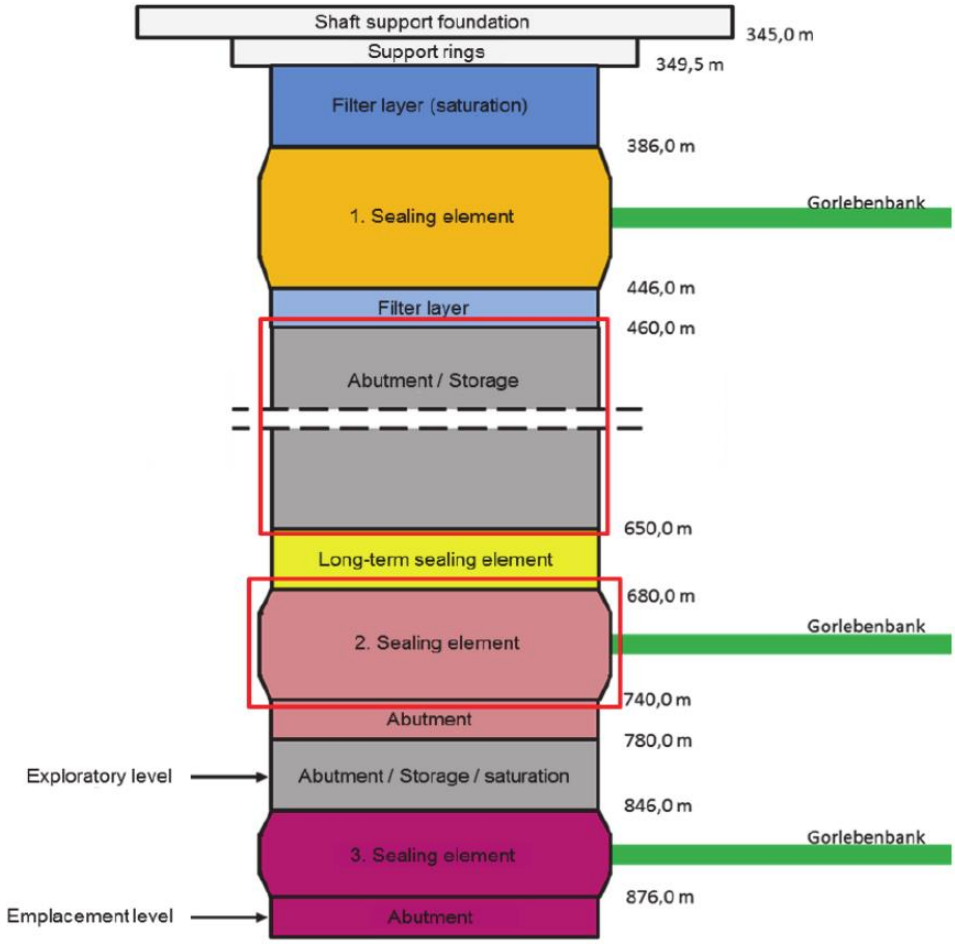

Fig. 2.10 Reference conceptual design for the German shaft seal. The elements considered in the safety assessment are framed in red (Müller-Hoeppe et al., 2012). The Gorlebenbank is a folded anhydrite layer in the rock salt.

Tests for seals in the vertical shafts, Entwicklung von Schachtverschlusskonzepten (ELSA) experiment was carried out by Technical University of Freiburg and associated partners (White and Doudou, 2014). The main objectives of the ELSA experiment were to develop generic design concepts for shaft seals in the salt and clay host rocks that comply with the requirements for a high-level waste repository and to carry out necessary preparatory work in the shaft cutoff seal design project. They investigated the sealing capacity of salt concrete cutoff seal elements and

surrounding rock salt at the laboratory scale (Fig. 2.10). The results showed that the permeable contact seam between the cutoff seal and the salt would not be closed in short term; however, confining stress of 5 MPa would be sufficient to stop brine flow along the cutoff seal element.

To test the effectiveness of drift cutoff seals, a rectangular test cutoff seal with dimensions 3.2 m by 3.5 m and 5 m in length was installed in a 35-year-old potash mine drift in Sondershausen, Germany (Sitz et al., 2002). The cutoff seal was installed in the Potash mine drift located at 700 m below the ground surface. The integrity of the seal was tested by applying a pressure of up to 8MPa to one side of the cutoff seal using a brine solution. The cutoff seal was constructed using bentonite and sand blocks, mixed in proportion 40 to 50% bentonite and remaining proportion as sand (Fig. 2.11). In order to cut off the EDZs, two rectangular slots were constructed and filled with the bentonite clay and sand mixture. To provide mechanical support to the cutoff seal a prismatic shape salt-brick block was constructed in the downstream face of the cutoff seal. Seepage rates at a fluid pressure of 1.5, 2.5, 4, and 8 MPa were monitored. Unfortunately, the system was failed after the pressure of 1.5 MPa due to the failure of the restrain system, and higher seepage rates were observed. At 1.5 MPa a seepage rate of 3 L/h was observed which decreased to 0.45 L/hr within 30 days (Sitz et al., 2002).

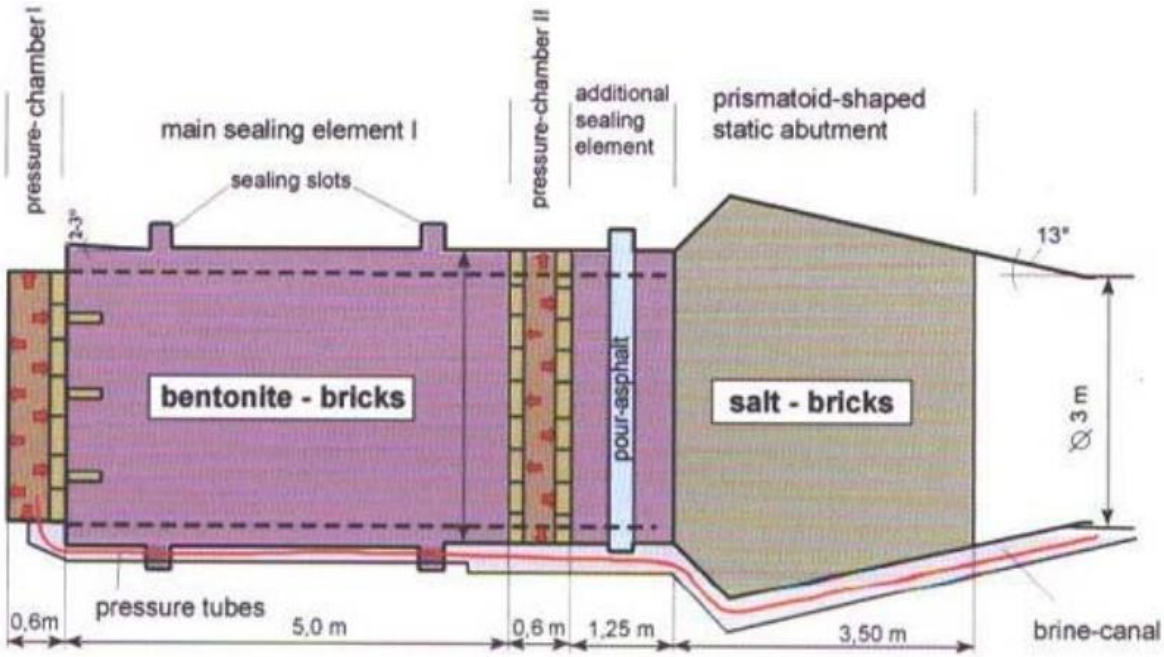

Fig. 2.11 Illustration of different components of the Tunnel Sealing Test in salt (Sitz et al., 2002).

The Underground Research Laboratory (URL) located near the Whiteshell Laboratory in Pinawa, Manitoba was built and maintained by Atomic Energy of Canada Limited (AECL) between 1983 and 2004 (Chandler et al., 2002a, b; Dixon et al., 2005). During this time, the URL conducted two field experiments for sealing the underground openings. Tunnel Sealing Experiment (TSX) and the Composite Seal Experiment (CSE) were carried out for drift sealing. The TSX was carried out to study the performance of concrete and bentonite bulkheads and to determine the importance of different parameters on bulkhead's performance.

The TSX was carried out in a drift constructed using drill and blast method and located at 420 m level of the URL. The TSX consisted of two bulkheads, one made of a bentonite-sand block (70% bentonite and 30% sand) and the other made of low-pH, low-heat, high-performance concrete (LHHPC). The two bulkheads were separated by a sand-filled chamber, which could be pressurized up to 4.2 MPa (Fig. 2.12). Hot water was used for circulation in the chamber to understand the effect of temperature on the performance of the bulkhead. To cut off the EDZ both the bulkheads were keyed into the walls of the drift. The clay bulkhead was 2.6 m long and located in a 3.5-m-high and 4.375-m-wide tunnel. The length and width of the keyed part of the bulkhead were 1 m and 2 m, respectively. To provide mechanical support to the clay bulkhead, a steel restraint system was used.

A high seepage rate was observed through clay bulkhead during the initial stages of bentonite hydration and pressurization. The high seepage rate was relatively for a short duration and did not involve any bentonite clay in the outflow. The high flow during the initial phases was attributed to discrete flow planes in the rock that gradually closed when the clay was hydrated. The bentonite clay bulkhead did not have any considerable seepage after 8 months and the flow rate continuously decreased after 8 months. At the time of decommissioning of the experiment, the flow rate was reduced to 0.7 L/h at a hydraulic pressure of 4 MPa and most of the seepage was occurring along the perimeter. At the other end of the drift, a 3.5-m-long concrete bulkhead was keyed to a depth of 1.75 m into the drift wall. Although it was a low-heat concrete, LHHPC does generate some heat during curing and so it was anticipated that at least a small degree of cooling shrinkage would occur. Cooling shrinkage could lead to shrinkage cracking or loss of contact strength between rock and concrete. At the initial stages of the experiment, a high seepage rate (96 L/h at 300 kPa

hydraulic head) was observed, and therefore, grouting was used. The grouting was used to improve the surrounding rock mass condition and to improve the contact strength between rock and concrete. After grouting, the rock mass condition was improved and a seepage rate of 0.07L/h at 400 kPa pressure was observed. While a seepage rate of 0.84 L/h at 4 MPa was observed at the end of the isothermal stage of the TSX. The experiment demonstrated that the heat from the hot water used for pressurization did not have a significant effect on the performance of both the bulkheads.

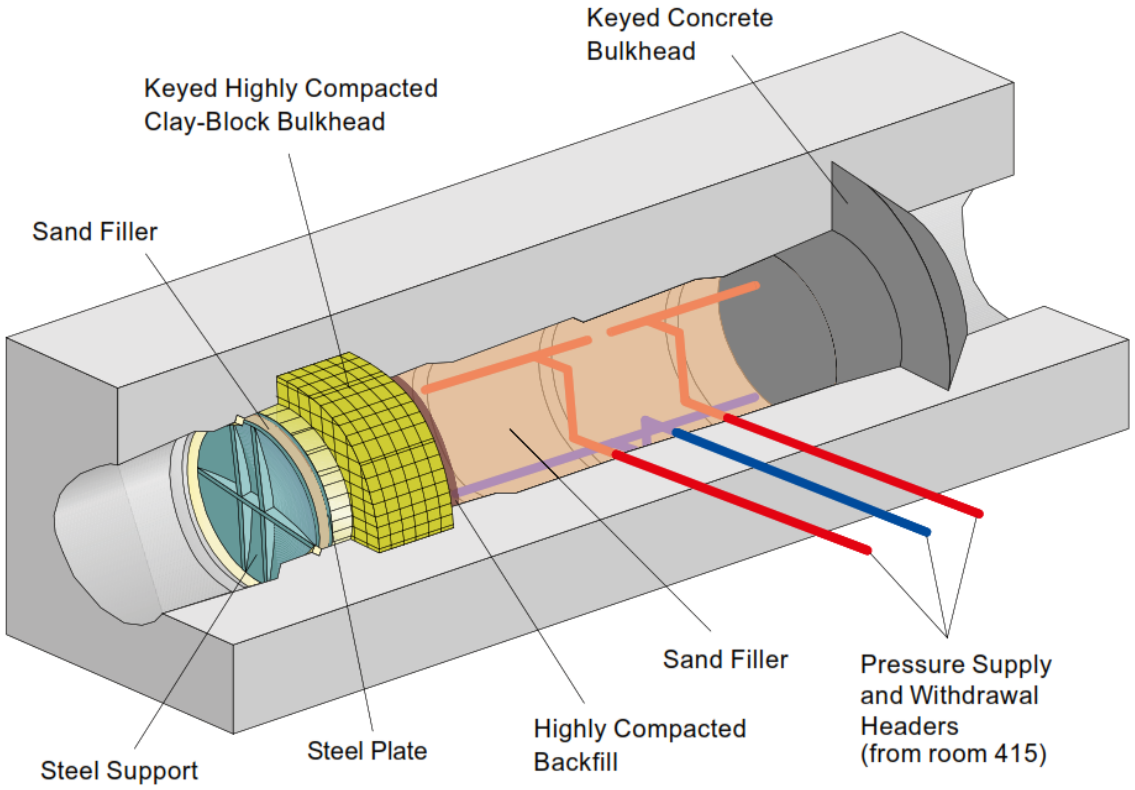

Fig. 2.12 Schematic diagram for the Tunnel Sealing Experiment designed to understand the performance of concrete and bentonite cutoff seals (Chandler et al., 2002a, b).

The composite seal experiment (CSE) (Martino et al. 2003) was installed at the 420 m level of the URL in a 6 m deep and 1.24 m diameter borehole (Fig. 2.13). The cutoff seal consisted of a 0.3-m-thick highly compacted bentonite-sand mixture (70% bentonite and 30% sand), overlain by a low-heat high-performance concrete. A layer of compacted, non-swelling backfill was placed between concrete and bentonite/sand mixture. To stop clay from moving towards the backfill, a layer of geotextile was also laced between them. Underlying all these components the remaining

1 m of the borehole was filled with sand to be used as a hydraulic pressurization chamber. The LHHPC concrete component was poured at the top of the clay block without any reinforcement. The concrete cutoff seal relies entirely on the contact strength between rock and concrete for mechanical support against the water pressure. Steel pins were keyed in the walls of the borehole to give mechanical support to the concrete in case the contact strength was not sufficient, and the concrete cutoff seal moves upward. The clay layer was found saturated after 1 year and the seepage rate was decreased from 0.0024 L/h to approximately 0.0015 L/h under a hydraulic pressure of 2.35 MPa. The seepage rate was decreased due to the hydration of clay and increased pressure between the clay-rock interface.

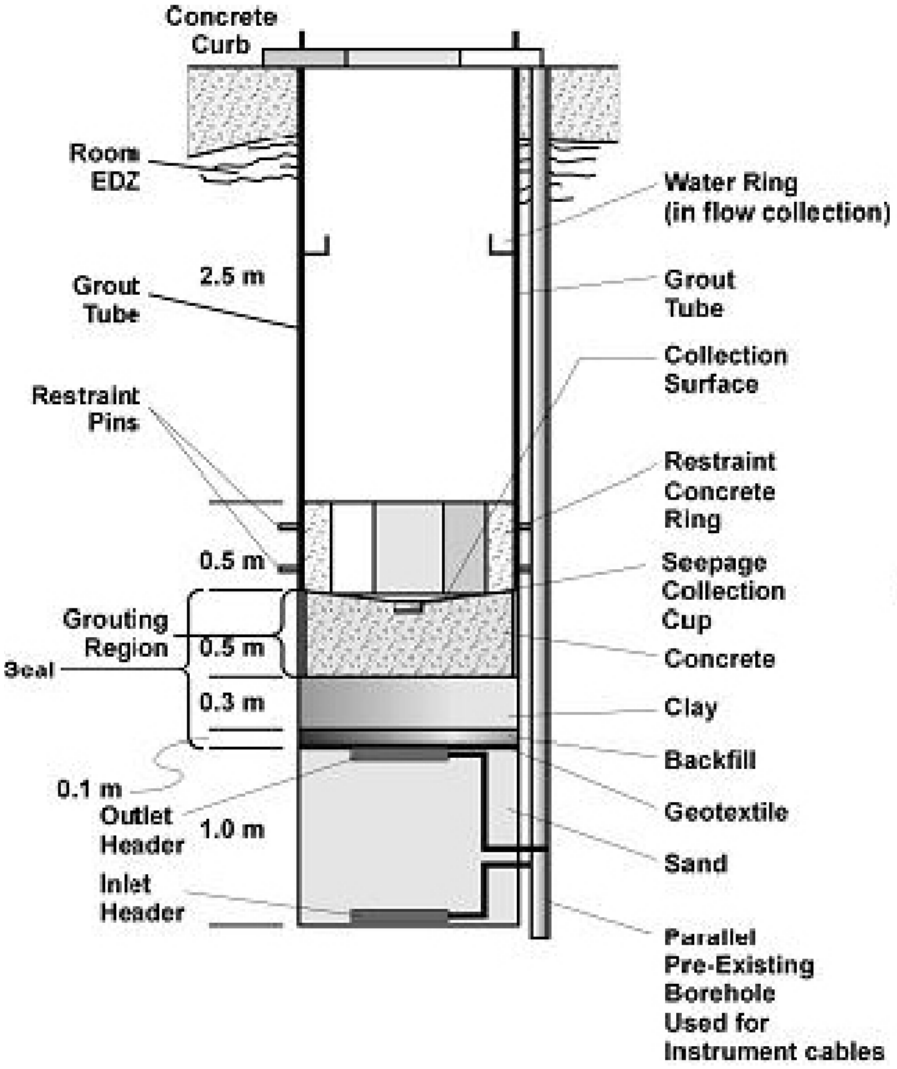

Fig. 2.13 Conceptual diagram for different components of the CSE (Martino et al., 2003).

2.3.3 DGR Perturbations on the Design of Cutoff Seal

Evolution of excavation damage zone around placement rooms and cutoffs will depend upon repository perturbations of different loading conditions such as used fuel container thermal history, glaciation, low probability strong ground motion earthquakes, and rock mass strength degradation with time.

The DGR at the depth between 500 to 1000 m would be affected by glaciation in terms of the increase in stress due to the weight of the ice sheet, increased frequency of earthquakes, and changes in the groundwater and geochemistry. Glaciation induced earthquakes will mainly occur along fault areas, locations of which should also be taken into consideration in the DGR site selection process (Frank, 2018). Although the seismic performance of DGR is better than the surface aboveground structures, however, given the long life of a repository and strict safety requirements it is important to consider the impacts of seismic events of different intensity on the long-term stability of the repository. The seismic analysis of any repository requires major steps such as determining the ground motion parameters at a certain depth and evaluating the complex dynamic interaction of containers with the multi-barrier environment. Kaláb et al. (2017) used the neo-deterministic method as an extension of the probabilistic method to evaluate seismicity and the impact of seismic effects on the Czech Republic's deep geological repository. The seismic wavefield excited by the particular seismic event and the corresponding maximum seismic load was evaluated. Radakovic-Guzina (2015) carried out a long-term stability analysis to evaluate rock mass damage for the proposed Canadian DGR under a seismic load of 0.5g for a long-term return period (1 million years) earthquake. Radakovic-Guzina (2015) also considered a load of 3 m thick ice sheet on the repository model to simulate the effect of future glaciation.

The time-dependent strength degradation of rock depends on stress intensity, chemical environment, temperature, and microstructure (Tuokko, 1990; Hagros et al., 2008). Eloranta et al. (1992) observed that the time-dependent effects on good quality rocks were insignificant, however, in DGRs, looking at the long time-scale and complex thermo-hydro-mechanical-chemical environment, these effects may be significant. The effect of strength degradation on rock mass damage can be analyzed by considering the crack initiation stress as the long-term strength of the

rock mass for design considerations (Damjanac and Fairhurst, 2010; Itasca 2011; Nickiar and Martin, 2013).

One important aspect of DGR design consideration is heat generated from the spent nuclear fuel. The Canadian DGR is designed to have a maximum temperature of 100 ^{o}C at the surface of spent fuel canisters (Guo, 2017). The heat from fuel will affect the mechanical behaviour of rock (Ranjith et al., 2012). For instance, the expansion of both rock and pore water will induce additional tensile stresses in the host rock mass. The thermal expansion in the rock will also change the existing hydraulic gradients in the rock mass, which will eventually affect the quantity and direction of flow of water altering the advective transport of water-borne radionuclides (Dixon et al., 2002). The performance of the engineered barrier is also dependent on the temperature of the canister. The heat from the spent fuel changes the moisture content in the sealing material, which causes a change in thermal parameters. Researchers have carried out physical and numerical modelling to analyze the effect of temperature on moisture migration and buffer drying (Dixon et al., 2002; Gens et al., 2002; Hökmark et al., 2007; Guo, 2011). The thermal load from the spent fuel canister also influences the rate of canister corrosion (King, 2013). Both three-dimensional and two-dimensional analyses were carried out to quantify thermo-hydro-mechanical behaviour of DGR at far- and near-field scales (Mathers, 1985; Tsui and Tsai, 1985; Baumgartner et al., 1994; Park et al., 2000; Hökmark et al., 2010; Guo, 2017). SKB carried out the Äspö pillar stability experiment (ASPE) to determine the effect of induced thermo-mechanical stress on the excavation damage zone both at the micro- and macro-scopic levels. Blaheta et al. (2013) analyzed the effect of temperature and confining stress on damage in the pillar, and was able to predict the location of damage zones. Rinne et al. 2013 simulated the temperature evolution in the pillar and showed the fracture propagation in the pillar due to thermo-mechanical stress using FRACOD. Koyama et al. (2013) used particle flow code to simulate the crack propagation in the pillar during the excavation, pressurizing, and heating process. It is evident from these studies that heat from nuclear fuel can influence the excavation damage zones and eventually affect the performance of cutoff seals.

2.4 Research Gap

The detailed literature review showed that extensive research had been carried out to understand the performance and EDZs for seals in underground nuclear waste repositories using experimental investigation. It is evident from these experiments that the seals are keyed into the surrounding rock mass to cut off the EDZ. However, the methodology to determine the depth of the keyed part of the seals is not clearly defined. The depth of the keyed part of the seals depends on the depth of the EDZi where connected fractures are present. It is difficult to determine the EDZi depth in the field due to the gradual transition between different excavation damage zones. Therefore, numerical modelling can be an important tool to determine the depth of the EDZi and the depth of the keyed portion of the cutoff seal.

The review of literature also showed that although extensive research had been carried out to understand the performance and EDZs for cutoff seals for underground nuclear waste repositories using experimental investigations. These tests are site-specific, and experiences from these projects can not be transferred to other DGR sites where geological conditions vary from site to site. Therefore, numerical modelling can be an important tool to understand the generic performance and EDZs for the cutoff located in different geological settings. While few researchers such as Perras et al. (2015), Holt (2016), and Yuan et al. (2017) have numerically simulated the mechanical behaviour of a particular shape and dimension of the cutoff located in a specific rock type, this study uses numerical modelling to develop a generic methodology for evaluating EDZi and EDZo for the cutoffs with different shape and dimensions located in different geological settings. Perras et al. (2015) used a continuum model to predict the depth of a thin slot cutoff based on the depth of EDZi. Based on similar guidelines, in this study, a continuum numerical model is used to determine depths of different shapes of cutoffs viz. triangular, rectangular, and trapezoid based on the depth of EDZi.

Furthermore, the literature review showed that researchers, for example, Guo (2017) used near field and far field thermal numerical models to understand the thermal behaviour of the repository. However, there is a scarcity of numerical modelling studies for the thermo-mechanical behaviour of the cutoff. Therefore, numerical modelling can be an important tool to determine the depth of

the EDZs and the optimum dimension and shape of the cutoff seals under the influence of heat from nuclear fuel. A conceptual 3-dimensional thermo-mechanical finite difference model is developed to analyze the potential response of the optimum cutoff geometry under hypothetical repository conditions. The effect of the temperature of the spent nuclear fuel on the optimum shape and the dimensions of the cutoff is also investigated.

Chapter 3: Methodology

3.1 Introduction

This chapter describes the methodology used to study the mechanical and thermo-mechanical response of the cutoff. A continuum model, based on the finite difference method using FLAC3D was used to simulate the mechanical and thermo-mechanical response of the cutoff. The backfill material was considered for the thermal model while for the mechanical model the placement room and cutoff were considered empty. The finite element method software COMSOL (COMSOL, 2015) was used to simulate the thermal response of the cutoff.

In the first step, FLAC3D was used to simulate the mechanical behaviour of a circular shaped room under different geological settings. The depth of the room varied in order to have stress to strength ratios that cover the typical range a repository might be constructed under. The dimensions of EDZs for a circular placement room located at different depths were determined using the mechanical numerical model.

In the second step of the study, based on the dimensions of EDZs from the first step, rectangular, triangular, and trapezoidal shape cutoffs were constructed for the circular placement room. The depth of the cutoff was kept equal to the dimension of EDZi as this zone can be a potential flow path for radionuclides due to the presence of connected micro-fractures. A parametric study was carried out to optimize the dimension of the cutoff by using the criterion that the cutoff should induce a minimal increase in the pre-existing EDZi after the construction of the cutoff. Furthermore, the effect of different variants such as shape and orientation of the room, rock mass properties, rock mass anisotropy on the extent of EDZi was analyzed.

In the third stage of the study, a finite element thermal model was used to determine the maximum temperature in the rock mass surrounding the cutoff. In addition, a 3-dimensional thermo-mechanical finite difference model was used to analyze the potential response of the optimum cutoff geometry under the heat load in hypothetical repository conditions. The effect of heat from the spent nuclear fuel on the EDZo and EDZi for the optimum cutoff was analyzed.

3.2 Model Setup

The Fast Lagrangian Analysis of Continua (FLAC 3D), a software developed by the Itasca consulting group, Inc. (Itas42ca, 2012) was used to analyze the extent of EDZi and EDZo for the placement room and cutoff. FLAC3D is based on the finite difference numerical method. In addition, the finite element software, COMSOL was also used to understand the thermal behaviour of the cutoff. The flow chart with different tasks to be carried out in order to achieve the objectives is shown in Fig. 3.1.

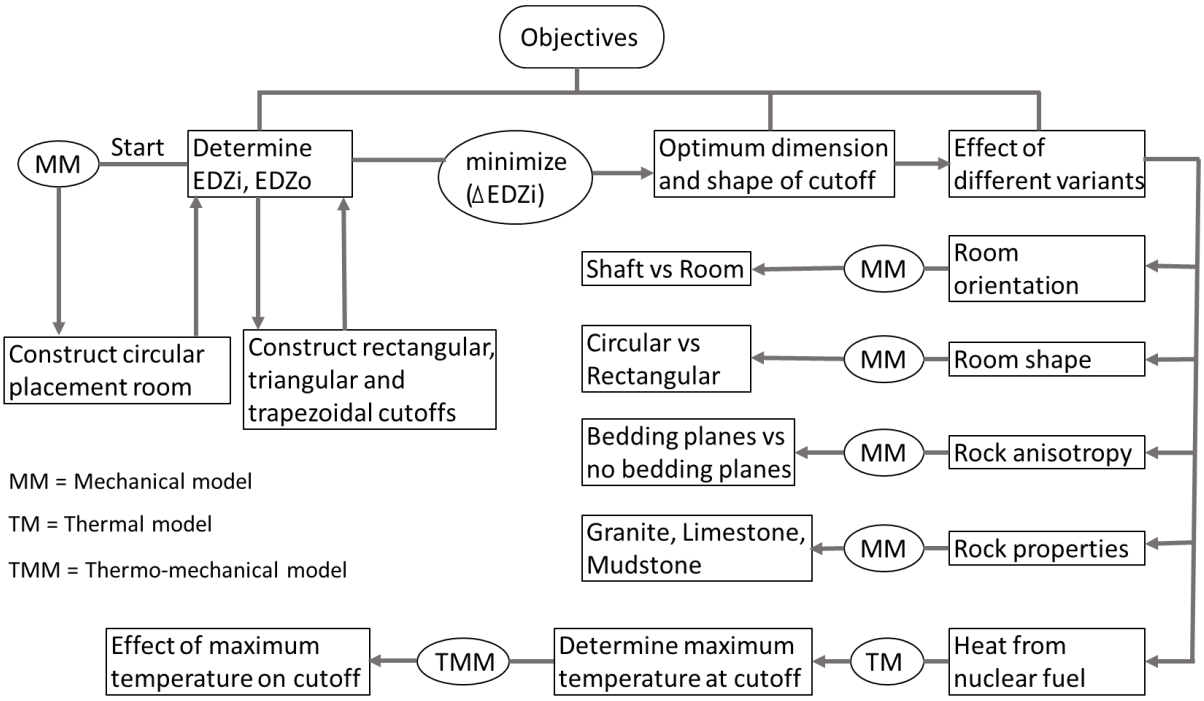

Fig. 3.1 The flow chart with different tasks carried out in order to achieve the objectives. Here ΔEDZi is the change in EDZi before and after the construction of the cutoff.

In general, the FLAC 3D software discretizes the continuous media into polyhedral elements using a three-dimensional grid to fit the modeled geometry. The equations of motions are then solved at the nodes of the grid to calculate displacement and velocities from the initially given stresses and displacements. New strain rates are derived from these calculated nodal velocities. Constitutive equations are then used to calculate new stresses from the strain rates and stresses at the previous time step. The equations of motion are again invoked to derive the new nodal velocities and displacements from the new stresses and forces. One calculation loop is completed in a single time

step and the loop is repeated at every time step. The maximum out of balance force for the given model is monitored. The force value either will become zero, indicating that the model has reached equilibrium or it will become constant, indicating that a portion (or all) of the model is at steady state (plastic) flow of material. The explicit, Lagrangian calculation scheme and the mixed-discretization zoning technique are used in FLAC3D to ensure that plastic collapse and flow were modeled very accurately.

In past, researchers such as (Hajiabdolmajid et al., 2002; Hajiabdolmajid et al., 2003; Walton, 2019) used FLAC3D to predict the depth of failure around underground openings in brittle rocks. The command-driven interface in the software and the FISH scripting language give the flexibility to modify the conventional constitutive models such as Mohr coulomb failure criteria to model the complex rock failure process.

3.2.1 Mechanical Model

A 3D Finite Difference numerical model was adopted to simulate the excavation of a circular and rectangular room with 1 m radius, and 1 m height and width respectively as shown in Fig. 3.2. Excavation of the drift was carried out in 12 stages with each 1 m excavation stage implemented in the model to determine the stress distribution with excavation advancement. The outer boundaries of the model were located 14 m away from the room surface. For the purpose of the mechanical model, a shotcrete liner was used in the excavated area to provide support for the room though it was not used inside the cutoff excavation. The liner was only used in the mechanical model; the thermo-mechanical model was simulated without the liner. This is because the mechanical modelling was a general modelling exercise to predict the EDZs and optimize the dimensions and shapes of cutoffs for underground excavations while the thermo-mechanical modelling exercise was to understand the thermo-mechanical behaviour of cutoff in underground nuclear waste repositories.

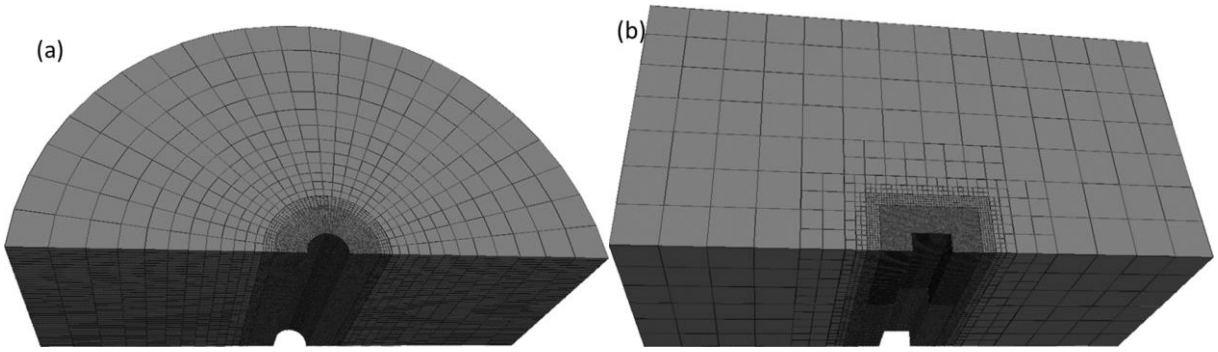

Fig. 3.2 (a) Circular excavation and (b) Rectangular excavation used in the numerical model.

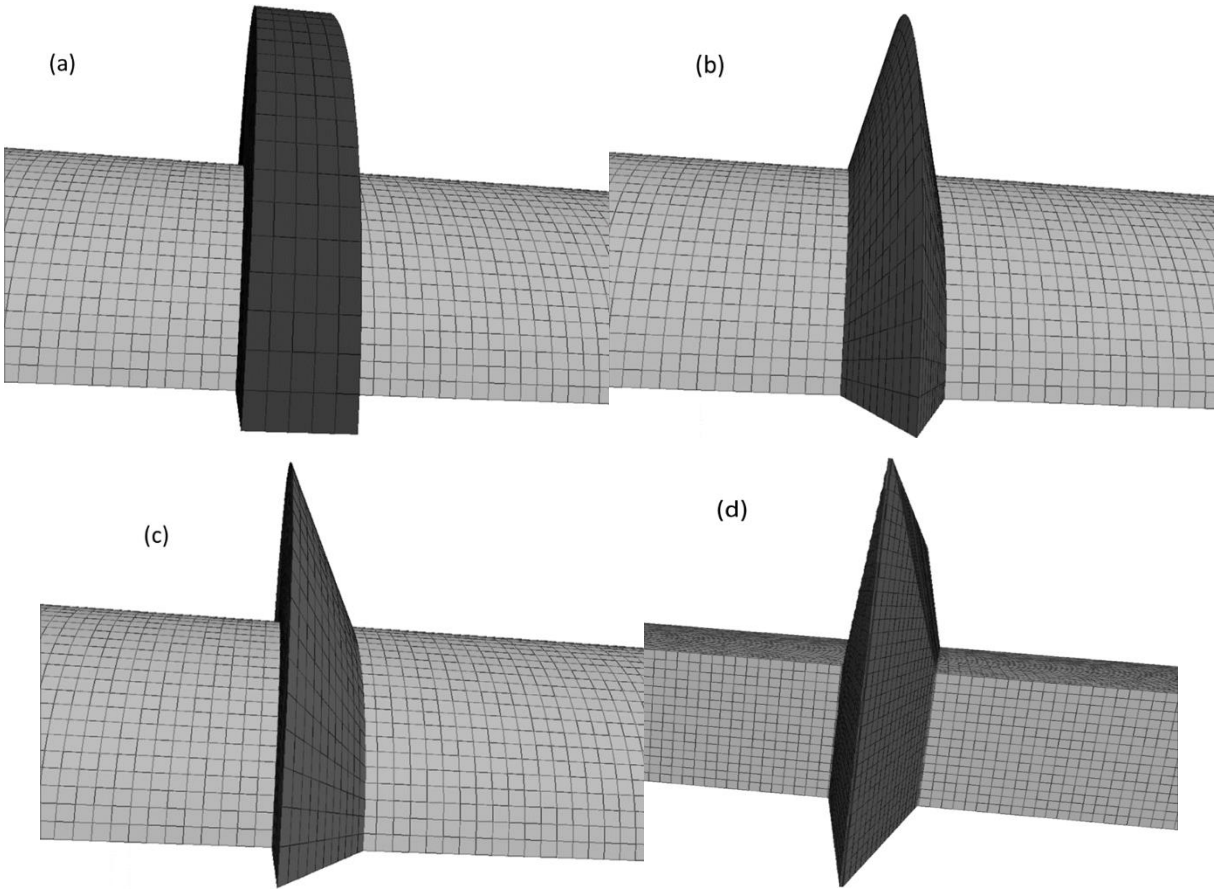

Fig. 3.3 (a) Rectangular cutoff with circular excavation (b) Triangular cutoff with circular excavation (c) Trapezoid cutoff with circular excavation (d) Trapezoid cutoff with rectangular excavation

First, the numerical model was solved to equilibrium for each stage of the excavation without the cutoff. The dimensions of EDZs were determined at this stage of the model for the circular room located in granite. Based on the depth of EDZi, different shapes and dimensions of the cutoffs were constructed around the circular room. A parametric study was conducted by solving the

numerical model with different types of cutoff geometries at different depths to study how their dimensions and shape can be optimized. Three different types of cutoff geometries (Fig. 3.3) were investigated - triangular, trapezoidal, and rectangular, to optimize the cutoff geometry aspect ratio for the circular room.After optimizing the dimension and shape of the cutoff, effects of different variants such as shape of the room, orientation of the room, influence of rock mass anisotropy, and properties of the rock mass were analyzed. To understand the effect of room-shape on the extent of EDZi for the optimum cutoff, the optimum shape and aspect ratio of the cutoff was used for the analysis of the cutoff for a rectangular shaped room. Similarly, to simulate the effect of other variants such as orientation of the room, influence of anisotropy, and properties of the rock mass, a circular room with cutoffs of the optimum shape and aspect ratio were used.

The effect of room orientation on the extent of EDZi and EDZo for the optimum cutoff was analyzed by simulating a vertical room (shaft). The influence of rock mass anisotropy on the extent of EDZi and EDZo for the optimum cutoff was analyzed by simulating horizontal bedding planes in limestone and mudstone. It should be noted that the horizontal bedding planes were considered in limestone and mudstone and not in granite as it is rare to see the bedding planes in granite in the real field scenario. Finally, to understand the effect of rock properties on the extent of EDZi and EDZo for the optimum cutoff, three rock mass types – granite, limestone, and mudstone were simulated.

3.2.2 Thermo-mechanical Model

Evolution of excavation damage zone around placement rooms and cutoffs will depend upon repository perturbations of different loading conditions such as used fuel container thermal history, glaciation, low probability strong ground motion earthquakes, and rock mass strength degradation with time. One important aspect of DGR design consideration is heat generated from the spent nuclear fuel.

Different panels of a conceptual repository in crystalline rock containing multiple rooms are shown in Fig. 3.4 (Noranha, 2016). The spacing between the adjacent rooms is 20 m and each room will contain 200 canisters along the length of the room. It is not possible to simulate all the canisters explicitly in the repository due to computational limitations. Guo (2017), and Radakovic-Guzina

et al. (2015) simulated the far field and near field response of the conceptual Canadian repository in sedimentary rock and crystalline rocks respectively. For the far field model, the repository was presented as a block of uniform material with a volume averaged heat source. Due to symmetry, only one-quarter of the repository was modelled. The two panels in the quarter of the repository were modeled as a 2 m thick plate-shaped heat source. The two meters represent the height of the two layers of buffer boxes. The assumption that the heat load is uniformly distributed throughout the repository panel in the far-field model does not simulate the temperature gradient between different components of the repository such as canister, backfill material, cutoff, and host rock. To understand the thermal response of canister, backfill material, and host rock, a near field model was also simulated by Guo (2017), and Radakovic-Guzina et al. (2015).

For the near field thermal model, the repository was assumed infinitely large and a unit cell – at the centre of the placement room (Fig. 3.4) of dimensions shown in Fig. 3.5 (a) was simulated. The near field model simulates the temperature gradients inside the panel along a cross-section perpendicular to the placement room (Y-direction, Fig. 3.4, Fig. 3.5 (a)). However, this model does not simulate the temperature gradient along the longitudinal direction (X-direction, Fig. 3.4, Fig. 3.5 (b)) of the placement room where cutoff will be located.

In order to simulate the temperature gradient between canister and cutoff, this study analyzed the maximum possible temperature at the cutoff in the longitudinal direction (X-direction, Fig. 3.4, Fig. 3.5 (b)) of the placement room by simulating multiple canisters in the room. The maximum temperature at the cutoff will occur when there will be 100 canisters (unit cell is located at the 100^{th} canister, Fig. 3.4) in the placement room because after the 100^{th} canister the cooling effect from the rock mass outside of the panel will be dominating. To analyze the effect of temperature on the optimum cutoff, the main purpose of thermal modelling was to create representative thermal history at the rock mass in the vicinity of cutoff by creating a thermal history similar to Radakovic-Guzina's near field model (Radakovic-Guzina et al., 2015) for the 100th canister located (at the unit cell, Fig. 3.4) at the middle of the placement room. This model will create a maximum temperature at the rock mass surrounding the cutoff and the thermal history from this model can be used to understand the effect of heat from nuclear fuel on the extent of EDZi and EDZo for the optimum cutoff.

To simulate the maximum possible temperature at the cutoff and the temperature gradient along the Y direction, a placement room scale model in COMSOL was used. For the placement room scale model, multiple canisters were simulated in the placement room. until the maximum temperature was achieved at the cutoff. The effect of the number of canisters in the room on the temperature at the cutoff was analyzed by simulating 10, 50, and 100 canisters in the placement room. The X and Z dimensions of the numerical model were 10 m and 2500 m, respectively (Fig. 3.5 (b)).

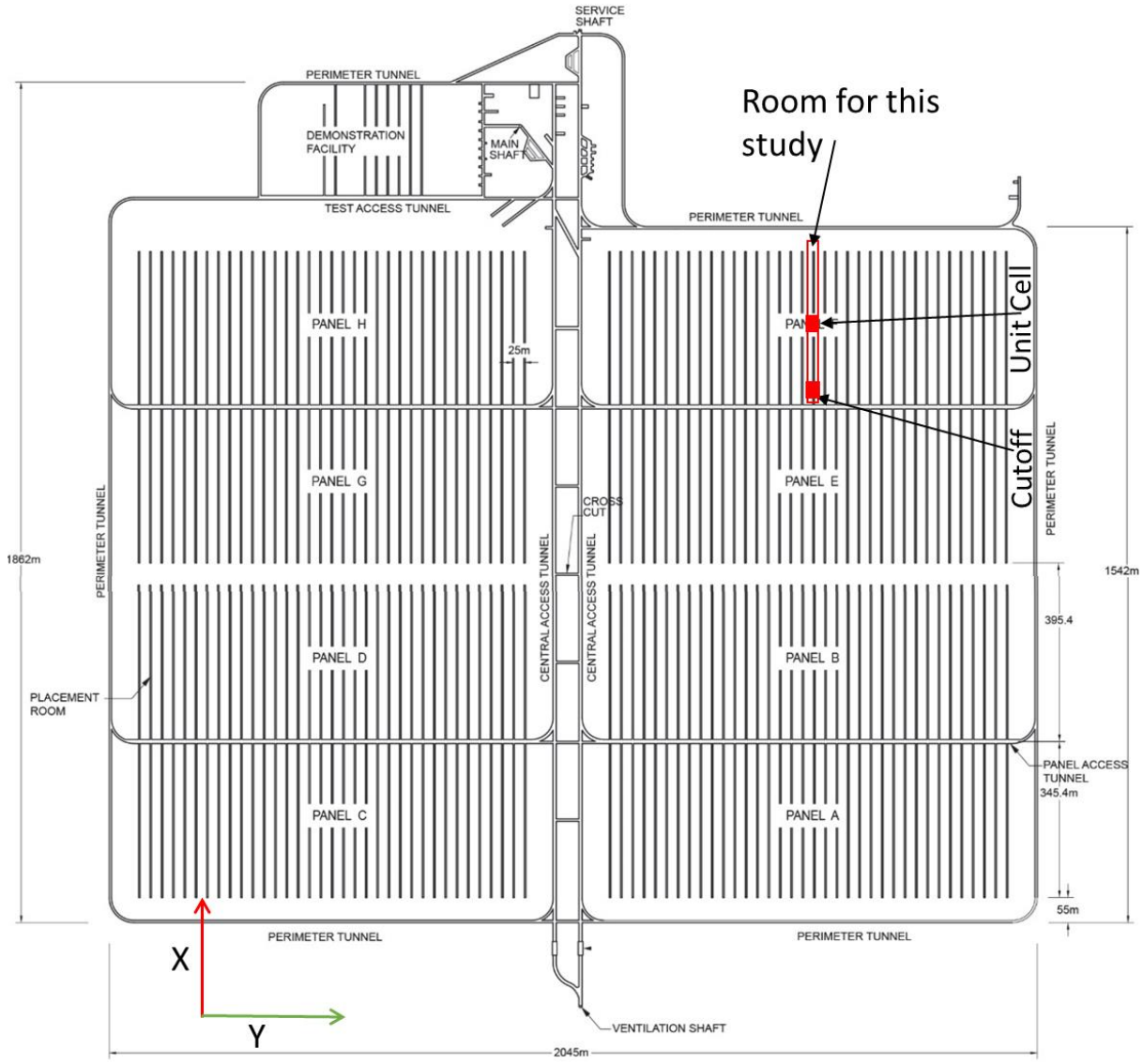

Fig. 3.4 Proposed layout for an underground nuclear waste repository in crystalline rock for 4.6 million spent nuclear bundles (modified after Radakovic-Guzina et al. (2015)).

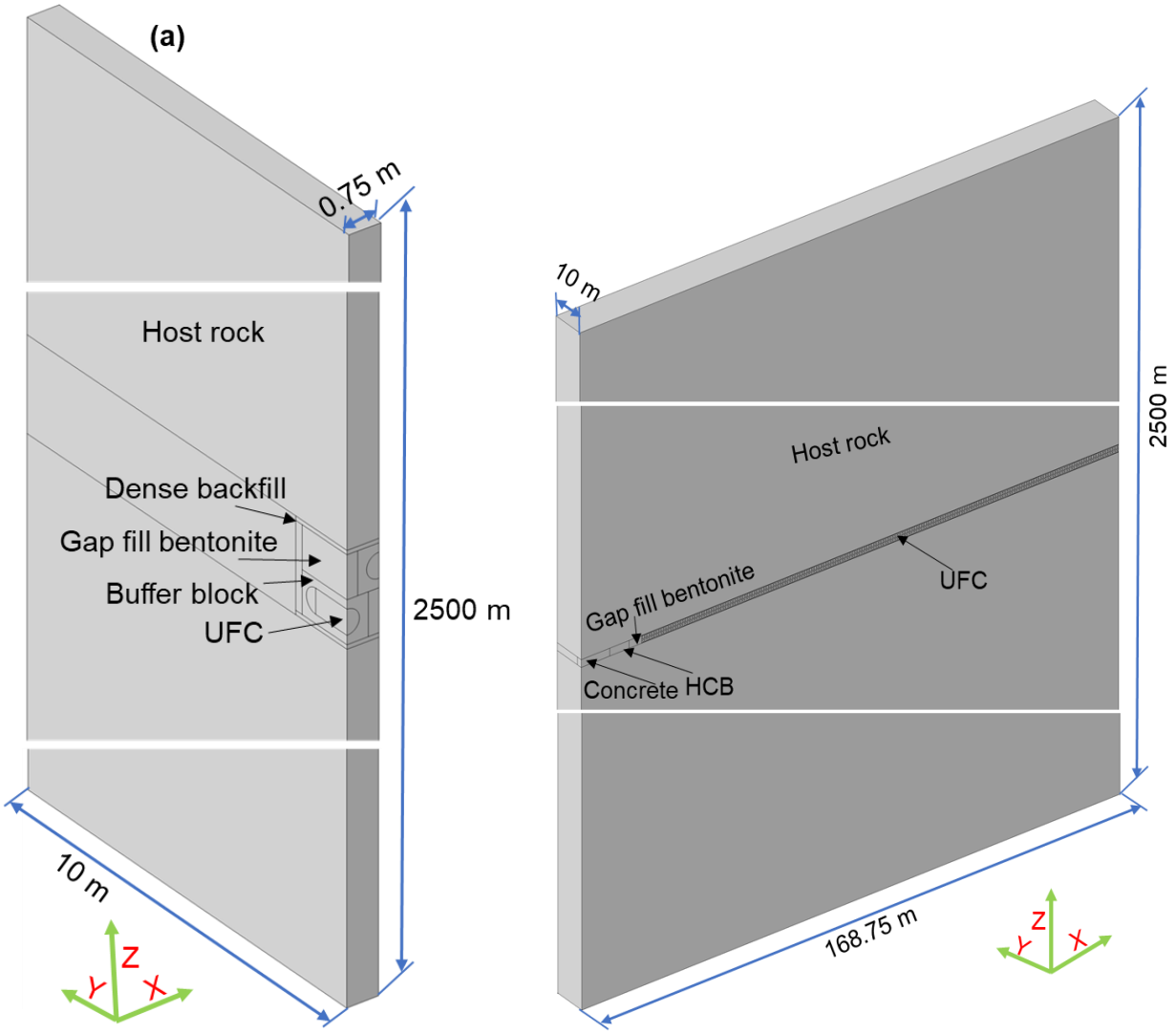

Fig. 3.5 (a) Near field thermal (unit cell) model for an infinite repository (b) thermal model with 100 canisters in the room used in this study. Both figures are not to scale.

The geometries used for the near field scale thermal model and placement room scale model are shown in Fig. 3.5. After determining the maximum temperature from the thermal analysis in COMSOL, FLAC3D was used to carry out the thermo-mechanical analysis of the extent of EDZi and EDZo for the cutoff. Due to the high computational time for the thermal model in FLAC3D, the maximum possible temperature at cutoff was determined using COMSOL using 100 canisters. Only 1.5 canisters were used in FLAC3D for the thermo-mechanical model, however, the power of each canister was increased to match the maximum temperature at the cutoff from the thermal modelling of 100 canisters from COMSOL. The variation of single canister power is shown in Fig.

3.6 (Guo, 2017). For the thermo-mechanical model in FLAC 3D, the repository was considered infinite in the X direction similar to Guo (2017) to generate the maximum possible temperature at the cutoff. In the Y direction, only 1.5 canisters with increased power were considered to minimize the computation time. Furthermore, to understand the variation of temperature with the canister power in FLAC3D, the power of a single canister was increased by 6, 12, 15, and 18 times to generate a range of thermal histories including the thermal history at the cutoff tip observed from the thermal model with 100 canisters in COMSOL.

For the thermo-mechanical model, a 3.2 m wide and 2.2 m high rectangular placement room with trapezoidal cutoff, located 500 m below the ground surface was numerically modeled using FLAC3D. The X, Y, and Z dimensions of the numerical model were 10 m, 20.25 m, and 1000 m, respectively as shown in Fig. 3.7. A simplified model containing 1.5 canisters and a single cutoff structure was considered. The canisters were modeled as enclosed in buffer blocks and the gap between them was filled with dense backfill. Initially, the model was solved without a cutoff excavation to determine the EDZi depth due to the room excavation and this depth was then used as the cutoff depth with an optimum aspect ratio for subsequent modelling. In a second step, a mechanical model with a cutoff was solved and this was followed by a coupled thermo-mechanical model to evaluate the effect of temperature on the cutoff.

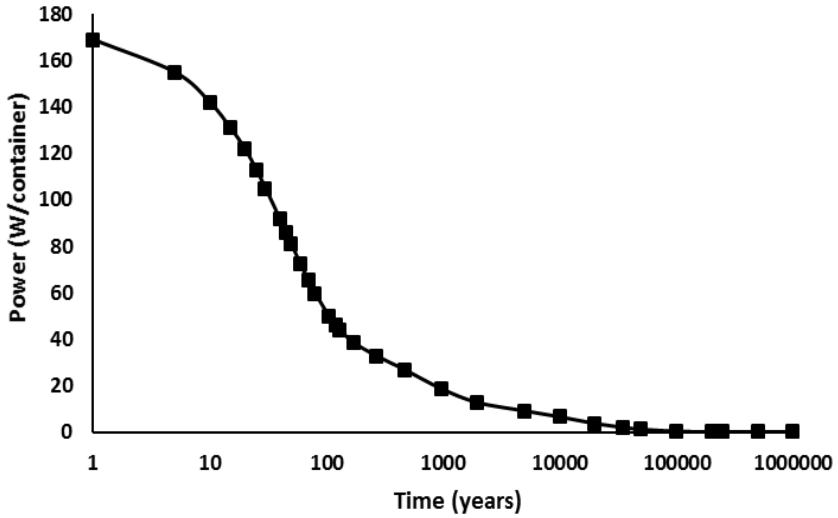

Fig. 3.6 Variation of single canister power with time (after, Guo (2017)).

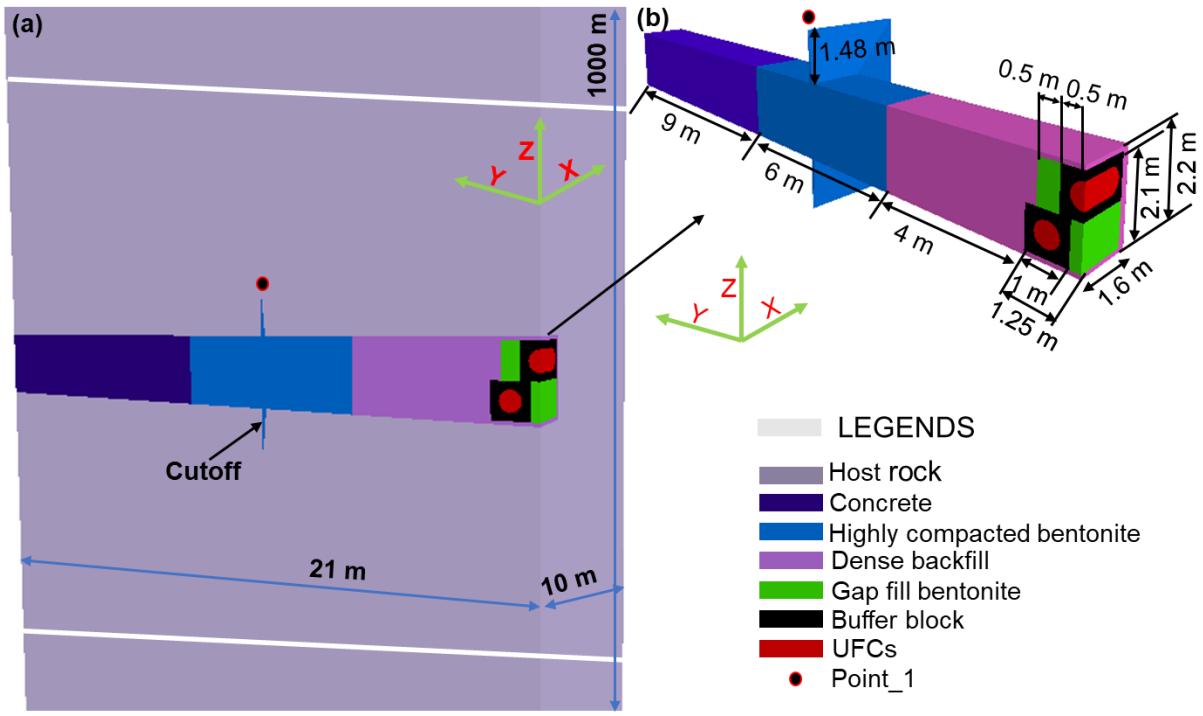

Fig. 3.7 Geometry of (a) room and host rock and (b) backfill material used in the numerical model to simulate the thermo-mechanical response of cutoff. Point_1 represents the temperature monitoring location. Backfill material was illustrated for the thermal model only and the room was considered empty for the mechanical model.

The thermal strains were evaluated after each time step of 2000 seconds. The coupling of the thermal and mechanical model was done at an interval of 1 year to enhance computational efficiency. Therefore, the mechanical model was solved to equilibrium after adding thermal strains at an interval of 1 year. Backfill material inside the placement room was only simulated for the thermal model, it was not included in the mechanical model. As explained before, it was computationally impractical to include all the canisters that would be in the proposed repository design into the numerical model at the scale being investigated. The variation of a single canister power (P) with time was taken from Guo (2017) but because of the difference in modelling strategies, the increased power approach was taken in the current work.

3.3 Constitutive Model

For brittle rocks, the evolution of strength during loading or excavation advancement was observed (by Martin and Chandler, 1994; Hajiabdolmajid et al., 2002; Hajiabdolmajid et al., 2003; Diederichs, 2003, 2007; Hoek and Brown, 1997) based on laboratory and field investigations of

hard rocks. It was concluded that the cohesion of rock decreases with inelastic strain due to the initiation and propagation of cracks. Initially, the friction angle increases with inelastic strain reaching a maximum value in the post-failure region and then becomes constant. Interestingly, the friction angle increases even after the maximum strength until a well-developed macroscopic failure surface was formed. The idea of cohesion loss and friction gain comes from the research by Schmertmann and Osterberg (1960) on soils. They suggested that there is a sequential mobilization of the friction angle, while there is a gain in cohesion reaching the maximum value and then a loss in the cohesion when the soil is sheared. The cohesion increases with strain reaching a maximum value, where almost negligible friction is present, and then decreases to become residual. A similar pattern was observed for friction which increases initially reaching a maximum value, and then reduces to a residual value (Schmertmann and Osterberg, 1960). These experiments were carried out on saturated clay with a high void ratio and strong plastic behaviour which may not be applied for the rocks with low void ratio and quasi-brittle behaviour. Martin and Chandler (1994) observed that cohesion is lost when friction is mobilized based on the assumption that the total strength of the rock mass varies little with rock fracturing damage. Later this approach was called cohesion weakening and friction strengthening (CWFS) and numerically used by Hajiabdolmajid et al. (2002). Diederichs (2003, 2007) proposed that brittle failure around an excavation can be simulated by a combined weakening-strengthening approach, similar to that of Hajiabdolmajid et al. (2002). This approach was designed to use in the software, especially finite element that did not allow the mobilization of peak and residual strength with inelastic strain.

It is important to simulate the correct evolution of stress and strength of the brittle rock mass as a result of excavation. Particularly, for the sedimentary and crystalline rocks being considered for HLW storage in Canada are hard rocks, which can be considered to behave in a brittle manner. The cutoff aspect ratio can be optimized by considering the strength of the rock mass as a function of damage. Many researchers (Martin and Chandler, 1994; Hajiabdolmajid et al., 2002; Hajiabdolmajid et al., 2003) incorporated the effect of damage to the failure criteria of commercially available software. For example, Hajiabdolmajid et al. (2002) implemented CWFS criteria by mobilizing cohesion and friction angle as a function of plastic strains in the numerical model.

The Mohr-Coulomb strain hardening/softening (MCSS) failure criteria in FLAC3D was chosen for numerical modelling in this thesis. The evolution of brittle rock mass strength was mathematically modeled by varying cohesion and friction angle with inelastic strain as suggested by Walton (2019). As shown in Fig. 3.8, the initial value of friction angle is very low (0 to 20 degrees) which indicates the behaviour of undamaged rock in low confinement conditions. The initial high value of cohesion indicates that there are fewer cracks in the rock. As the number of cracks initiates and propagate in the rock, cohesion decreases and becomes almost zero, representing the progressive failure of rock at the levels of damage (typically quantified as inelastic shear strain, e.g. γp or ε^{ps}) less than or equal to those at which the maximum (or mobilized) friction angle is attained (Fig. 3.8). The variation of cohesion and friction angle was approximated by a bi-linear curve, as suggested by Walton (2019), who based his recommendation on back analysis of calibrated models of various case studies. The peak and residual friction and cohesion were determined from the experience of the authors for strong granitic rock (Table 3.1). The mechanical properties of the rock, liner and bedding planes used in the model are given in Table 3.2 and Table 3.3.

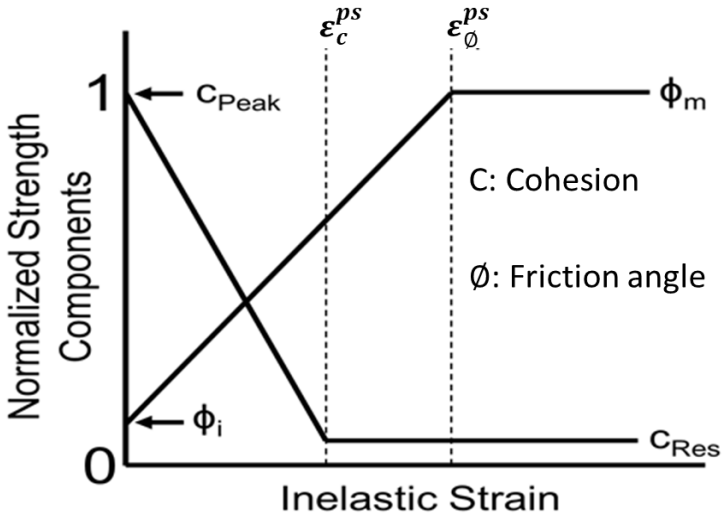

Fig. 3.8 Mathematical evolution of cohesion and friction angle with inelastic strain in cohesion weakening and friction strengthening approach (after Walton, 2019).

To understand the effect of rock mass anisotropy on the extent of EDZi and EDZo for the optimum cutoff, horizontal bedding planes were considered in the rock mass. The bilinear strain-hardening/softening ubiquitous joint model was used to describe the constitutive behaviour of rock

mass with horizontal bedding planes. In the bilinear model, the failure envelopes for the matrix and joint are the composite of two Mohr-Coulomb criteria with a tension cutoff that can harden or soften according to specified laws. A nonassociated flow rule is used for shear-plastic flow, and an associated flow rule is used for the tensile-plastic flow. The softening parameters for the matrix and the bedding planes are specified in tables in terms of four independent hardening parameters (two for the matrix and two for the bedding planes) that measure the amount of plastic shear and tensile strain, respectively. The values for hardening and softening parameters for the rock matrix and bedding planes are given in Table 3.1 and Table 3.4. In this failure criteria, failure is first detected for the matrix, and relevant plastic correction is applied. The new stresses after applying the plastic correction are used to detect the failure along the bedding planes and updated accordingly. The hardening parameters are incremented if the plastic flow has taken place, and the parameters of cohesion, friction, dilation, and tensile strength are adjusted for the matrix and the bedding planes using the tables.

Table 3.1 Data points to generate the CWFS, a bi-linear model used in the numerical simulation (Perras and Diederichs, 2016).

Rock type	Inelastic strain (millistrain)	Cohesion (MPa)	Friction angle (degree)	Tensile strength (MPa)
Granite	0	52	12	15.6
	2	4	33.5	0.1
	4	4	55	0.1
Limestone	0	15.5	15	6.5
	2	1.2	35.3	0.1
	3	1.2	50	0.1
Mudstone	0	7.2	20	4
	2	0.4	45	0.1

Table 3.2 Mechanical properties used in the mechanical study and thermo-mechanical study (Perras and Diederichs, 2016).

Mechanical Property	Granite	Limestone	Mudstone	Concrete liner
Density (kg/m^3)	2650	2660	2680	2000
Young's modulus (GPa)	75	40	17.4	10
Crack initiation stress (MPa)	128.4	17.4	20.6	NA
Poisson's ratio	0.2	0.25	0.3	0.2
Tensile strength (MPa)	15.6	6.5	4	NA
Uniaxial compressive strength (MPa)	246	101	48	NA

Table 3.3 Mechanical properties of bedding planes used in the mechanical study (Perras and Diederichs, 2016).

Mechanical Property	Bedding planes in Limestone	Bedding planes in Mudstone
Bedding planes dilation (degree)	5	5
Bedding planes tensile strength (MPa)	0.66	1.4

Table 3.4 Bedding plane data points to generate the CWFS, bi-linear model used in the numerical simulation (after Walton, 2019).

Rock type	Inelastic strain (millistrain)	Bedding cohesion (MPa)	Bedding friction angle (degree)	Bedding tensile strength (MPa)
Limestone	0	3.3	38	0.66
	3	0.01	30	0.1
Mudstone	0	6	20	1.4
	3	0.1	15	0.05

Table 3.5 Thermal properties used in the thermo-mechanical study (Radakovic-Guzina et al., 2015; Guo, 2017).

Thermal Property	Limestone	Highly compacted bentonite	Bentonite backfill pellets	Dense bentonite backfill	Container	Backfill concrete
Thermal conductivity (W/(m.K))	2.5	0.5	0.4	0.8	45	1
Specific heat (J/(kg.K))	845	1440	910	1110	434	880
Bulk density (kg/m^3)	2660	1880	1439	2120	5345	2400

Because the numerical dimensions of the different excavation damage zones, especially for EDZi, were determined based on the volumetric strain in the rock, accurate prediction of the numerical volumetric strain was vital. The volumetric strain in the post-failure region is highly dependent on the constitutive behaviour of the rock mass in the region. Studies have shown that due to the variation of dilation angle in the post-failure region, the volumetric strain is highly non-linear (Alejano and Alonso, 2005; Zhao and Cai, 2010; Walton and Diederichs, 2015a). Because of the complexity of including a varying value of dilation angle in FLAC3D, a constant dilation angle was evaluated using equation (1) from Walton and Diederichs (2015b). The dilation angle value obtained through this equation provided a close approximation to the more complex dilation models mentioned above in terms of overall rock displacement trends within the damage zone.

$$\frac{\psi}{\phi_m} = (\sigma_{crm}/\sigma_{e\_t}) - 0.1 \qquad (1)$$

Here σ_{crm} is the in-situ unconfined strength of the rock mass and σ_{e_t} is the maximum elastic tangential (compressive) stress expected along the excavation boundary.

To simulate heat transfer in the repository environment, Fourier's law of heat transfer for stationary, homogeneous, isotropic rock was used. Different components inside the placement room – highly compacted bentonite, gap fill bentonite, and concrete were considered homogenous,

isotropic, and non-porous for the thermal and thermo-mechanical model. The thermo-mechanical properties used in the mechanical model and thermo-mechanical model are given in Table 3.2 and Table 3.5. Thermal properties of the intact limestone were used for the rock, including when damaged, with a thermal expansion coefficient equal to 5.4E-06 1/K.

3.4 Initial Stress and Boundary Conditions

The mechanical model was a general modelling exercise to optimize the cutoff and it was not a real representation of any site for the underground nuclear waste repository. On the other hand, for the thermo-mechanical model, a representative room from the conceptual Canadian nuclear waste repository was considered to use the actual power of the canister. Different stress scenarios were considered for the mechanical model to understand the extent of EDZi and EDZo for cutoff with the in-situ stresses, while only one in-situ stress value was used for the thermo-mechanical model.

3.4.1 Mechanical Model

The numerical model was considered at different depths by using different values of σ_{max} in order to adjust the σ_{max}/CI ratio between 1 to 3 (Fig. 3.9), the latter was done to induce the brittle failure of the rock as suggested by Diederichs (2007), where σ_{max} is the maximum tangential stress at the excavation boundary and CI is the crack initiation stress. Initially, the numerical model was set up with 46 MPa principal stress in zz and xx direction and 69 MPa in the yy direction for a k ratio of 1.5 (horizontal (yy) to vertical (zz) stress ratio).

All the boundaries in the numerical model were fixed except for the excavation surface of the drift and cutoff. For the purpose of this study, a shotcrete liner was used in the excavated area to provide support for the drift, however, it was not considered for the thermo-mechanical model as it will not be present in the stable crystalline rock mass conditions in the actual repository conditions. This liner was not installed inside the cutoff excavation for both the thermal and thermo-mechanical models.

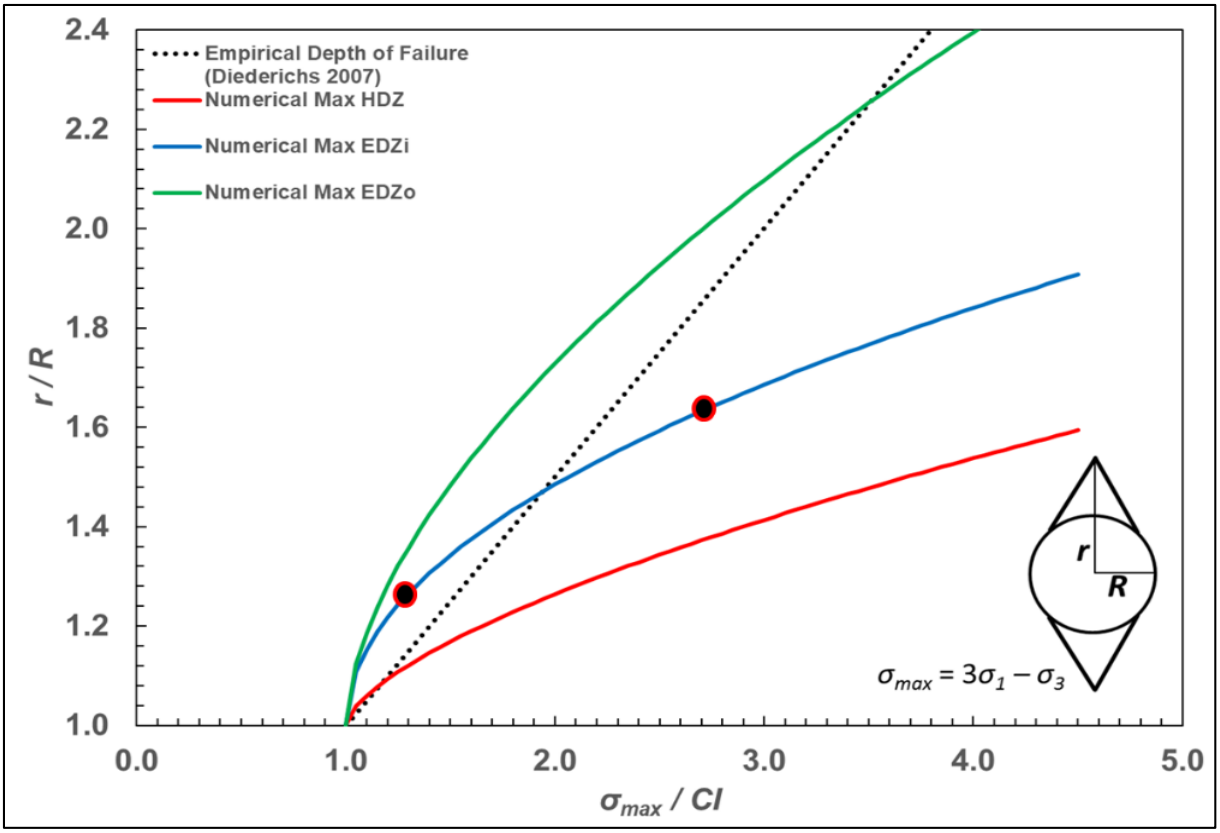

Fig. 3.9 Empirical and Numerical depths of EDZs (modified after Perras and Diederichs (2016)). The two dots in the figure show the range of σ_{max} to CI ratio used in this study.

3.4.2 Thermo-mechanical Model

For the thermo-mechanical model (Fig. 3.7), the conceptual repository was set at a depth of 500 m with 13.5, 23.1, and 40.5 MPa principal stresses in the zz, xx, and the yy directions, and a 0.027 MPa/m vertical stress gradient using a K ratio of 3 (horizontal (xx) to vertical (zz) stress ratio) and K_h ratio of 1.75 (horizontal (xx) to horizontal (yy) stress ratio). This value of K was selected to induce measurable EDZs and represents the worst-case scenario for a repository. The initial temperature in the model was set with a geothermal gradient of 0.012 ^{o}C/m considering a surface temperature of 5 ^{o}C, following Baumgartner et al. (1994).

Normal displacements along all the vertical boundaries except the excavation walls were set to zero. The bottom boundary of the model was fixed in all three directions while the top boundary, representing the ground surface was kept free. For heat transfer, the top and bottom boundary were considered isothermal with the top boundary set at 5 ^{o}C and the bottom boundary set at 17 ^{o}C in

accordance with the geothermal gradient. The vertical boundary passing through the center of two adjacent rooms represented a symmetry boundary between two rooms in an infinite repository and therefore was considered adiabatic. The vertical boundary passing through the center of the room also represented the symmetry boundary through the center of the room in an infinite repository and therefore was considered adiabatic. The vertical boundary perpendicular to the room axis and passing through the axis of the material handling drift is a symmetry boundary between two repository panels and considered adiabatic. The vertical boundary passing through the canister was also assumed adiabatic. Therefore, all the vertical boundaries were considered adiabatic while the top and bottom boundaries were considered isothermal.

3.5 Summary

The methodology used to understand the mechanical and thermo-mechanical response of a cutoff was described in this chapter. A continuum finite element method using COMSOL was used to understand the thermal behaviour of the cutoff. On the other hand, a continuum finite difference method using FLAC 3D was used to understand the mechanical and the coupled thermo-mechanical response of the cutoff.

The important aspects of mechanical and thermo-mechanical models were described here. The geometry of the model, model setup, constitutive models, and in-situ and boundary conditions used for the mechanical and thermo-mechanical model were described in the chapter. Furthermore, the steps to carry out a parametric study to optimize the shape and dimension of the cutoff was described. The results of the mechanical modelling are presented in chapter 4 while the results of thermo-mechanical modelling are presented in Chapter 5. For the model verification, the results of the mechanical model were compared with the past empirical and numerical modelling studies. Further the results of thermo-mechanical model were verified by comparing them with past numerical modelling studies, for instance, Guo (2017).

Chapter 4: Mechanical Modelling Results

4.1 Introduction

This chapter analyzes the results of mechanical modelling to understand the extent of EDZi and EDZo for the cutoff. Dimensions of EDZs were determined for a circular room located at different depths in the granite rock mass. Based on the dimensions of the EDZi, rectangular, triangular, and trapezoid cutoffs were constructed. Dimensions of EDZi after the construction of the cutoff were determined to analyze the effect of cutoff construction on EDZi.

A parametric study was conducted to analyze the extent of EDZi and EDZo for different shapes and dimensions of the cutoff under different stress conditions. The cutoff shape and dimension were optimized based on the criteria that the construction of the cutoff should induce a minimum increase in the pre-existing EDZi.

After optimizing the cutoff, the next step was to study the effects of different variants on the extent of EDZi and EDZo for the cutoff. Different variants such as shape and orientation of the placement room, rock mass properties, and rock mass anisotropy were considered to analyze the extent of EDZi and EDZo for the optimum cutoff under different scenarios.

4.2 Mechanical Modelling Results and Discussion

The yielded elements and volumetric strain around a room with a rectangular cutoff at the equilibrium state of the numerical model are shown in Fig. 4.1. Numerically, yielded elements indicate the plastic yield region, and these elements have lost some cohesion and gained frictional strength. Practically speaking, the rock mass in the region of plastic yielding is damaged due to connected and unconnected macro and microfractures (Diederichs, 2003, 2007). The zone beyond the plastic yield region is in an inelastic state (EIZ). The plastic zone is comprised of EDZi and EDZo (Fig. 4.1). The maximum extent of the plastic zone is the outer limit of EDZo. The black iso-line in Fig. 4.1 shows the boundary between EDZi and EDZo. It can be observed that the iso-line has shifted away from the excavation surface right above the cutoff. This shift in iso-line is due to the construction of the cutoff which increases the pre-existing EDZi before the construction of cutoff.

The volumetric strain is positive near the cutoff boundary and it increases away from the boundary becoming zero at a certain distance away from the cutoff tip (Fig. 4.1). Perras and Diederichs (2016) suggested that this transition should be considered the EDZi to EDZo transition boundary. In FLAC3D, positive volumetric strain represents a volumetric expansion of the rock mass and negative volumetric strain represents volumetric contraction. Physically, this behaviour in a rock mass can be understood using the analogous behaviour of rock under tri-axial test conditions. Under low confinement triaxial loading, pre-existing cracks close and new cracks initiate parallel to maximum principal stress, which causes an increase in volumetric strain. When tensile cracks start interacting with each other, there is a rapid increase in radial strain and this, in turn, causes a decrease in the volumetric strain. Similarly, around the room under low confinement conditions, tensile cracks interact with each other, causing large extensional strains.

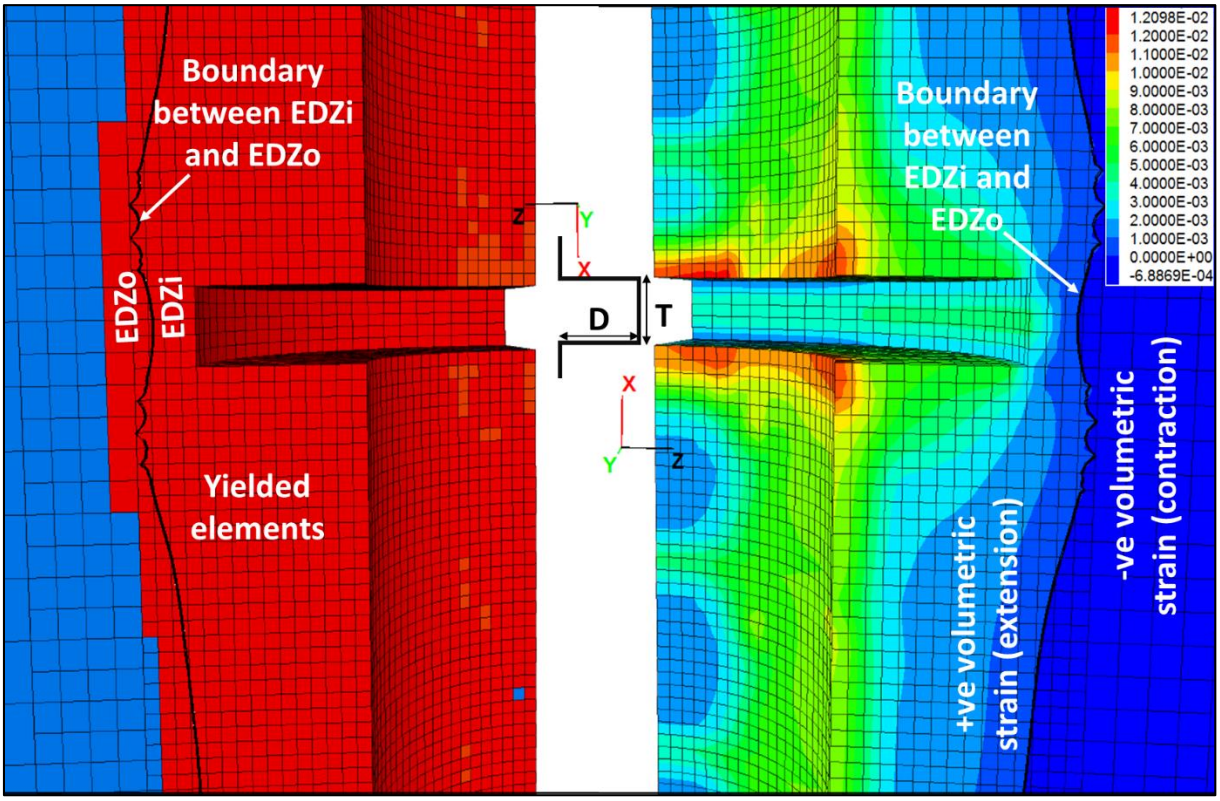

Fig. 4.1 Different excavation damage zones interpreted from volumetric strain and yielded elements (Sharma et al., 2019).

The contours of volumetric strain around the cutoff, with the extent of EDZi 1.91 m and EDZo 2.12 m for the triangular shaped cutoff with an aspect ratio of 1:2 are shown in Fig. 4.2. Moving

out beyond the EDZi zone into EDZo, the volumetric strain becomes negative and indicates volumetric contraction. With the CWFS constitutive model, plastic yielding can still occur under negative volumetric strain (contraction). This represents cracks forming under high confining stress, similar to a volume of rock away from the excavation surface. This confinement limits crack growth, thereby limiting crack interactions. This has been shown by Hoek (1965) for tests under triaxial loading where equilibrium crack lengths at a given compressive load are smaller under confinement. Similarly, in the field, the zones in which volumetric strain is negative in the model, may not have connected fractures and therefore smaller tensile strains. The extent of the EDZi and EDZo are increased by 0.18 m and 0.33 m, respectively, from the pre-cutoff dimensions for the triangular shaped cutoff with an aspect ratio of 1:2.

The contours of volumetric strain around the excavation of the trapezoidal shaped cutoff are shown in Fig. 4.3. The extent of the EDZi and EDZo is 1.78 m and 2.00 m, respectively, for the trapezoidal shaped cutoff with an aspect ratio of 1:2. The extent of the EDZi and EDZo is increased by 0.05 m and 0.21 m, respectively, after the cutoff construction.

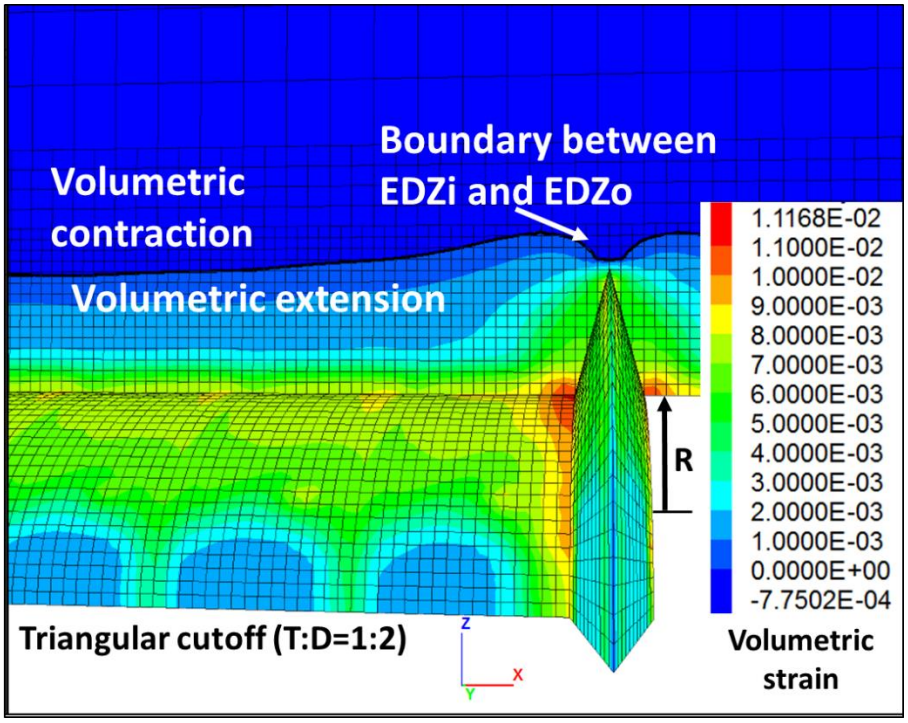

Fig. 4.2 The EDZi to EDZo transition around a triangular shaped cutoff.

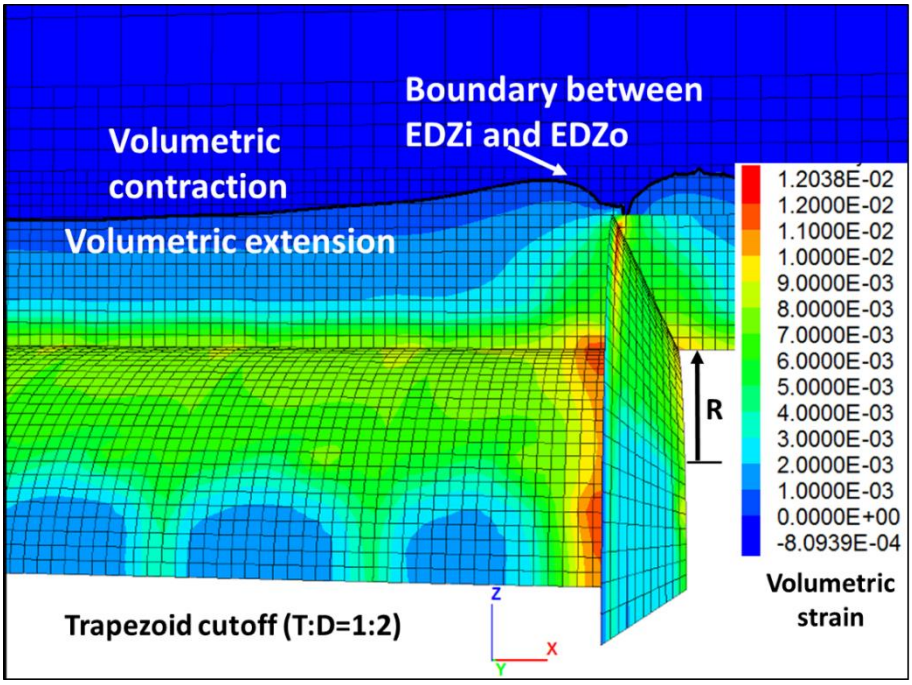

Fig. 4.3 The EDZi to EDZo transition around a trapezoidal shaped cutoff.

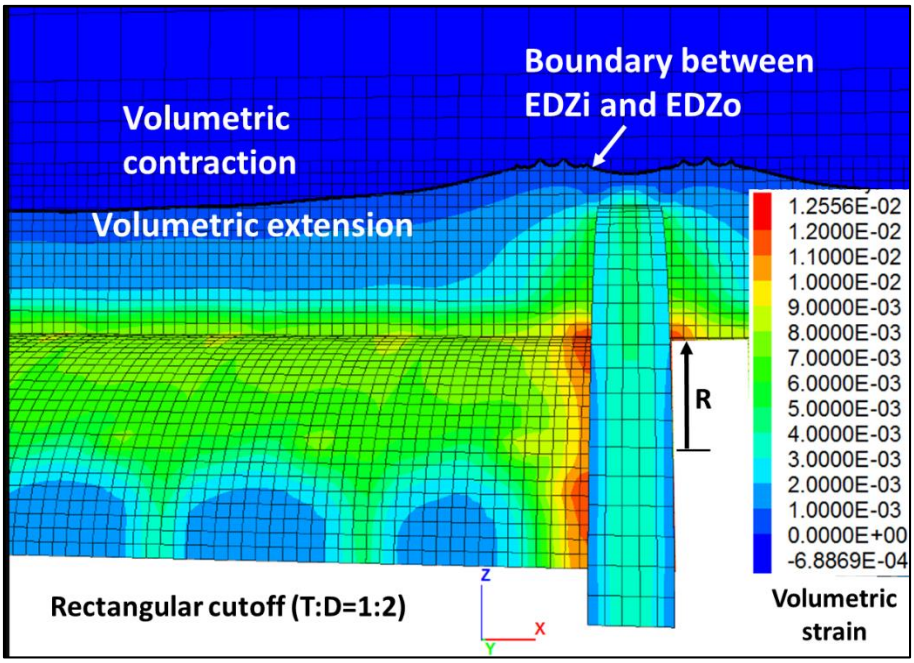

Fig. 4.4 The EDZi to EDZo transition around a rectangular shaped cutoff.

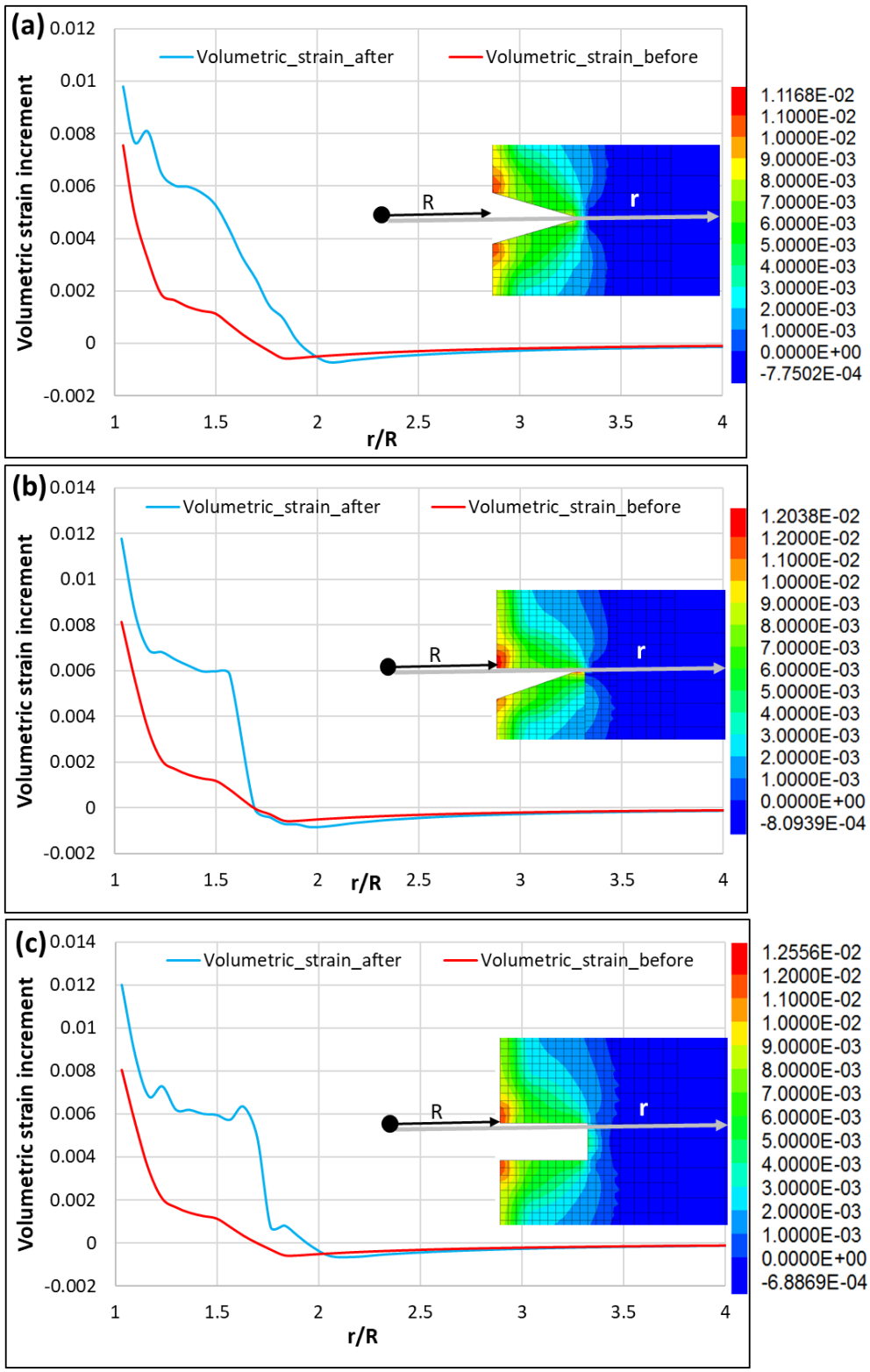

Fig. 4.5 Extent of rock mass dilation before and after the construction of (a) triangular, (b) trapezoid, and (c) rectangular cutoff.

The contours of volumetric strain around the rectangular cutoff are shown in Fig. 4.4. The extent of the EDZi and EDZo are 1.94 m and 2.12 m, respectively, for the rectangular shaped cutoff with an aspect ratio of 1:2. The extent of the EDZi and EDZo increased by 0.21 m and 0.33 m, respectively, after the cutoff construction.

The variation of rock mass dilation around the room before and after the construction of the cutoff is shown in Fig. 4.5 (a), (b), and (c). For a thickness to depth ratio of 0.5 for the trapezoid, triangle, and rectangular cutoff, the dilation has increased significantly. A maximum increase in dilation is observed for the rectangular cutoff followed by the triangular and finally the trapezoid cutoff. The trapezoid cutoff results showed that the depth of transition from extensile to compressional strain for the pre- and post- construction of the cutoff remains minimum as compared to the rectangular and triangular cutoff.

4.3 The Optimum Cutoff

The cutoff dimension was optimized by ensuring minimum or zero extension in the pre-existing numerical EDZi when the cutoff was constructed. The numerical results of the parametric study for different inner excavation damage zone dimensions for different shapes of cutoff are shown in Fig. 4.6 (a), (b), (c). The in-situ stress ratio and cutoff depth to width ratio were varied to optimize the cutoff dimensions. The variation of normalized change in EDZi before and after the construction of the cutoff for different aspects and σ_{max}/CI ratios was analyzed. The results of the parametric study for the rectangular, triangular, and trapezoidal cutoffs are shown in Fig. 4.6 (a), (b), and (c) respectively. It can be observed that with an increase in the aspect ratio and the σ_{max}/CI ratio, the extent of the normalized ΔEDZi increased. For each shape of cutoff, the increase in EDZi after construction is minimum for low aspect and low σ_{max}/CI ratios. The trapezoidal shaped cutoff with a low aspect ratio (0.2) caused the smallest increase in pre-existing numerical EDZi when compared to the triangular and rectangular shaped cutoffs and therefore was selected as the optimum.

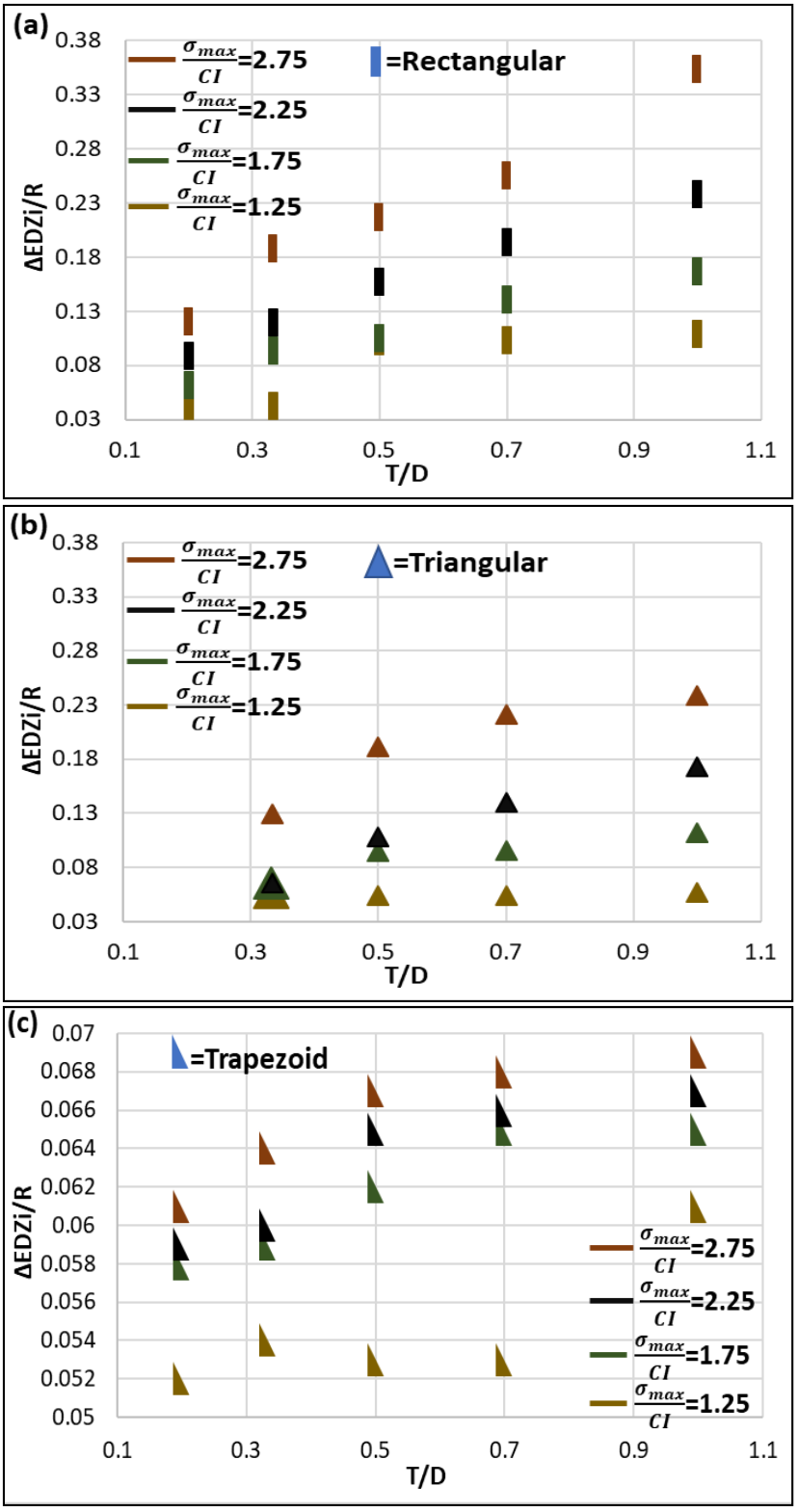

Fig. 4.6 Normalized extent of ΔEDZi with T/D ratios and σ_max/CI ratios for (a) rectangular cutoff (b) triangular cutoff and (c) trapezoid cutoff

4.4 Effect of Different Variants on the Cutoff

After optimizing the cutoff, the effect of different variants such as orientation and shape of the room, rock mass properties, and rock mass anisotropy on the extent of EDZi and EDZo for the optimum cutoff was analyzed. First, to analyze the effect of room orientation, a cutoff for a vertically oriented room (circular shaft) of radius 1 m was constructed with the shape and aspect ratio of the cutoff similar to that of the optimum cutoff. Second, to analyze the effect of rock mass properties, a cutoff for circular placement room located in different rock types was constructed with aspect ratio and shape similar to the optimum cutoff. Third, to analyze the effect of rock mass anisotropy, the cutoff located in rock mass with horizontal bedding planes, and with shape and aspect ratio similar to the optimum cutoff was constructed. And fourth, to analyze the effect of room shape, a cutoff for a rectangular placement room was constructed with a shape and aspect ratio similar to the optimum cutoff.

4.4.1 Comparison between Cutoff for Shaft and Room

To simulate the cutoff for the shaft, the direction of the gravity in the base numerical model was changed to horizontal. The model with a trapezoid cutoff of aspect ratio 0.2 for circular placement room was considered the base model. Also, the major horizontal stress was changed to vertical stress while the vertical stress was changed to major horizontal stress in the base numerical model. The contour of volumetric strain for the optimum shaft-cutoff is shown in Fig. 4.7 (a). The black iso-line shows the boundary between the EDZi and EDZo. The zone with positive volumetric strain represents the volumetric extension while the zone with negative volumetric strain shows volumetric contraction. The magnitude of EDZi before the construction of the cutoff for the shaft is 1.70 m and the magnitude of EDZo is 1.73 m. The magnitudes of EDZi after the construction of the cutoff is 1.78 m and the magnitude of the EDZo is 2.00 m. The extent of EDZi for the optimum cutoff depends on the in-situ stress condition. For the given stress condition for this thesis, the extent of EDZi before and after the construction of the cutoff with optimum shape and dimension is approximately the same for the shaft and the horizontal placement room.

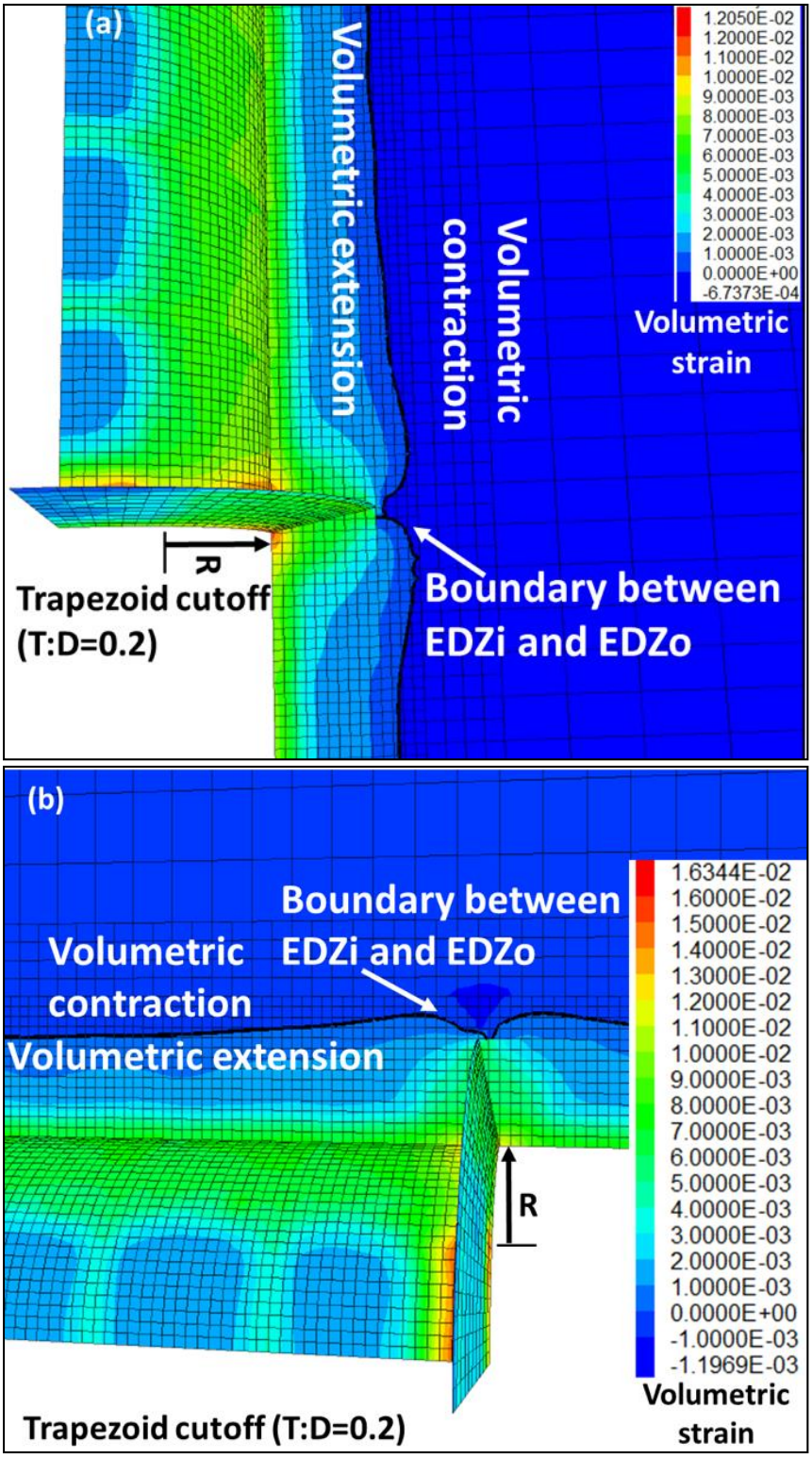

Fig. 4.7 Contours of volumetric strain, and the boundary between EDZi and EDZo for a trapezoid shape cutoff for (a) circular shaft and (b) circular room.

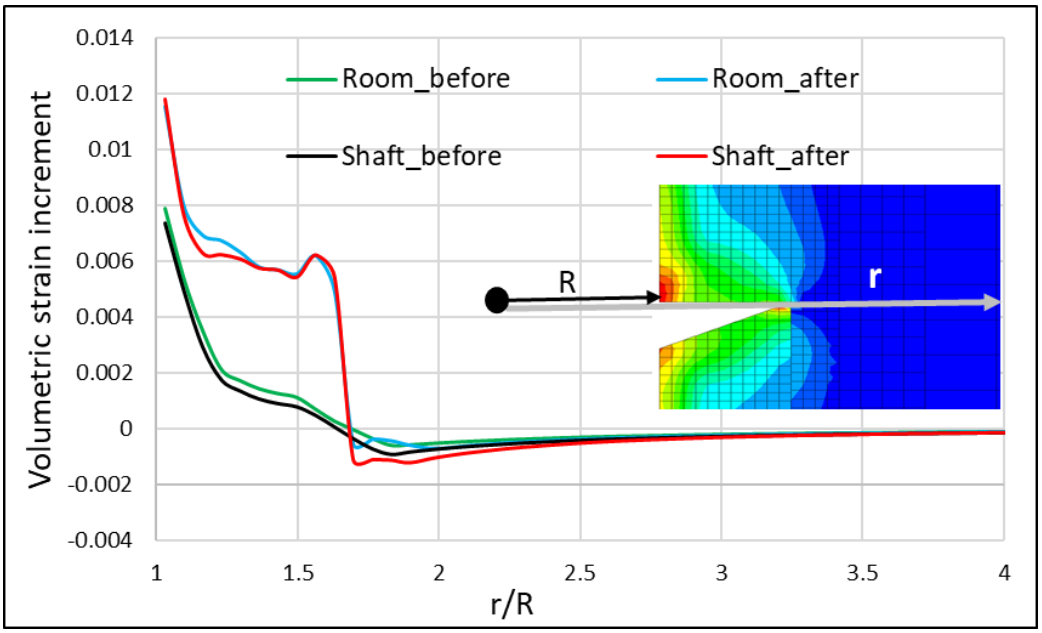

Fig. 4.8 Volumetric strain before and after the construction of the trapezoid cutoff for the shaft and its comparison with the volumetric strain for the room with the optimum trapezoid cutoff.

The extent of dilation along a line, passing through the tip of the cutoff is shown in Fig. 4.8 for the shaft and the placement room. It can be observed that the volumetric strain is positive along the line up to a certain value of r/R and then it becomes negative after a certain value of the r/R. The value of r/R represents the normalized distance and the point of transition from the negative to positive volumetric strain is the boundary between EDZi and EDZo. Dilation of rock mass in the vicinity of the cutoff can be observed from Fig. 4.8. The dilation before and after the construction of the optimum cutoff for the shaft and placement room is approximately the same.

4.4.2 Cutoff for Anisotropic Rock Mass Properties

To understand the effect of anisotropic rock mass properties, the bilinear strain hardening-softening model for anisotropic rock mass was used in the numerical model. In this constitutive model, the weak planes located inside a zone are simulated using the Mohr-coulomb failure criteria. The most frequently observed orientation of the weakness plane in rock i.e. the horizontal bedding planes were considered in the numerical model. It is rare to observe the bedding planes in granite, therefore, only limestone and mudstone rocks were considered with the horizontal bedding planes to understand the effect of rock mass anisotropy in a realistic field scenario.

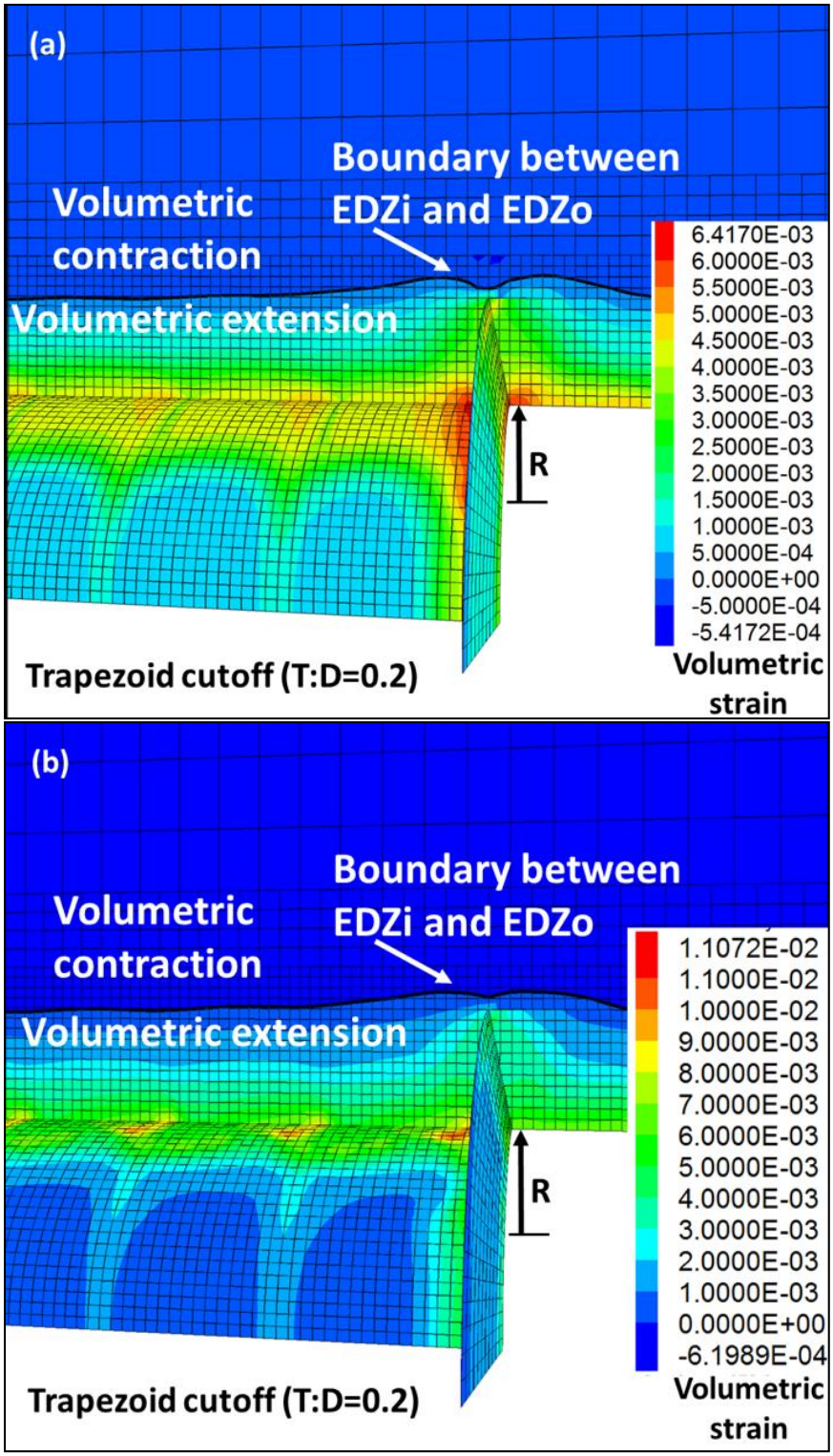

Fig. 4.9 Contours of volumetric strain, and the boundary between EDZi and EDZo for a trapezoid shape cutoff for circular placement room in limestone (a) without bedding planes and (b) with bedding planes.

The contours of volumetric strain for an optimum trapezoid cutoff around circular placement room located in limestone without and with bedding planes are shown in Fig. 4.9 (a) and (b). The positive volumetric strain represents the volumetric expansion while the negative volumetric strain represents the volumetric contraction of the rock mass. The boundary between positive volumetric strain and negative volumetric strain is the separation boundary between EDZi and EDZo.

The dimension of EDZi and EDZo are 1.73 m and 1.93 m for the circular placement room with trapezoid cutoff located in limestone without bedding planes. The extent of EDZi and EDZo is increased to 1.8 m and 2 m for the circular placement room with trapezoid cutoff located in limestone with bedding planes. Both EDZi and EDZo are increased due to the presence of horizontal bedding planes. The bedding planes have lower shear strength than the shear strength of the intact limestone. The high shear stresses in the rock mass caused failure along the weak plane before the failure in the intact rock. Therefore, higher EDZi and EDZo were observed for the optimum cutoff located in limestone with bedding planes as compared to limestone without bedding planes.

The contours of volumetric strain for the optimum cutoff around the circular placement room located in mudstone with and without bedding planes are shown in Fig. 4.10 (a) and (b). The dimension of EDZi and EDZo are1.64 m and 1.8 m for the optimum cutoff located in mudstone without bedding planes. The extent of EDZi and EDZo are increased to 1.96 m and 2.06 m for the optimum cutoff located in mudstone with the bedding planes. The extent of EDZi and EDZo is increased due to the presence of bedding planes. Similar to the case of limestone, the high shear stresses in the rock mass caused failure along the bedding planes before failure in intact rock eventually causing a higher extent of EDZi and EDZo in the mudstone with bedding planes as compared to mudstone without bedding planes.

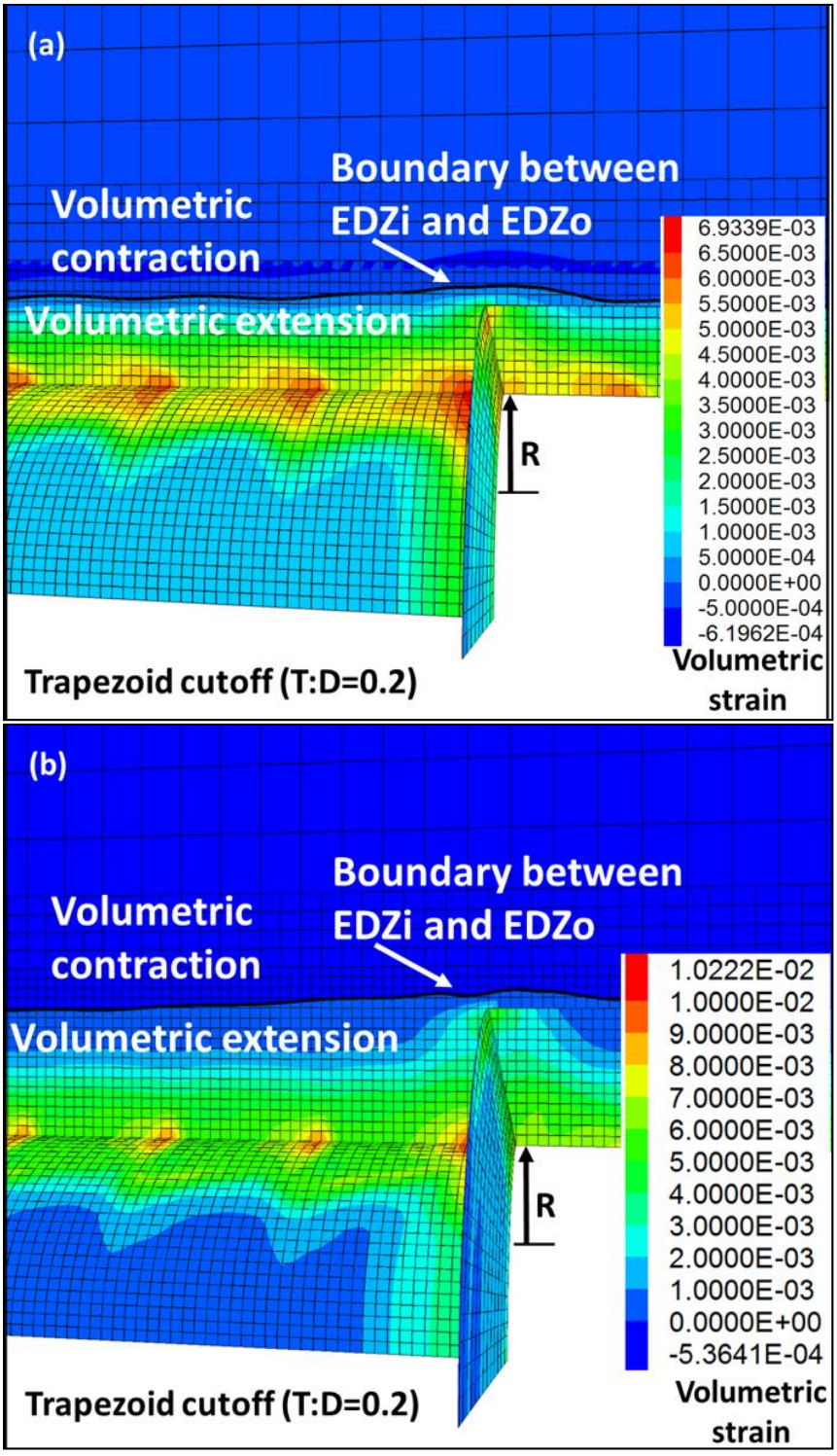

Fig. 4.10 Contours of volumetric strain, and the boundary between EDZi and EDZo for a trapezoid shape cutoff for circular placement room in mudstone (a) without bedding planes and (b) with bedding planes.

The rock mass dilation along a straight line originating from the roof of the placement room and moving into the rock mass up to a depth of 4 m is shown in Fig. 4.11. The rock mass dilation for the optimum cutoff is positive near the placement room, showing a volumetric expansion of the rock. It becomes negative after a certain distance from the placement room representing the volumetric contraction of the rock. The boundary where the volumetric dilation becomes positive to negative represents the boundary between EDZi and EDZo. Moreover, going beyond the EDZo, the dilation becomes zero after a certain distance which shows that the construction of the placement room does not have any effect in this zone. It can be observed that the rock mass dilation is greater when the horizontal bedding planes are present in the limestone. This is because the bedding planes due to their lower strength cause large shear strains in the rock mass as compared to the rock mass with no bedding planes in it. The failure in the rock mass occurs along the weak planes due to their lower strength as compared to the intact rock.

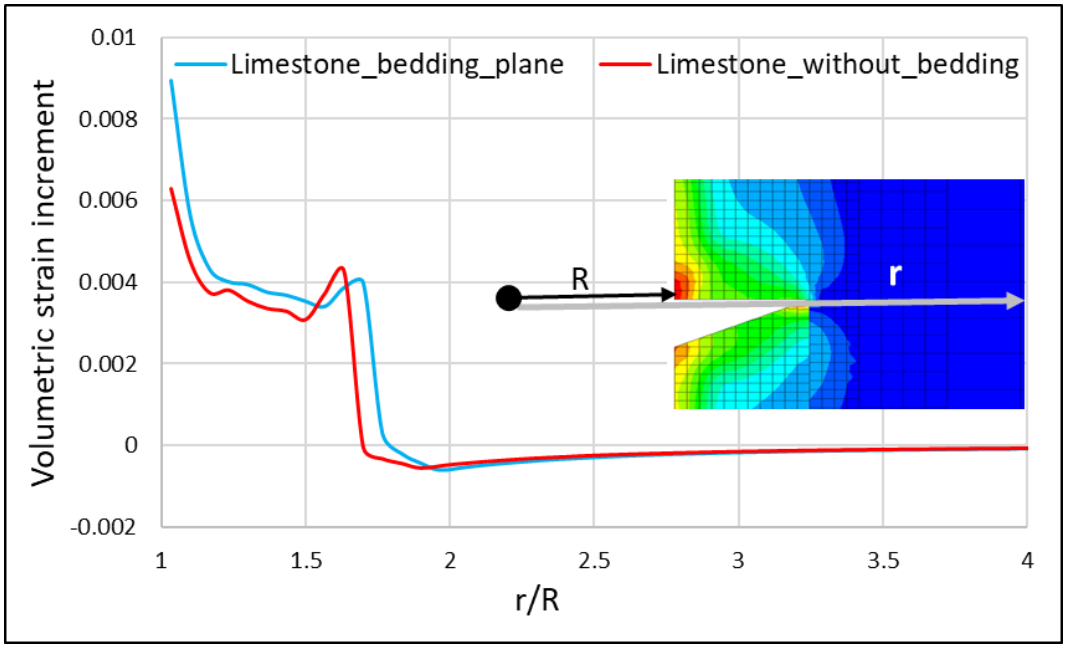

Fig. 4.11 Rock mass dilation for a cutoff with optimum shape and dimension located in limestone with and without the presence of bedding planes.

Similar to limestone, the rock mass dilation for mudstone along a straight line originating from the roof of the placement room and moving into the rock mass up to a depth of 4 m is shown in Fig. 4.12. It can be observed that the rock mass dilation is greater when the horizontal bedding planes are present in the mudstone. This is because the weak plane due to its lower strength causes large

shear strains in the rock mass as compared to the mudstone with no bedding planes in it. The change in rock mass dilation with and without the bedding planes was more pronounced for mudstone as compared to limestone.

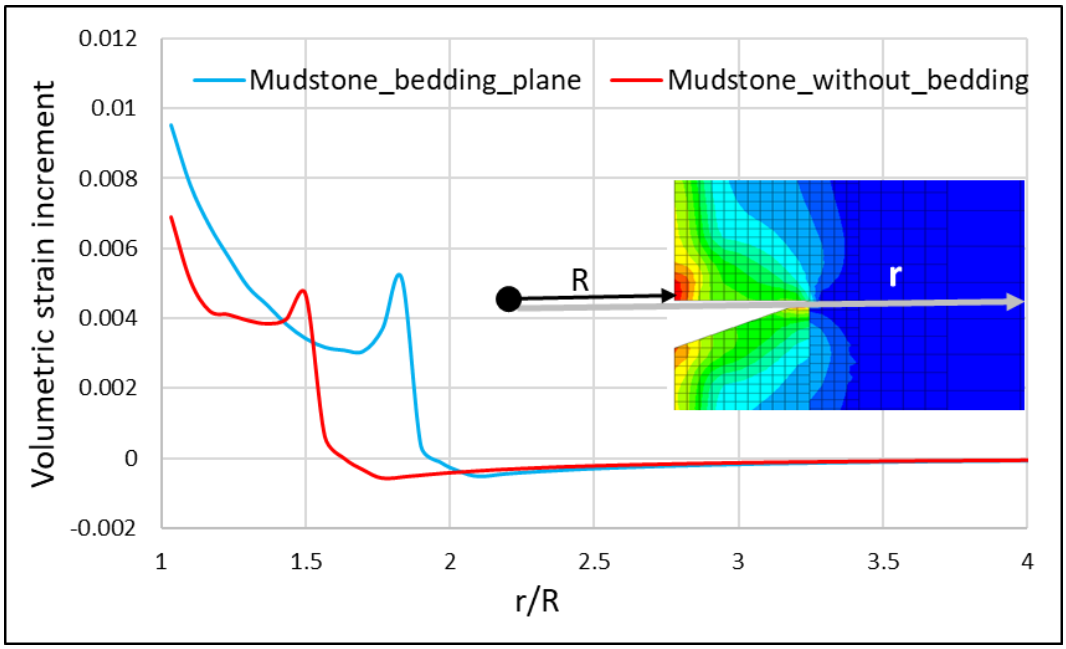

Fig. 4.12 Rock mass dilation for a cutoff with optimum shape and dimension located in mudstone with and without the presence of horizontal bedding planes.

The contours of shear stress in the rock mass for intact limestone and mudstone are shown in Fig. 4.13 (a) and (b) respectively. It can be observed that the magnitude of the shear stress is greater for the limestone as compared to mudstone when there are no bedding planes in the rock. The higher values of shear stress cause a high value of shear strain eventually causing high values of volumetric strain and the higher extent of EDZi for limestone. The higher values of shear stress are caused due to high value of modulus of elasticity of limestone. The extent of EDZi depends on the ratio between shear strength to shear stress values in the rock mass. Although, the shear strength of mudstone is lower than limestone, however, the low value of modulus of elasticity of mudstone induces lower values of the shear stress for mudstone. For the given elastic and strength parameters of limestone and mudstone, the ratio between shear strength to shear stress is higher for mudstone than limestone in this study. The higher value of the ratio between shear strength to shear stress caused a lower value of EDZi for mudstone as compared to limestone. Therefore, the extent of

EDZi for the optimum cutoff in intact mudstone was found to be lower than the optimum cutoff in intact limestone.

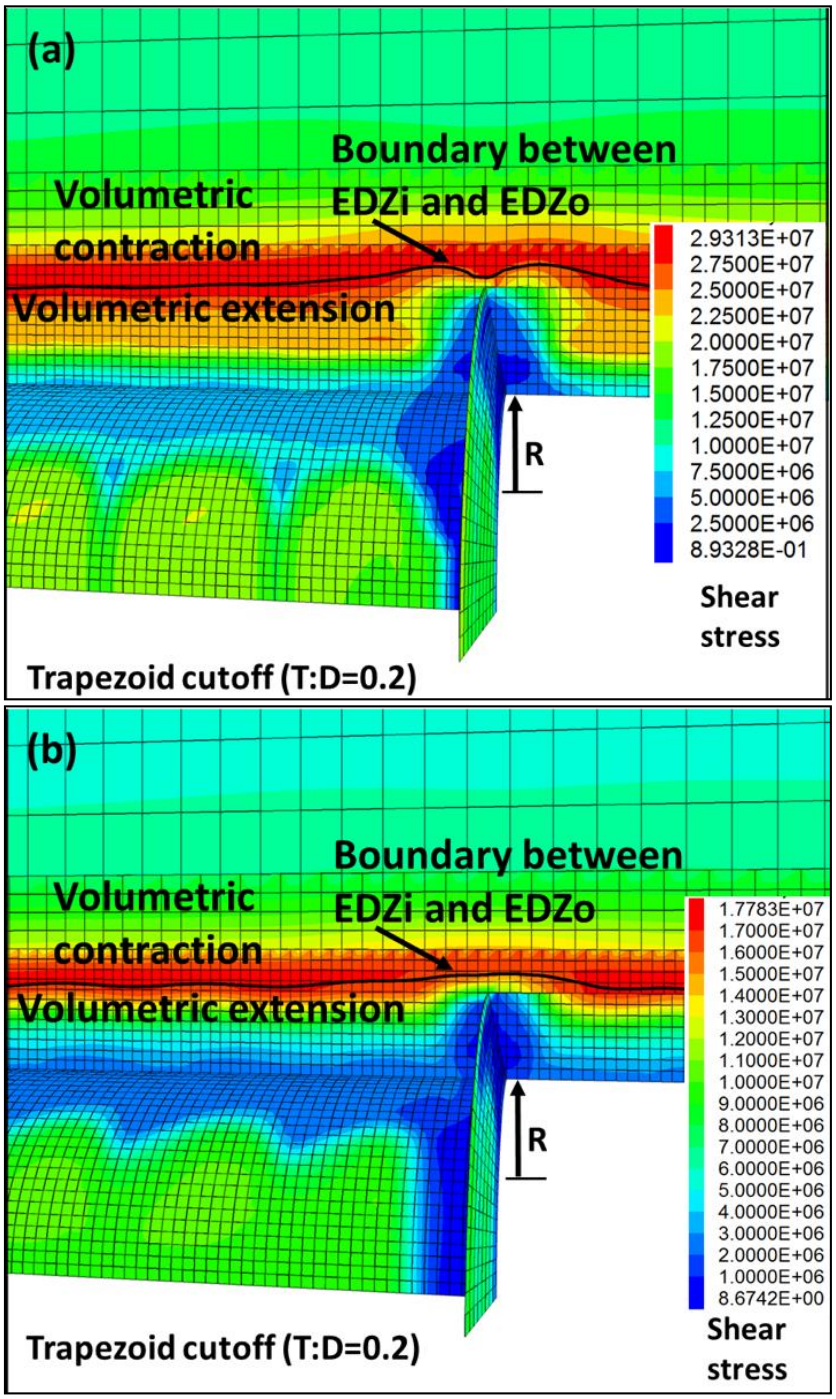

Fig. 4.13 Contours of shear stress, and the boundary between EDZi and EDZo for a trapezoid shape cutoff for circular placement room in (a) limestone and (b) mudstone without horizontal bedding planes.

4.4.3 Cutoff for Different Rock Mass Types

The optimum cutoff for a circular placement room was modelled for granite, limestone, and mudstone rock mass to understand the effect of rock mass properties on the extent of EDZi and EDZo around the optimum cutoff. Granite was considered without bedding planes while limestone and mudstone were considered with horizontal bedding planes to simulate realistic field conditions.

The contours of volumetric strain for the cutoff located in granite, limestone, and mudstone are shown in Fig. 4.14 (a), (b), and (c). The black iso-line shows the boundary between EDZo and EDZi. The zone with positive volumetric shows the volumetric extension of the rock while the zone with negative volumetric strain shows the volumetric contraction of the rock. The extent of EDZi is 1.7 m, 1.71m, and 1.83 m for the circular room located in granite, limestone, and mudstone, respectively. Further, the extent of EDZo is 1.86 m, 1.87 m, and 2 m for the circular room located in granite, limestone, and mudstone, respectively. The extent of EDZi is 1.78 m, 1.8 m, and 1.96 m after the construction of optimum cutoff in granite, limestone, and mudstone rocks, respectively. Similarly, the extent of EDZo is 2 m, 2 m, and 2.1 m after the construction of optimum cutoff in granite, limestone, and mudstone rocks, respectively. The dimension of EDZi and EDZo is the largest for the optimum cutoff located in mudstone followed by limestone and granite. For the case when the horizontal bedding planes are present in limestone and mudstone, the failure of rock mass occurs along the weak planes present in the limestone and mudstone. Due to the lower strength of the horizontal bedding planes, as compared to the intact rock mass, higher values of shear strains are observed in the rock mass. Therefore, the dimension of EDZi is greatest for mudstone followed by limestone and granite.

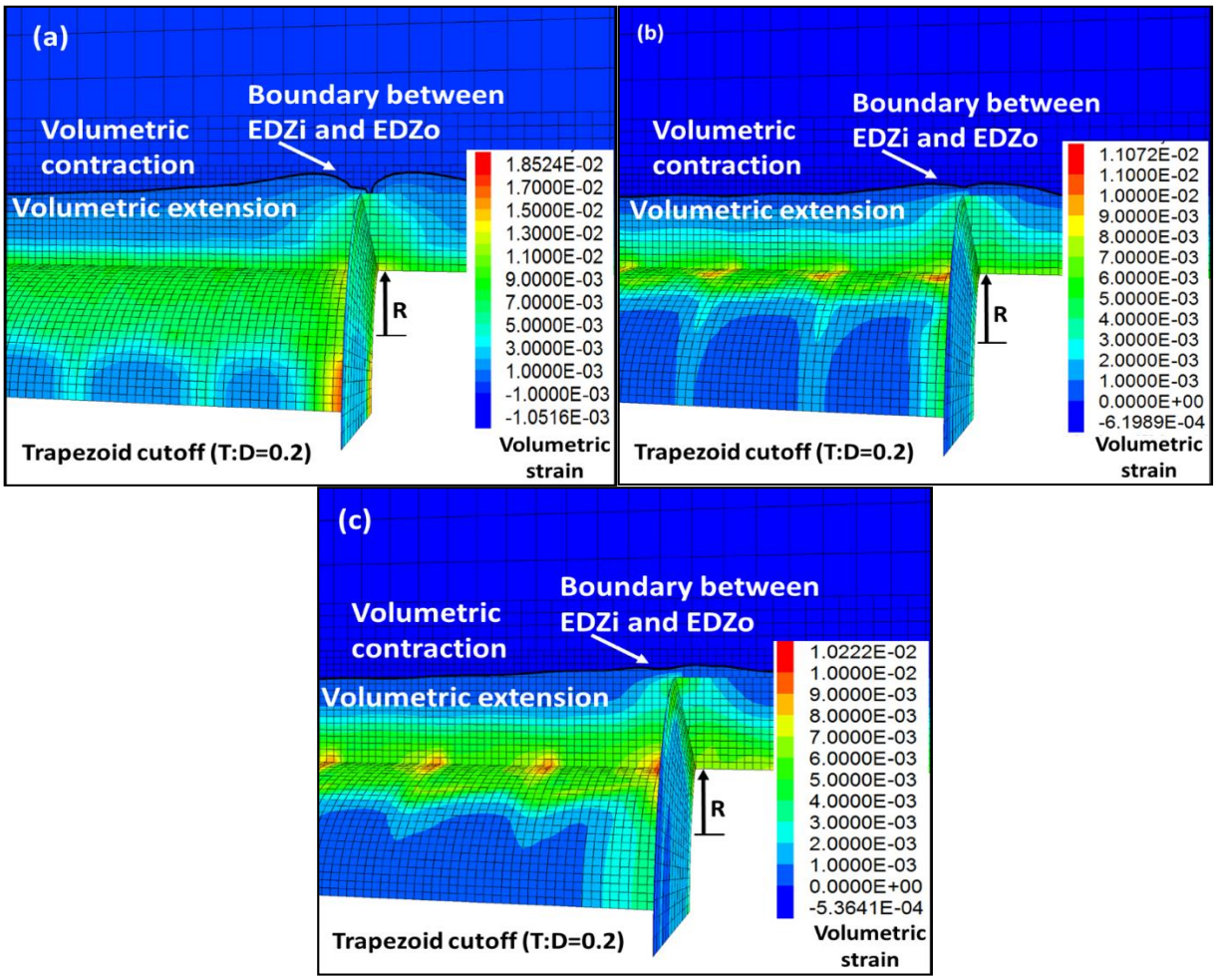

Fig. 4.14 Contours of volumetric strain, and the boundary between EDZi and EDZo for a trapezoid shape cutoff for circular placement room in (a) granite (b) limestone, and (c) mudstone.

The rock mass dilation along a straight line parallel to the vertical side of the optimum cutoff and passing through the tip of the cutoff is shown in Fig. 4.15 for the optimum cutoff located in granite, limestone, and mudstone. The volumetric strain is positive for the low values of r/R and then becomes negative after a certain distance. The boundary of transition from positive volumetric strain to the negative volumetric strain is the separation boundary between EDZi and EDZo. It can be observed that the extent of EDZi for the optimum cutoff is greater for mudstone followed by limestone and granite.

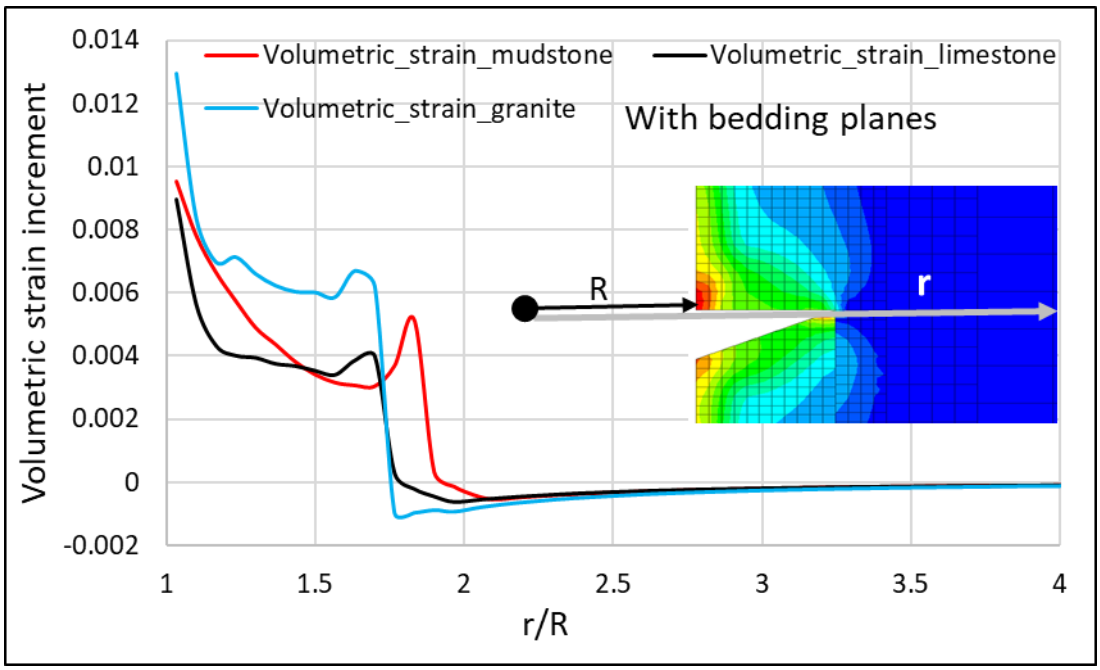

Fig. 4.15 Rock mass dilation for a cutoff with optimum shape and dimension located in granite, limestone, and mudstone with the presence of horizontal bedding planes.

Interestingly, the order of rock mass dilation was found to be the opposite of that which one would expect when the bedding planes were absent in the limestone and mudstone rock masses (Fig. 4.16). This order is because of the difference in the values of shear strengths and modulus of elasticities of the rocks. The extent of EDZi and EDZo depends on the ratio between the shear strength and shear stress in the rock mass. Although the shear strength of intact granite is higher followed by limestone and mudstone, the high value of modulus of elasticity of granite followed by limestone and then mudstone induces higher shear stress in the intact granite. For the given strength and elastic properties of the rocks used for this study, the higher values of shear stress in the intact granite followed by intact limestone and then intact mudstone caused a lower value of the ratio between shear strength and shear stress for the granite followed by limestone and then mudstone. The low values of shear strength to stress ratio induce higher values of shear strain eventually causing a higher extent of EDZi and EDZo for the granite followed by limestone and mudstone.

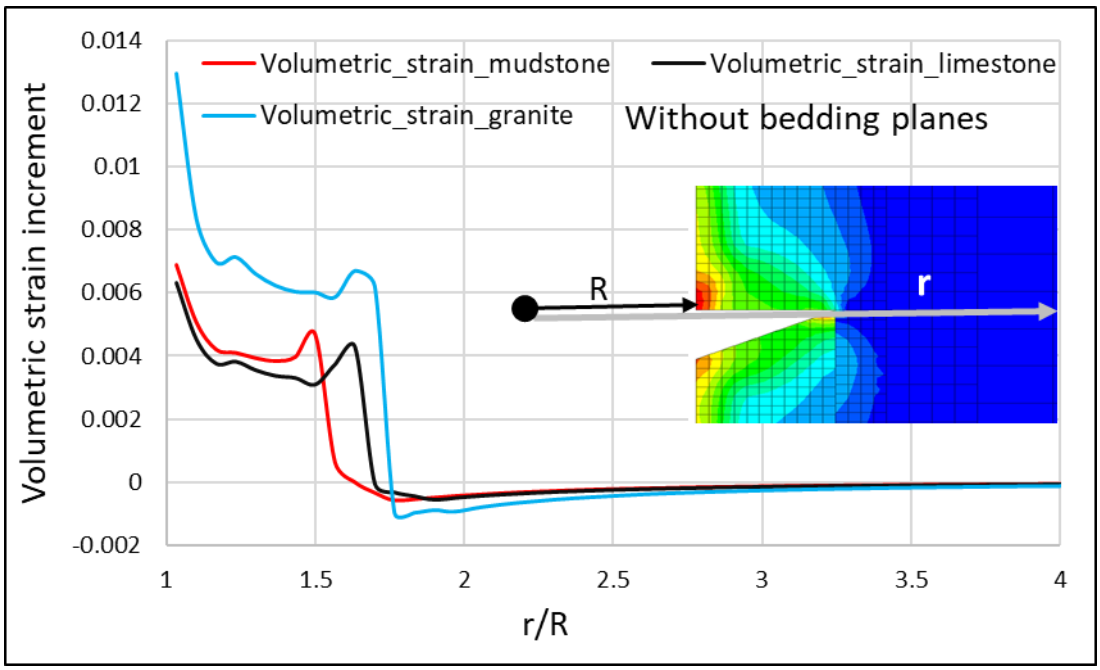

Fig. 4.16 Rock mass dilation for a cutoff with optimum shape and dimension located in granite, limestone, and mudstone without the presence of horizontal bedding planes.

4.4.4 Cutoff for Rectangular Placement Room

A cutoff with optimum shape and aspect ratio, as determined from the previous modelling in this thesis, was constructed for the rectangular placement room to understand the effect of placement room shape on the extent of EDZi and EDZo for the optimum cutoff shape. The contours of volumetric strain for the rectangular placement room and circular placement room with trapezoid shape cutoff is shown in Fig. 4.17 (a) and (b). The positive volumetric strain shows the volumetric expansion of the rock while the negative volumetric strain shows the volumetric contraction of the rock. The boundary between the positive and negative volumetric strain, shown by the black isoline is the separation boundary between the EDZi and EDZo. The dimensions of the EDZi and EDZo for the rectangular placement room are 2.11 m and 2.33 m before the construction of the optimum cutoff. The dimensions of the EDZi and EDZo for the rectangular placement room are 2.13 m and 2.4 m after the construction of the optimum cutoff. The dimension of EDZi and EDZo are more for the rectangular placement room as compared to the circular placement room.

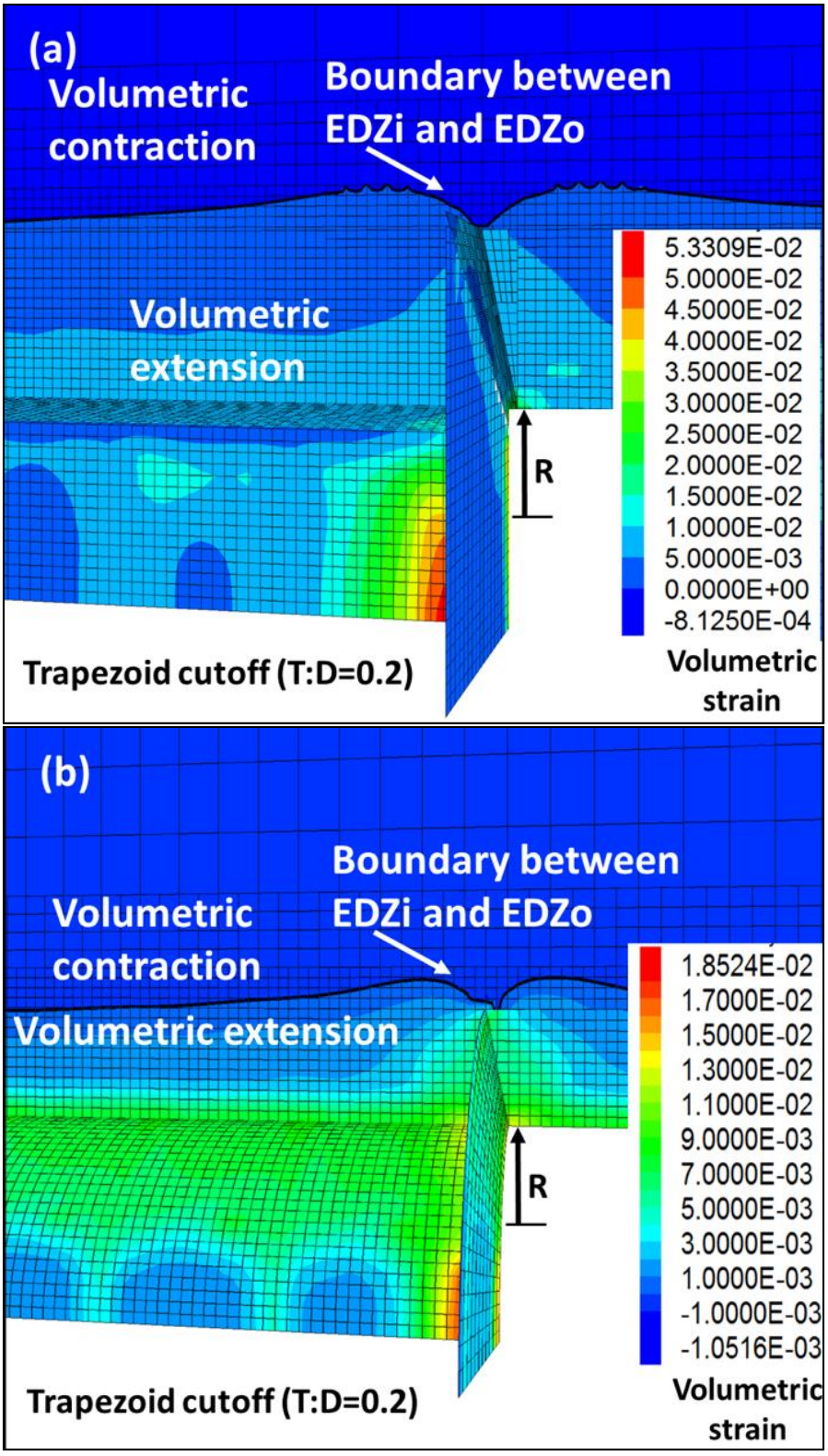

Fig. 4.17 Contours of volumetric strain, and the boundary between EDZi and EDZo for a trapezoid shape cutoff for (a) rectangular placement room and (b) circular placement room.

The rock mass dilation along a straight line parallel to the vertical side of the optimum cutoff and passing through the tip of the cutoff up to a distance of 4 m into the rock is shown in Fig. 4.18. The volumetric strain is positive near the roof of the placement room and decreases on moving into the roof rock mass. The volumetric strain becomes negative after a certain distance beyond the cutoff. The positive to negative volumetric transition boundary is known as the separation boundary between the EDZi and EDZo. The increase in EDZi and EDZo before and after the construction of the cutoff is greater for the rectangular room as compared to the circular placement room. This happens due to stress concentration around the sharp corners present in the rectangular placement room.

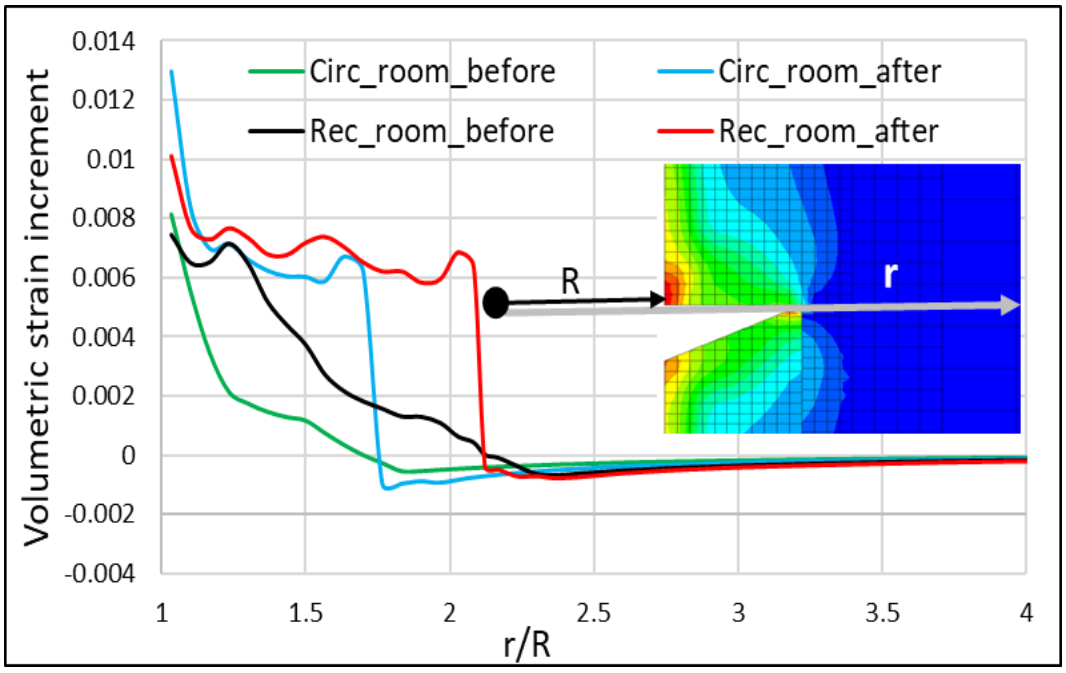

Fig. 4.18 Rock mass dilation for a cutoff with optimum shape and dimension for a rectangular placement room as compared to the circular placement room.

The results of the numerical modelling showed that the radial extent of EDZi for the optimum cutoff is smaller for the granite followed by limestone and mudstone. The radial extent of EDZi for the optimum cutoff is lower for the limestone and mudstone with the absence of bedding planes compared to when bedding planes are present. Furthermore, for the given stress situation in this study, the radial extent of EDZi for the optimum cutoff for the horizontal placement room and

vertical room (shaft) is found approximately equal. Finally, the radial extent of EDZi for the optimum cutoff for a circular placement room is smaller than the rectangular placement room.

The results of mechanical modelling to understand the mechanical behaviour of the cutoff was presented in chapter 4. The shape and dimension of the cutoff were optimized by using the criteria that the construction of the cutoff should have a minimum influence on the dimension of the pre-existing numerical EDZi. A trapezoid shape cutoff with a minimum aspect ratio (0.2) was found to be optimum of the three different shaped used in this study. After optimizing the shape and dimension of the cutoff, the effect of different variants such as orientation and shape of the placement room, rock mass properties, and rock mass anisotropy on the extent of EDZi and EDZo for the optimum trapezoidal cutoff were analyzed.

Chapter 5: Thermo-Mechanical Modelling Results

5.1 Introduction

This chapter describes the thermal and thermo-mechanical response of the optimum cutoff under conceptual Canadian repository conditions. The effect of heat from the spent nuclear fuel was analyzed on the optimum cutoff. Dimensions of EDZs induced from the thermo-mechanical stresses were determined to understand the optimum cutoff response under heat from spent nuclear fuel.

The first stage of the study consisted analysis of rock mass temperature in the vicinity of the cutoff. A finite element thermal model was used to analyze the maximum possible temperature at the cutoff due to the heat from the spent nuclear fuel in the repository.

In the second step of the study, the thermo-mechanical response of the optimum cutoff was analyzed. The effect of maximum possible temperature due to the heat from spent nuclear fuel on the EDZs was analyzed.

5.2 The Maximum Temperature inside the Repository

Guo (2017), and Radakovic-Guzina et al. (2015) simulated the far field and near field response of the conceptual Canadian repository in crystalline and sedimentary rocks respectively. Guo (2017) observed for a repository in the crystalline setting from the far-field thermal model that the peak temperature at the center of the panel occurs after 78 years with a magnitude of 71 ^{o}C. The peak temperature at the center of the repository was 43 ^{o}C after 2200 years. Guo (2017) also carried out a near field thermal model simulation to understand the temperature for the different components inside the placement room explicitly. The results showed that there is an influence of adiabatic boundary condition in the near field model due to the assumption of the infinite extent of the repository. After the correction of the adiabatic boundary effect, the results of the study showed a peak temperature of 84 ^{o}C at the surface of the container after 45 years, while a peak temperature of 77 ^{o}C at the roof of the room after 65 years.

Radakovic-Guzina et al. (2015) simulated the far-field and near-field thermal response of conceptual Canadian repository in sedimentary rock settings. The temperature from the far-field models was consistently observed lower than the temperature from the near field models as shown in Fig. 5.1. The reason for this was that the heat load in the case of the far field model was uniformly distributed throughout the panel, while in the near field model, it was concentrated to the canister volume which produces a higher temperature at the canister surface compared to the temperature at the panel center as observed in the far-field modelling. The peak temperature at the center, in the close proximity of the canister, was 97 ^{o}C after 42 years, while the peak temperature at the panel center was 81 ^{o}C after 800 years (Fig. 5.1).

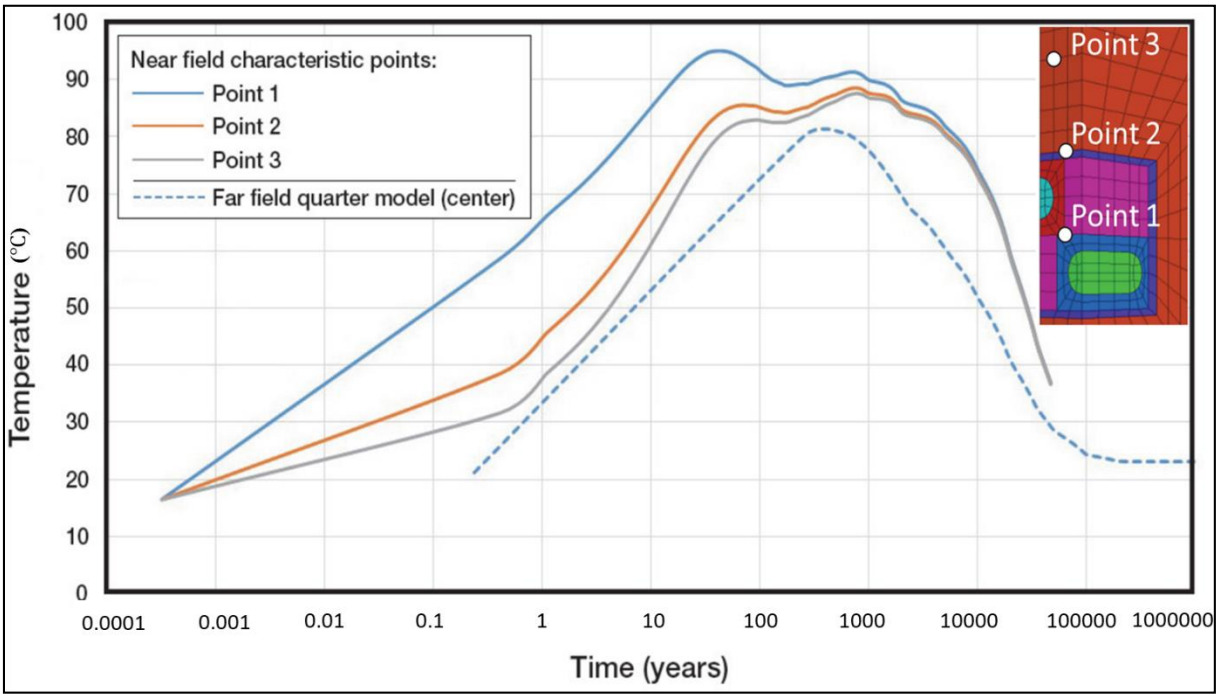

Fig. 5.1 The far-field response and near-field response (without adiabatic boundary effect correction) of the conceptual Canadian repository (modified after Radakovic-Guzina et al. (2015)).

The assumption that the heat load is uniformly distributed throughout the repository panel in the far-field model does not simulate the temperature gradient between different components of the repository such as the canister, backfill material, cutoff, and host rock. The near field model simulates the temperature gradients inside the panel along a cross-section perpendicular to the placement room (Y-direction, Fig. 3.5). However, this model does not simulate the temperature

gradient along the longitudinal direction (X-direction, Fig. 3.5) of the placement room where the cutoff will be located.

In order to simulate the temperature gradient between canister and cutoff, this study analyzed the maximum possible temperature at the cutoff in the longitudinal direction (X-direction, Fig. 3.5) of the placement room by simulating multiple canisters in the room. The results of this study also predict temperature more than expected due to the effect of adiabatic boundary condition as explained by Guo (2017). To analyze the effect of temperature on the optimum cutoff, the main purpose of thermal modelling was to create representative thermal history at the rock mass in the vicinity of cutoff by creating a thermal history similar to Radakovic-Guzina et al. (2015) (Fig. 5.1) for the 100^{th} canister located at the middle of the placement room.

5.3 Thermal Modelling Results and Discussion

In the first stage, the maximum possible temperature at the canister surface located at the center of the panel for an infinite repository was evaluated from the near-field thermal model. The variation of temperature with time at the canister surface, at the surface of the excavated rock, and inside the rock is shown in Fig. 5.2. The second peak in the temperature after 1000 years occurs due to the effect of the adiabatic boundary condition as explained by Guo (2017). A maximum temperature of 98 ^{o}C is observed in the vicinity of the container (Pt1) after 42 years while a maximum temperature of 84 ^{o}C is observed at the room roof (Pt2) after 57 years and a maximum temperature of 78 ^{o}C is observed inside the rock (Pt3) after 75 years. The maximum temperature from this study at Pt1 was equal to the maximum temperature from Radakovic-Guzina et al. (2015) (Fig. 5.1).

The temperature contours after 42 years when the temperature of the canister surface becomes maximum are shown in Fig. 5.3. The thermal gradients in the perpendicular direction (Y direction, Fig. 3.5) of the placement room can be observed from the different colors along the plane. A maximum temperature of 75 ^{o}C was observed in the middle of the two placement rooms located 20 m away from each other. The model results do not show the temperature gradient in the longitudinal direction (X-direction, Fig. 3.5) of the room because of the limited thickness (0.75 m) of the model. In order to simulate thermal gradients along the longitudinal direction of the

room, the longitudinal length of the numerical model, and the number of canisters in the placement room were increased.

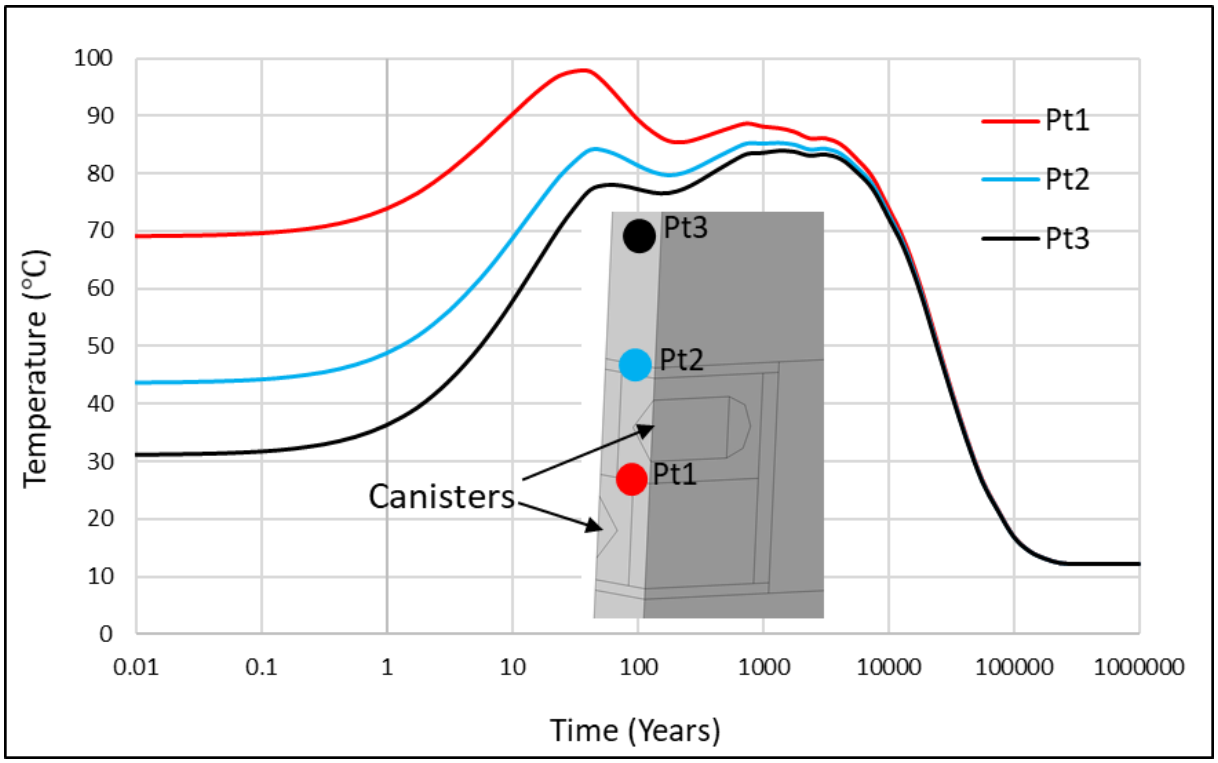

Fig. 5.2 Evolution of temperature with time at characteristic points for the near field model assuming an infinitely large repository.

In order to simulate the representative temperature of the rock mass in the vicinity of the cutoff, the number of canisters in the placement room was increased until the temperature at the 100th canister located in the middle of the room becomes equal to the maximum temperature from the near field model. The effect of the number of canisters on the temperatures at the cutoff was analyzed by simulating different number of canisters in the placement room. The evolution of temperature with time for 10 canisters in the placement room is shown in Fig. 5.4. The temperature evolution is plotted at the characteristic points along a longitudinal (X direction, Fig. 3.5) horizontal line which passes through the center of the placement room. The first two pairs of points along the line are separated by 3.5 m while other points are separated by a distance of 3 m.

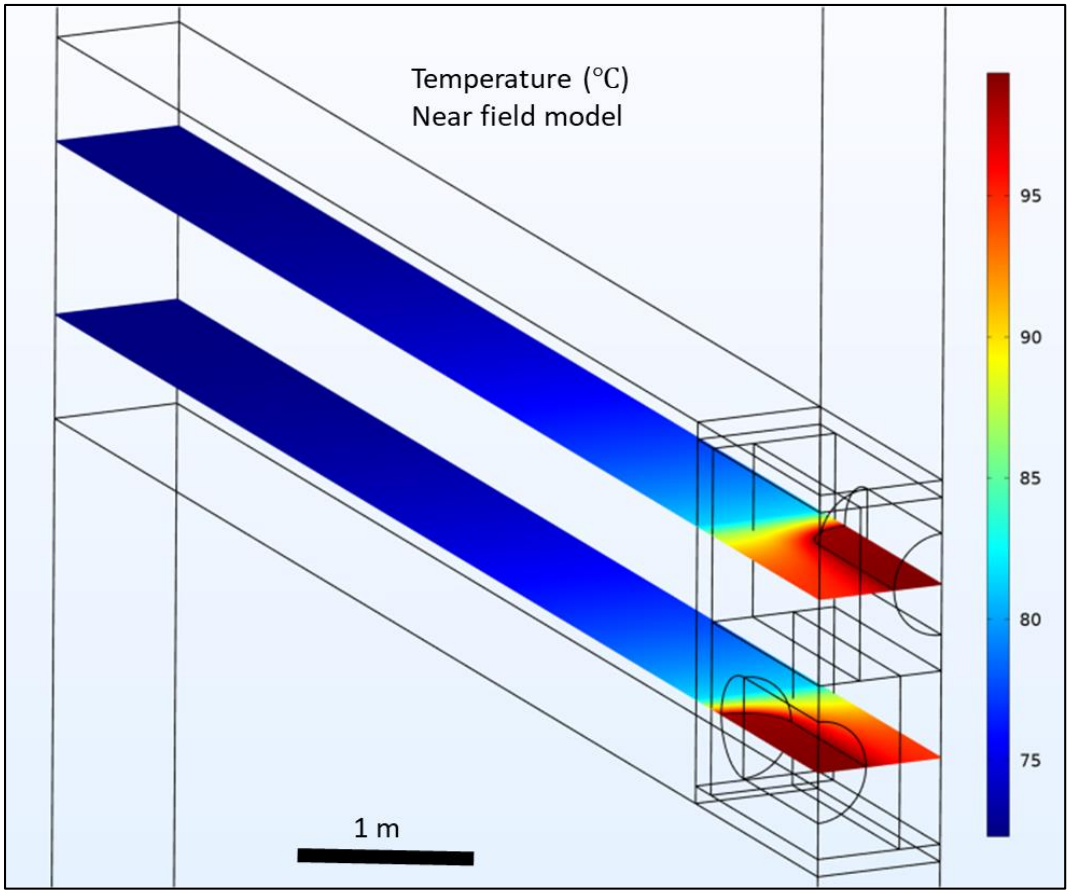

Fig. 5.3 Contours of temperature along a horizontal plane passing through the center of the room when the temperature at the canister surface becomes maximum.

In general, the temperature at all the points increases with time becoming maximum after a certain time and then again decreases with time. The temperature in the vicinity of cutoff and at Pt1 (Fig. 5.4) becomes maximum and equal to 41 ^{o}C and 42 ^{o}C after 1333 years. The temperature at Pt2 (Fig. 5.4) becomes maximum and equal to 52 ^{o}C after 17 years. After point 2, the temperature at all the points becomes maximum with values between 69 ^{o}C and 76 ^{o}C between 7 to 10 years. It can be observed that the thermal gradient in the horizontal direction decreases on moving from cutoff to the Pt7. The peak temperature at the surface of the 10th canister (Pt7) (Fig. 5.4) is less than the canister temperature predicted from the near-field model (Pt1) (Fig. 5.2). Also, the time taken to reach the maximum temperature is lower than the time taken to reach the maximum temperature in the near-field model. This is because the heat load from the 10 canisters was not enough to heat the rock mass as present in the near-field model.

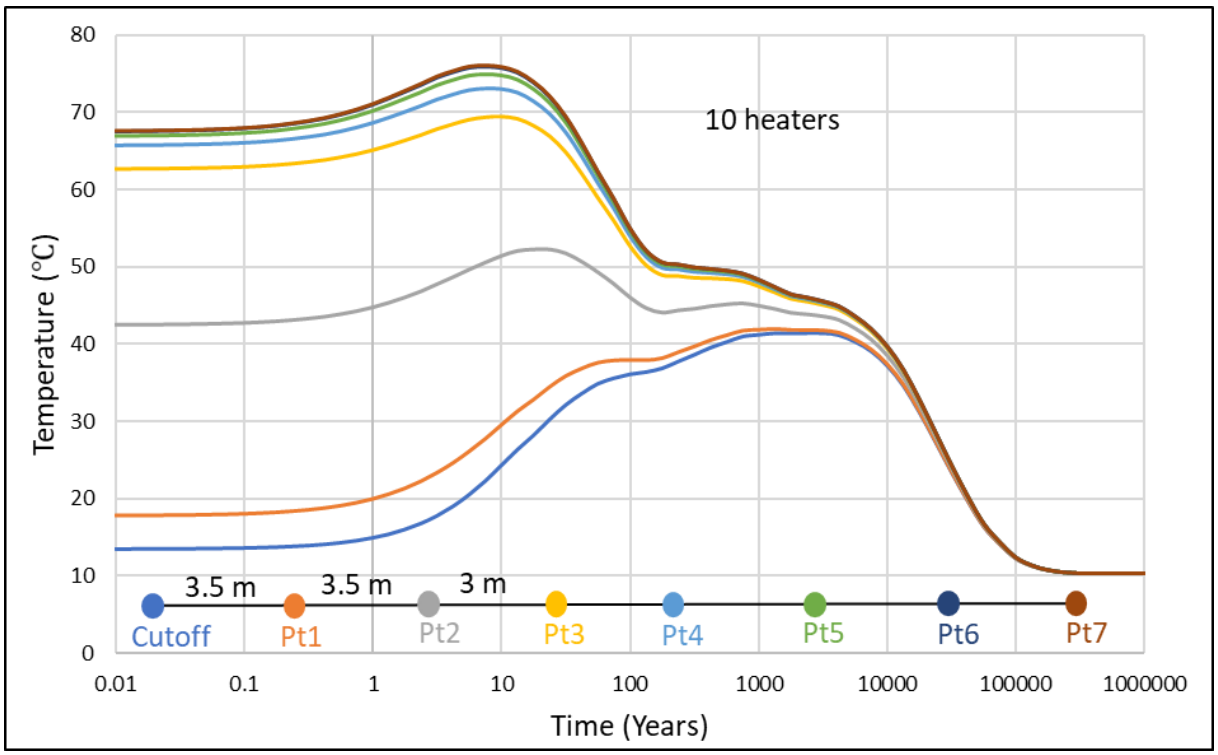

Fig. 5.4 Evolution of temperature at characteristic points with time for 10 canisters in the placement room. The horizontal distance between cutoff, Pt1, and Pt1, Pt2 is 3.5 m while the distance between all other points is 3 m.

The evolution of temperature with time for 50 canisters in the placement room is shown in Fig. 5.5. The temperature evolution is plotted at the characteristic points along a longitudinal horizontal line passing through the center of the room. The first two pairs of points along the line are separated by 3.5 m while other points are separated by a distance of 12 m. In general, the temperature at all the points increases with time and becomes maximum after a certain time and then again decreases with time. The temperature at the rock mass in the vicinity of cutoff, Pt2, and Pt3 (Fig. 5.5) becomes maximum and equal to 67 ^{o}C, 67 ^{o}C, 70 ^{o}C after 1333 years. After Pt3, the temperature at all the points becomes maximum with values between 84 ^{o}C and 96 ^{o}C after 24 years, and the thermal gradients along the line between Pt4 to Pt8 (Fig. 5.5) in the room decrease. The peak temperature at the surface of the last canister (Pt8) is more than the peak temperature at the last canister when there are 10 canisters in the room and less than the canister temperature predicted from the near-field model, assuming an infinitely large repository. Also, the time taken to reach the maximum temperature is higher than the model with the 10 canisters and lower than the near field model. This is because the heat load from the 50 canisters is enough to heat the rock mass to

get the temperature more than with the model with 10 canisters but not large enough to heat the rock mass as present in the near-field model.

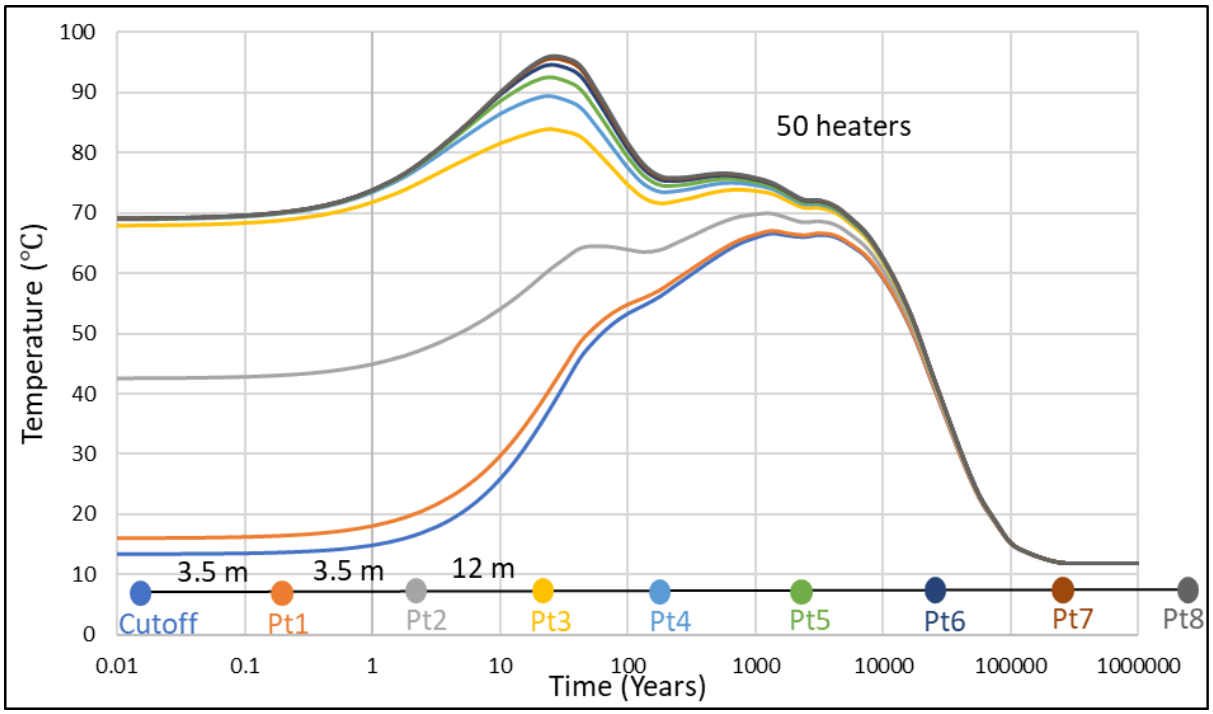

Fig. 5.5 Evolution of temperature at characteristic points with time for 50 canisters in the placement room. The horizontal distance between cutoff, Pt1, and Pt1, Pt2 is 3.5 m while the distance between other points is 12 m.

The evolution of temperature with time for 100 canisters in the placement room is shown in Fig. 5.6. The temperature evolution is plotted at the characteristic points along a longitudinal horizontal line passing through the center of the room. The first two pairs of points along the line are separated by 3.5 m while other points are separated by a distance of 21 m. In general, the temperature at all the points increases with time becoming maximum after a certain time and then again decreases with time. The temperature at the rock mass in the vicinity of cutoff, Pt1, and Pt2 (Fig. 5.6) becomes maximum and equal to 72 ^{o}C, 73 ^{o}C, 72 ^{o}C after 1778 years. The temperature at the rock mass in the vicinity of cutoff after 1000 years is 71 ^{o}C. After Pt3 (Fig. 5.6), the temperature at all the points becomes maximum with values between 94 ^{o}C and 98 ^{o}C between the years 24 and 42. The thermal gradients along the line between Pt4 to Pt8 in the room in the horizontal direction decrease after point 3.

The peak temperature at the surface of the last canister (Pt8) is 2 ^{o}C more than the peak temperature at the last canister when there are 50 canisters in the room and approximately equal to the canister temperature predicted from the near-field model, assuming an infinitely large repository. Also, the time taken to reach the maximum temperature is higher than the model with the 50 canisters and approximately equal to the near field model. The simulation results from the 100 canisters show that the heat load is large enough to create a maximum temperature equal to the maximum temperature from the near field model. The near field model simulates the maximum possible temperature that can be observed in the actual repository at the centre of the panel. Therefore, the model with 100 canisters simulates the maximum possible temperature at the last canister (100th) that can be observed in the actual repository. It also implies that the thermal gradients in the longitudinal direction of the placement room can be assumed equal to observed in the actual repository condition. Based on the thermal gradients in the longitudinal direction, the observed temperature at the cutoff (72 ^{o}C) can be assumed as a representative temperature in the actual repository conditions for the rock mass in the vicinity of the cutoff.

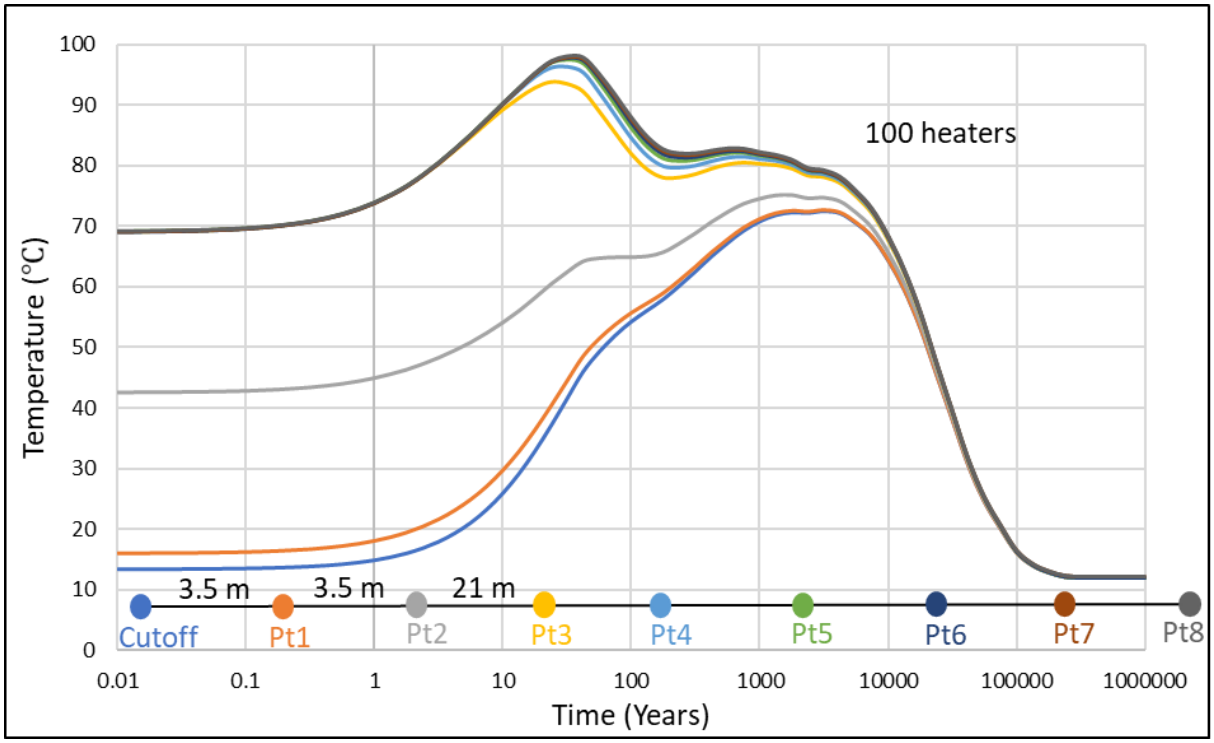

Fig. 5.6 Variation of temperature with time for characteristics points along a line passing through the center of the room. The horizontal distance between cutoff, Pt1, and Pt1, Pt2 is 3.5 m while the distance between other points is 21 m.

The temperature at the rock mass in the vicinity of the cutoff becomes maximum (72 ^{o}C) after 1778 years while the temperature at the same point is 71 ^{o}C after 1000 years. The maximum temperature at the rock mass in the vicinity of the cutoff is 1 ^{o}C greater than the temperature after 1000 years. In order to decrease the solve time (to 25 days) for the thermo-mechanical model, the maximum temperature was assumed to be 71 ^{o}C and reached after 1000 years.

The temperature contours after 1000 years when the temperature of the rock mass in the vicinity of the cutoff becomes maximum are shown in Fig. 5.7. The thermal gradients in the perpendicular (Y-direction, Fig. 3.5) and (X direction, Fig. 3.5) direction of the placement room can be observed from the different colors on the plane passing through the center of the placement room. A maximum and minimum temperature of 82 ^{o}C and 70 ^{o}C are observed in the longitudinal direction (L1, Fig. 5.7) after 1000 years when the temperature at cutoff becomes maximum. The temperature difference between the two endpoints along a line perpendicular to the placement room (L3, Fig. 5.7), and passing through the left end of the placement room is approximately 0.4 ^{o}C. The temperature difference between the two endpoints along a line (L4, Fig. 5.7) perpendicular to the placement room, and passing through the right end of the placement room is 6 ^{o}C.

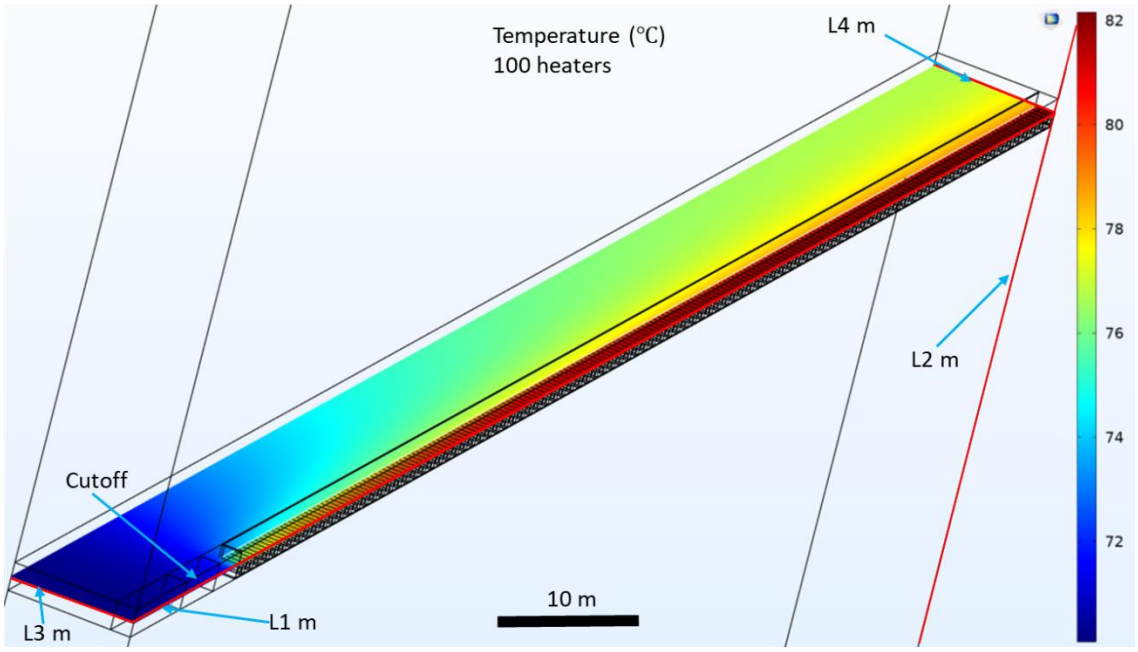

Fig. 5.7 Contours of temperature along a horizontal line passing through the center of the room after 1000 years when the temperature at the cutoff becomes maximum. The two lines used for data plotting are shown in red color and represented by L1 and L2.

The variation of temperature along a horizontal line (L1, Fig. 5.7) passing through the center of the placement room with distance is shown in Fig. 5.8. The temperature increases with distance for all the characteristic times after the placement of fuel in the room. There is an abrupt increase in the temperature after 20 m for all the times after the nuclear fuel placement. This is because the first canister in the placement room is located at a distance of 19 m from the access drift. The increase in temperature for the time one year is greatest than for the time 42 years at which the temperature at the last canister (100^{th}) becomes maximum. Similarly, the increase in the temperature for the times 1000 years and 100000 years are lower than for 1 and 42 years. This happens because of the exponential decay of the canister power with time. There is no change in the temperature for the time 1 million years because all the canister power is dissipated by this time and rock mass temperature becomes equal to the in-situ rock mass temperature. The thermal gradient along the horizontal line (L1, Fig. 5.7) decreases with distance and then became negligible after a distance of 100 m.

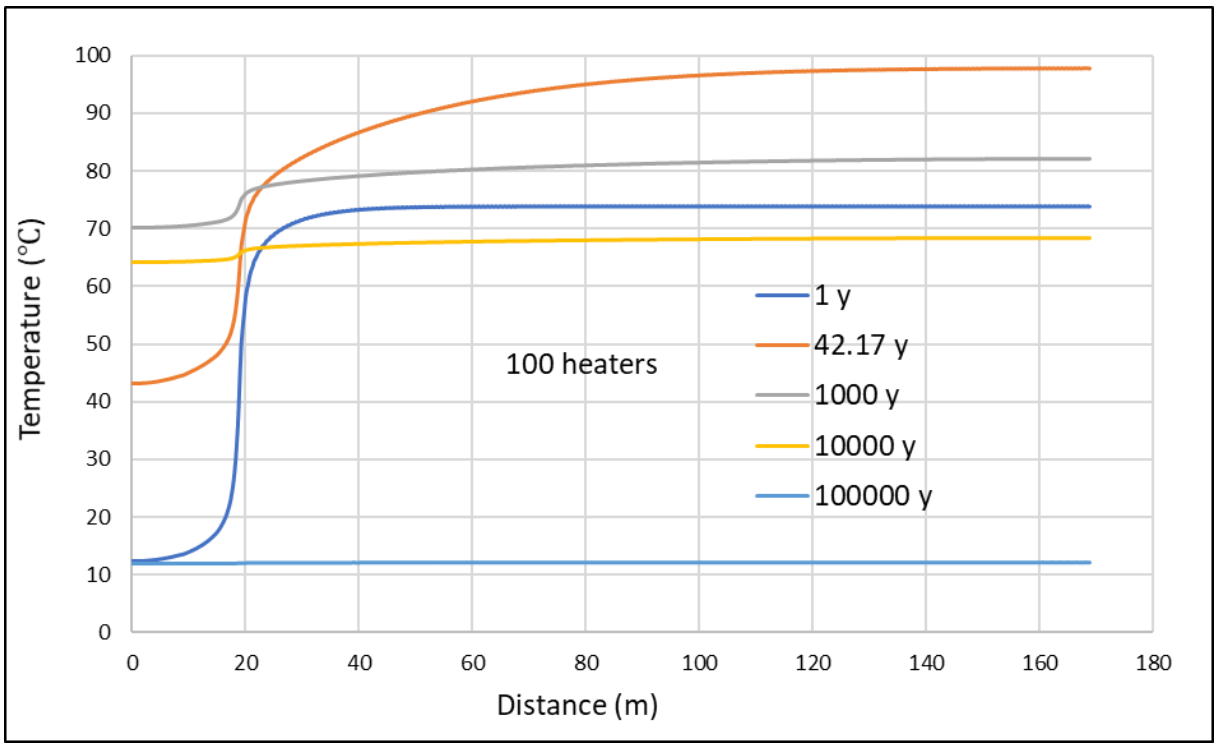

Fig. 5.8 Variation of temperature along a horizontal line (L1, Fig. 5.7) passing through the center of the room at characteristic times.

The variation of temperature with distance along a vertical line (L2, Fig. 5.7) passing through the right end of the model near to the last canister is shown in Fig. 5.9. The temperature increases with depth for all the times after the placement of nuclear fuel, becoming maximum at a depth of 500 m and then decreases with depth. The temperature becomes maximum at a depth of 500 m where the conceptual repository is constructed. The maximum temperature at the repository level is observed after 42.17 years of nuclear fuel placement. The maximum temperature at the repository level (500 m) increases with time, becoming maximum after 42 years and then decreases with time. This happens because of the exponential decay of the canister power. The increase in temperature with depth after 1 million years is linear which shows that all the heat is dissipated from the repository and the linear increase in temperature with depth is due to the in-situ geothermal gradient. It should also be noted that the increase in temperature with depth for all the times becomes linear after 2500 m depth which shows that the bottom boundary of the numerical model is sufficiently far to not have the isothermal boundary effect.

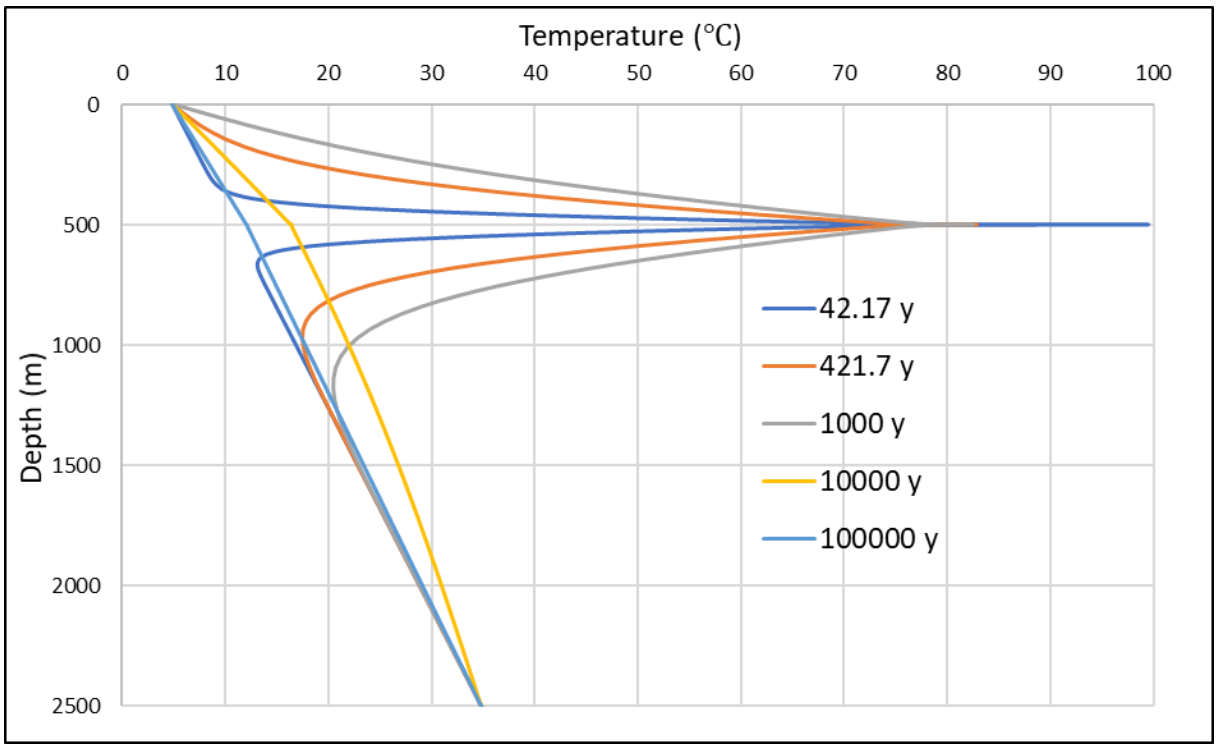

Fig. 5.9 Temperature along a vertical line (L2, Fig. 5.7) passing through the right end, away from the storage adit entrance, of the numerical model.

The thermal modelling exercise showed that a maximum temperature of 71 ^{o}C in the vicinity of cutoff can be assumed as a representative temperature for the conceptual repository conditions. To analyze the thermo-mechanical behaviour of the cutoff, four temperature histories were used in order to generate a temperature range between 35-90 ^{o}C. This temperature range includes the temperature (71 ^{o}C) at the rock mass in the vicinity of the cutoff from the thermal model with 100 canisters in the placement room.

5.4 Thermo-Mechanical Modelling Results

A thermo-mechanical model (Appendix A) was used to understand the response of optimum cutoff under thermal load for a conceptual repository. To simulate the representative temperature in the rock mass surrounding the cutoff, a thermal history equivalent to the thermal history (Fig. 5.6) at the cutoff from the thermal model in COMSOL was used. The power of the single canister was increased to simulate the latter mentioned thermal history in FLAC 3D. Furthermore, the power of the canister was varied to simulate a range of thermal histories to understand the evolution of the extent of EDZi and EDZo for the cutoff with temperature. The contours of temperature for canisters with power 6 times the actual canister power and when the rock mass temperature at Point_1 (Fig. 5.10 (d)) becomes 38 ^{o}C are shown in Fig. 5.10 (d). The plastic state of the elements and volumetric strain around the placement room with a trapezoidal shaped cutoff is shown in Fig. 5.10 (a) and Fig. 5.10 (b), respectively. Perras and Diederichs (2016) showed that positive (dilatant) numerical volumetric strain correlated with measured regions of connected microfractures around underground excavations, therefore, the zones within the plastic region with positive volumetric strain represent EDZi.

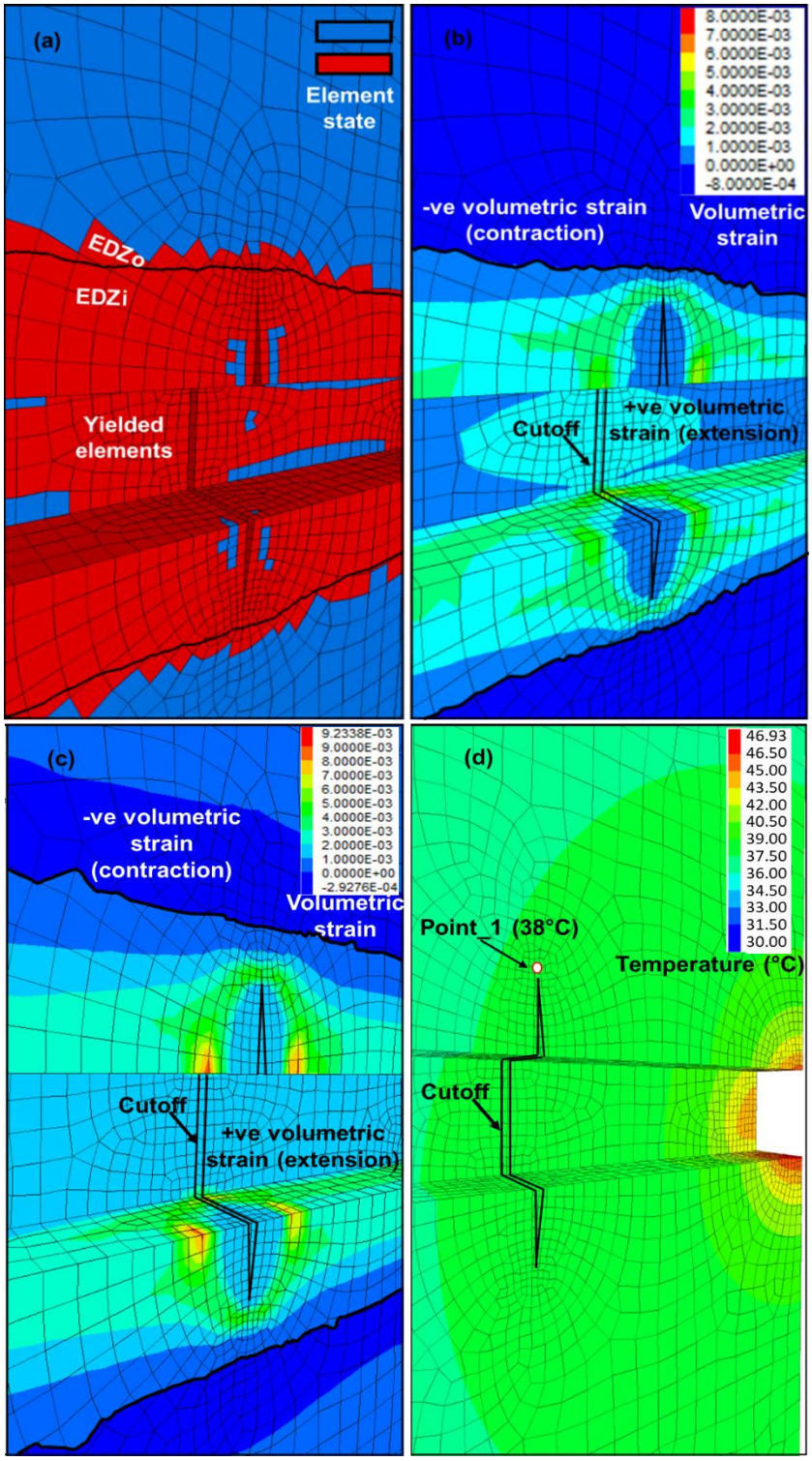

Fig. 5.10 Different excavation damage zones interpreted from (a) yielded elements (b) volumetric strain without temperature effects. The black iso-line showed the boundary between positive and negative volumetric strain. (c) Volumetric strain when the temperature around cutoff becomes maximum and (d) Contours of temperature

The remaining zones in the plastic region above the black isoline (Fig. 5.10 (a)) are considered to be the EDZo, which contains zones that have undergone volumetric contraction. Higher temperature gradients are observed inside the backfill material than the rock mass, which shows the insulation effect of the backfill material. Fig. 5.10 (c) shows the extent of EDZi and EDZo when the temperature of the rock mass in the vicinity of the cutoff reaches 38 ºC. The extent of the EDZi increased from 2.93 m to 3.18 m and the EDZo increased from 3.12 m to 3.50 m, respectively, due to thermally induced perturbations.

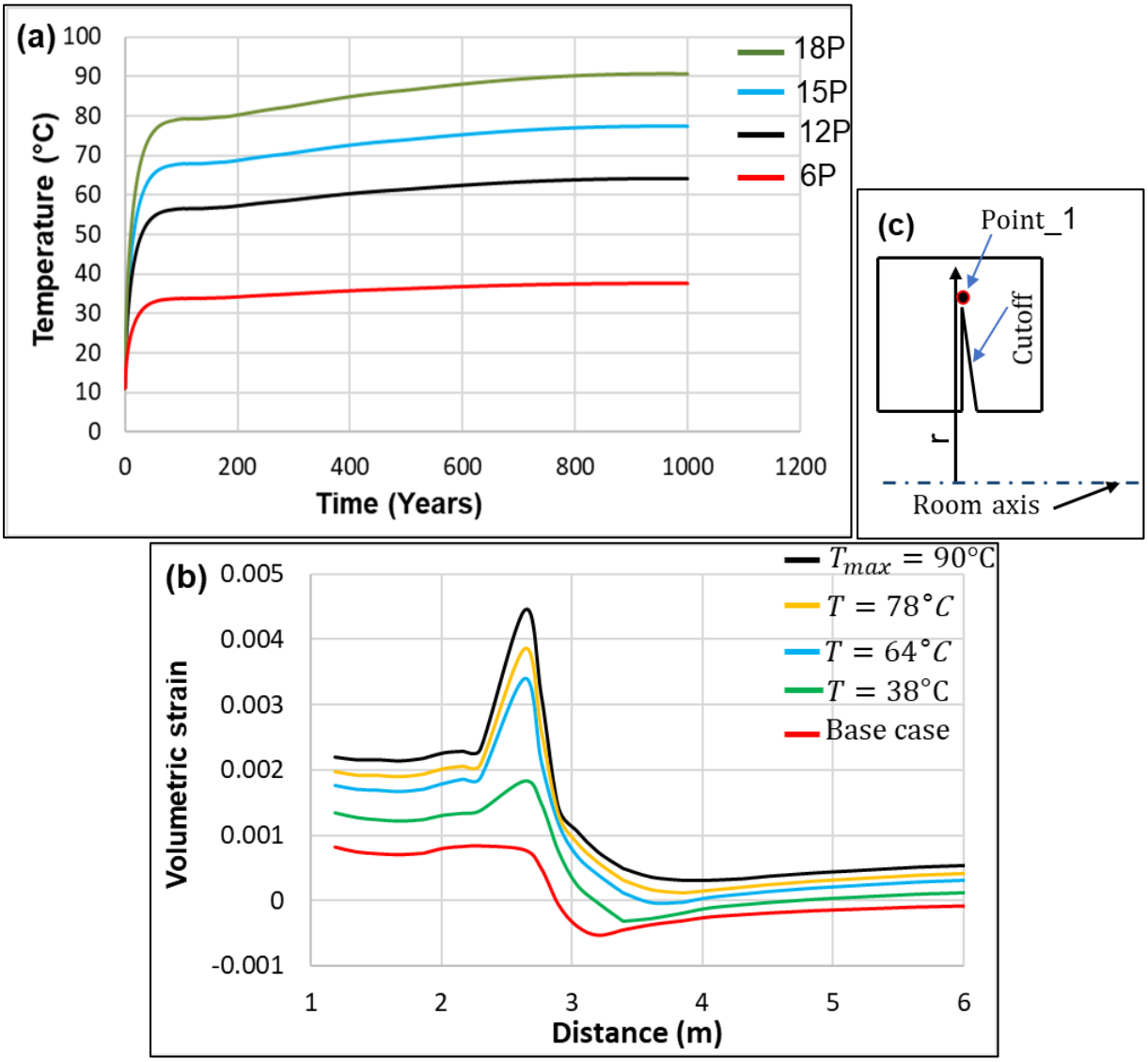

Fig. 5.11 (a) Evolution of rock mass temperature at Point_1 from the thermo-mechanical model. P represents the actual power of the canister. (b) Volumetric strain before and after rock mass heating. (c) Description of Point_1 and Distance (r) used for figures (a) and (b)

The variation of rock mass temperature at Point_1 for different canister powers is shown in Fig. 5.11 (a). Temperatures increase exponentially for the initial 50 years and then increase slowly thereafter. The increase in temperature was found to be negligible after 1000 years, so the analysis was stopped at this point in numerical time. Rock mass temperatures of 38 ^{o}C are observed at Point_1 for a canister power of 6 times the actual power, 64 ^{o}C for 12 times, 78 ^{o}C for 15 times, and 90 ^{o}C for 18 times the actual canister power, respectively, as observed in Fig. 5.11 (a).

The extent of EDZi increased by 0.25 m and 0.72 m after heating when the rock mass temperatures at Point_1 reached 38 ^{o}C and 64 ^{o}C, respectively. The increase in temperature caused an increase in the principal stresses and volumetric strain, which caused an increase in the EDZi. Fig. 5.11 (b) indicates changes in the rock mass dilation before and after heating along a line perpendicular to the room axis and parallel to the vertical side of the cutoff. The change in dilation due to thermal stress is more pronounced at the roof of the room, although the induced strains are higher at the tip of the cutoff due to high stress concentrations. It can be observed in Fig. 5.11 (b) that with an increase in temperature, the zone with negative (contracting) volumetric strain decreased and the volumetric strain became positive again after a certain distance beyond the plastic yield limit due to thermally induced strain. Negative volumetric strains within the plastic yield zone are not observed when the rock mass temperature at Point_1 is between 78 ^{o}C and 90 ^{o}C. This is due to the thermal expansion and the lack of resisting (backfill) material within the mechanical model that would be present in a real repository.

Further study is needed to determine what these numerical results mean in terms of the extent of disconnected or connected micro-fractures beyond the cut-off tip. The extent of EDZo is increased by 0.38 m, 0.61 m, 0.94 m, and 0.94 m after the rock mass temperature at Point_1 reached 38 ^{o}C, 64 ^{o}C, 78 ^{o}C, and 90 ^{o}C, respectively. It should be noted that the numerical increase in EDZo when the temperatures surpassed 78 ^{o}C is less than 0.1 m based on the size of the model zones; specifically, the zones are 0.1 m thick and therefore this is the limiting factor. The induced thermal stresses caused an overall increase in thermo-mechanical stresses which caused an increase in the number of plastically yielded elements and hence an increase in the EDZo size.

The results of the thermal and thermo-mechanical modelling were presented in this chapter. The thermo-mechanical behaviour of the cutoff was simulated using FLAC 3D. It was computationally impractical to simulate all the canisters present in the repository, therefore a placement room scale model was used to determine the maximum temperature at the cutoff. The computational time to simulate the placement room was 25 days, therefore, COMSOL is used to simulate the maximum possible temperature at the cutoff inside the repository. The maximum temperature from the COMSOL was recreated in FLAC 3D using a near field model to decrease the computational time. Finally, using the temperature history from COMSOL into FLAC 3D, the thermo-mechanical behaviour of the cutoff was simulated. The thermo-mechanical model showed a significant effect of temperature on the extent of EDZi and EDZo for the optimum cutoff.

Chapter 6: Result Discussion and Limitations

6.1 Introduction

This chapter analyzes the results of the mechanical and thermo-mechanical study in context to the past numerical modelling and empirical studies. Researchers conducted empirical studies in the past to predict the extent of damage zones around the underground excavations in hard rocks. The results of these studies are compared to the numerical modelling results from this study. In addition, the thermo-mechanical behaviour of underground nuclear waste repositories is studied by different researchers. The results of the thermo-mechanical model from this study are compared to the thermo-mechanical modelling results for the conceptual Canadian repository from the past studies.

This chapter also outlines different assumptions made for mechanical and thermo-mechanical modelling studies. Assumptions regarding the geometry of the numerical model selected for the mechanical and thermo-mechanical models are discussed. The important supposition regarding the constitutive model and thermo-mechanical properties used in the numerical model are also discussed.

The effect of important input parameters for the numerical model and their sensitivity to the numerical modelling results are discussed here. The size of the mesh is optimized by the sensitivity analysis to avoid errors due to discretization for both the mechanical and thermo-mechanical models.

6.2 Discussion of Results

A comprehensive comparison of normalized EDZo and EDZi dimensions predicted in this study from the past numerical and empirical studies by other researchers is shown in Fig. 6.1. The empirical depth of damage was proposed by Diederichs (2007) based on the data from underground excavations around the world. The empirical model under predicts the depth of damage as compared to the dimensions of the damage (EDZo) observed in this study for the lower values of σ_{max} to CI, however, it over predicts the depth of damage for higher values of σ_{max} to CI ratio (greater than 2.75). This is due to the fact the radial extent of EDZo increases in a non-linear

fashion as opposed to the linear model from Diederichs (2007) (Fig. 6.1). The depth is under-predicted for the lower values of σ_{max} to CI ratio as compared to higher values of the ratio. Perras and Diederichs (2016) used the DISL approach using a finite element method to determine the depth of different EDZs around a circular tunnel. The extent of normalized EDZi and EDZo from Perras and Diederichs (2016) are shown in Fig. 6.1 by the red and light blue color curves.

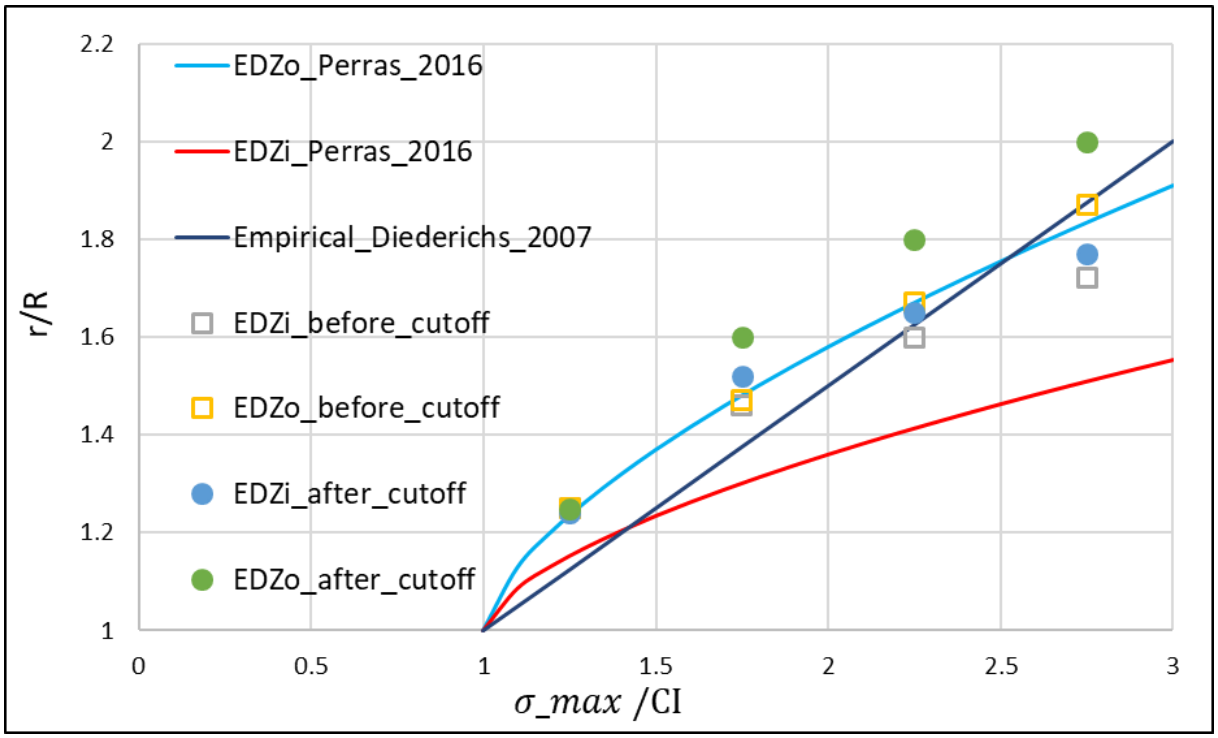

Fig. 6.1 The extent of EDZi and EDZo before and after the construction of the optimum trapezoidal cutoff from this study (data in circular and rectangular markers) in comparison with the past numerical and empirical studies.

The proposed depth of EDZo by Perras and Diederichs (2016) matched well with the depth of the EDZo from this study for the values of σ_{max} to CI ratio lower than a value of 2.5. However, the model from Perras and Diederichs (2016) under predicts the extent of EDZo for the σ_{max} to CI ratio greater than 2.5, while the empirical model by Diederichs (2007) accurately predicts the depth of EDZo for the σ_{max} to CI ratio greater than 2.5. The predicted depth of EDZi by Perras and Diederichs (2016) is observed lower than the depth of EDZi from this study. The difference in the values of the EDZi is attributed to the different modelling approaches used in the two studies. The DISL approach does not explicitly simulate the post-peak failure behaviour of the rock mass as simulated by the CWFS approach in FLAC 3D. The DISL approach does not explicitly simulate

the transition to the post-peak failure envelope in the same manner as the CWFS approach in FLAC 3D. In addition, the accurate simulation of dilation in the post-peak failure region is important to predict the dimensions of EDZi as the extent of EDZi is determined based on the volumetric strains. It can be observed that the extent of the normalized values of EDZi and EDZo before and after the construction of the cutoff is lower at the lower values of σ_{max} to CI ratio.

The optimum cutoff in this study is defined based on the criteria that it should induce a minimum increase in the pre-existing EDZi after the construction of the cutoff. Among the three cutoffs – trapezoid, triangular, and rectangular modelled in this study, the trapezoid shape cutoff with minimum aspect ratio was found optimum. Further study is needed to understand the change in EDZi for other shapes of the cutoffs. It was observed that for each shape of the cutoff, the increase in EDZi after the construction of the cutoff is minimum for lower values of aspect ratio (T by D ratio). Although the minimum value of aspect ratio would induce minimum increase in EDZi, it would impose limitations in terms of the constructability of the cutoff. These cutoffs can be constructed using controlled drilling and blasting, and wire sawing. Controlled drilling and blasting can induce damage in the rock mass which can be a potential path for radionuclide transport. Furthermore, controlled drilling and blasting will create irregular cutoff surfaces which can negatively affect the sealing capacity of backfill material. Grahm et al. (2015) noted that although the wire sawing method had a lower production rate compared to drilling, it created smooth cutoff surfaces and minimized the EDZs.

Guo (2017) studied the far field and near field thermal behaviour of the underground nuclear waste repository in the crystalline rock setting. For the far field thermal model, the whole repository is simulated by replacing the canisters in a panel with a uniformly distributed plate-shaped heat source. The thickness of the plate was equal to the vertical distance between the two left corners of the top and bottom dense backfill blocks (2m) in the placement room while the width and length of the plate are equal to the width and length of the panel. A maximum temperature of 71°C is observed at the centre of the repository panel after 78 years from the far field model. For the near field model, the repository was assumed infinite in the horizontal direction and a small portion of the placement room was simulated. The near field model included canisters, backfill material inside the placement room, and rock mass vertically above the placement room. A maximum

temperature of 84°C is observed at the surface of the canister after 45 years from the near field model. Radakovic-Guzina et al. (2015) simulated the far field and near field thermal behaviour of the underground nuclear waste repository for the sedimentary rock mass setting using a similar methodology as Guo (2017) but using finite difference simulator. A maximum temperature of 81°C is observed at the center of the repository panel from the far field model. A maximum temperature of 97°C is observed at the surface of the canister after 42 years from the near field model.

In this study, a finite element model was used to simulate the near field behaviour of the underground nuclear waste repository in the sedimentary rock mass setting using a similar methodology as used by Guo (2017) and Radakovic-Guzina et al. (2015). A maximum temperature of 98 °C is observed in the vicinity of the canister after 42 years from the near field model. A maximum temperature of 84 ^{o}C is observed at the tunnel roof after 57 years while a maximum temperature of 78 ^{o}C is observed inside the rock after 75 years (Fig. 5.2). The time for reaching the maximum temperature at all the points from the near field model matched well with the times predicted by Guo (2017) and Radakovic-Guzina et al. (2015). Moreover, the maximum temperature (98 °C) from the near field thermal model in this study matched well with the predicted temperature (97 °C) by Radakovic-Guzina et al. (2015).

For this study, the EDZi boundary was defined as the boundary in the plastic zone where the transition from the positive volumetric strain to negative volumetric strain occurs, this recommendation was based on the study from Perras and Diederichs (2017). At higher temperatures (beyond 78 °C), volumetric strain in the plastic zone became positive and the transition between positive to negative volumetric strain was not observed. This may represent that the extent of EDZi became equal to the extent of EDZo at higher temperatures. Further study is needed to determine what these numerical results mean in terms of the extent of disconnected or connected micro-fractures beyond the cut-off tip at temperatures higher than 78 °C.

6.3 Important Assumptions and Limitations

To optimize the shape and dimension of the cutoff, this study considered a circular placement room of radius 1m for the mechanical model. The effect of the size of the placement room should be

taken into consideration when simulating the actual placement room in the underground nuclear waste repositories. To minimize the errors due to the effect of size on the value of EDZs, the values of EDZs were normalized by the radius of the placement room for this study. Similarly, for the rectangular placement room in the mechanical model, the width and height of the placement room were 1 m which may differ based on the design requirements of the repository. However, for the thermo-mechanical model, the dimension of the placement room was considered equal to the dimension of the conceptual Canadian repository.

For the mechanical model, the liner was considered which provided additional support to the excavation surface. In the absence of the liner, the extent of EDZi will be more than the predicted value in this study. The liner was only used in the mechanical model; the thermo-mechanical model was simulated without the liner. This is because the mechanical modelling was a general modelling exercise to predict the EDZs and optimize the dimensions and shapes of cutoffs for underground excavations while the thermo-mechanical modelling exercise was to understand the thermo-mechanical behaviour of cutoff in underground nuclear waste repositories. The underground excavations in the underground nuclear waste repository will be constructed without the liner due to safety requirements.

The CWFS approach was used to simulate the brittle failure of the rock mass using the continuum finite difference numerical method. However, sometimes the brittle failure of the rock mass can be a discontinuum process or induced by a discontinuity in the rock mass. Simulation of progressive fracture initiation in rock mass and the rock mass interaction along the interface of the discontinuity can not be captured explicitly using the continuum models. The continuum models simulate the latter behaviour implicitly using the complex constitutive models for the rock mass material. The explicit simulation of progressive fracture initiation at grain scale and rock mass discontinuity interaction using discontinuum models can generate further insight into the nature of the brittle failure of the rock mass.

To simulate the variation of temperature with time in the rock mass surrounding the cutoff, a continuum finite element model was used. The model considered the rock mass homogenous up to a depth of 2500 m from the ground surface. This may not be true depending upon the geological

settings of the repository. Therefore, if the discontinuities such as faults and joints are present, the effect of inhomogeneity in the rock mass should be taken into consideration in the thermal numerical model to simulate representative temperature around the cutoff. Furthermore, given the size of the repository, it is computationally impractical to simulate all the canisters present in the repository to evaluate the actual temperature in the rock mass surrounding the cutoff.

The far field model can be used to simulate the maximum possible temperature at the center of the repository (Guo, 2017). However, the far field model does not simulate the placement room scale temperature in the repository. To simulate the temperature gradient along a vertical section of the placement room, the near field model can be used (Guo, 2017). The near field model can determine the temperature gradients along a vertical cross-section to the room but it can not simulate the temperature gradient along the longitudinal direction of the placement room. In order to determine the temperature gradients in the longitudinal direction of the placement room where cutoff will be located, a placement room scale model was used in this study. The placement room scale model simulates 100 canisters in the placement room so that the temperature at the last canister becomes the temperature at the center of the repository as observed in the near field model. This model assumed the vertical boundaries of the numerical model adiabatic similar to the near field model which may not be the case in the actual repository. In actual repository conditions, some of the heat will dissipate in the rock mass located outside of the repository as opposed to the whole heat reflecting from the adiabatic boundaries. The assumption of the adiabatic boundary conditions along the placement room will over predict the temperature at the cutoff and hence it will over predict the value of thermal stresses. The additional thermal stress will cause over prediction of EDZi therefore, the adiabatic boundary condition assumption was conservative. Furthermore, the spacing between different components of the placement room – between cutoff and canisters, and between canisters etc. will depend upon the type of the rock in which the repository is located. The larger the spacing between the canisters and cutoff, the lower will be the value of EDZi due to lower values of thermal stress in the vicinity of the cutoff. The effect of spacing was not considered in this study and therefore can be a potential area for future research.

Finally, this study did not consider the damage due to temperature in the CWFS approach. The CWFS approach was assumed to be independent of temperature. The thermal stresses were only

coupled with the mechanical stresses to determine the effect of temperature on the EDZs. Chen et al. (2018) carried out experiments on granite between the temperature 25 °C to 130 °C, and showed that the strength and brittleness of granite are dependent on the temperature. With the increase in temperature, the brittleness of granite increased at temperatures below 60 °C while it decreased at temperatures above 60 °C. It was also observed that below 60 °C, crack damage stress increased while the crack initiation stress decreased when the temperature rose. However, this trend was found opposite for the temperature values higher than 60 °C. Chen et al. (2018) concluded that the effect of temperature on the rock mass is dependent on the microscopic structure of the rock. This study was a general modelling exercise to understand EDZs evolution and cutoff mechanical behaviour for the underground excavations where the influence of temperature may or may not be present. Considering the effect of temperature in the constitutive model can generate further insight into the brittle damage of the rock mass which can help in accurate prediction of dimensions of EDZs as a function of temperature for underground excavations in repositories.

6.4 Sensitivity Analysis

The transition between different excavation damage zones in the field is continuous and it is difficult to measure the accurate depth for each damage zone. The size of the mesh plays an important role in deciding the dimensions of the damage zones because the gradual transition between the zones is represented by the mesh size. For the mechanical model, hexagonal elements were used in the numerical model to determine the dimensions of EDZs. The average side length of the mesh elements was set to 0.067 m at the placement room surface. The size of the mesh gradually increases moving away from the placement room surface. A fine mesh was adopted in the vicinity of the cutoff to improve depth resolution for damage zone determinations. The extent of EDZi for a mesh size of 0.067 m in the vicinity of the cutoff is shown in Fig. 6.2.

To understand the effect of mesh size on the extent of EDZi, different mechanical models without cutoff with mesh sizes 0.04 m, 0.05 m, 0.06 m, 0.08 m, 0.09 m, 0.1 m, and 0.2 m were solved. The variation of shear stress at the EDZi boundary (for the optimum cutoff) right above the cutoff with mesh size is shown in Fig. 6.3. It can be observed that the value of shear stress increases with decreasing the mesh size. After the mesh size of 0.067 m, the change in the value of shear stress

is negligible, therefore, the mesh size of 0.067 m was selected for the mechanical numerical model. It should be noted that the value of shear stress was plotted against mesh size instead of the EDZi. This is due to the fact that EDZi is calculated based on the volumetric strain and the nodal volumetric strain is determined based on the weighted average of the surrounding element values. The change in mesh size will change the volume of elements surrounding the node and therefore the volumetric strain at a point in the rock mass will depend upon the type of averaging method used to calculate the value of nodal volumetric strain. To avoid errors due to the type of averaging method on the sensitivity analysis, the values of shear stress were used to understand the effect of the mesh size.

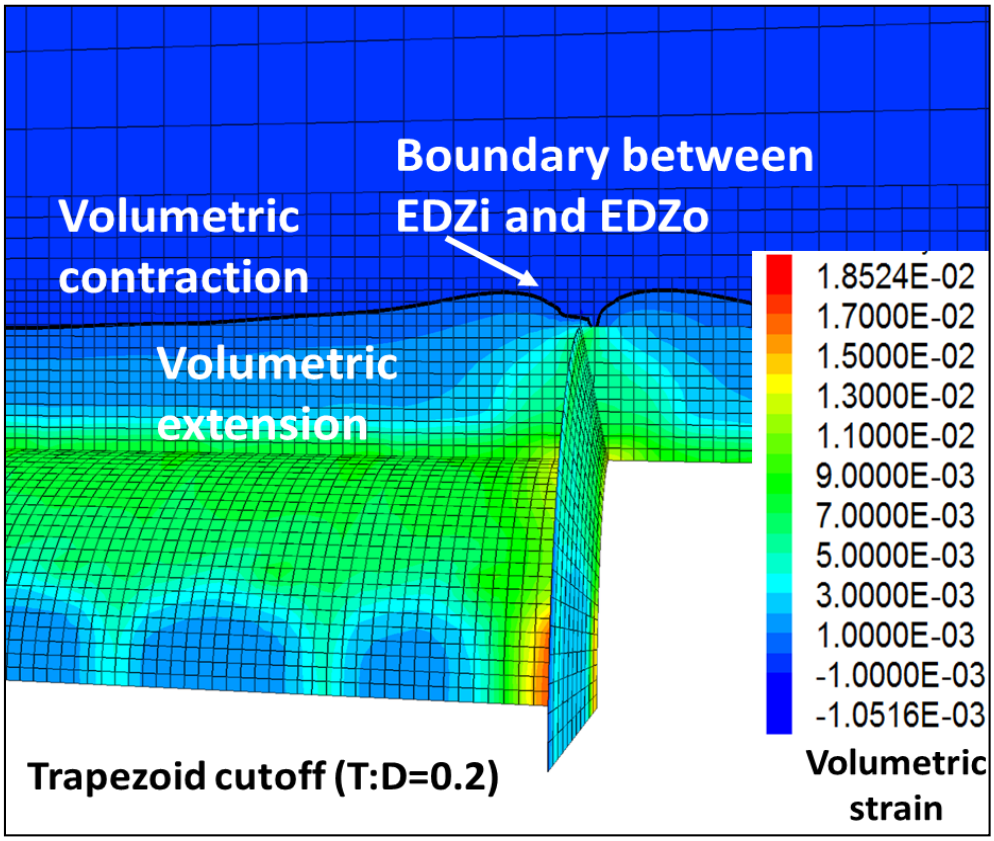

Fig. 6.2 Contours of volumetric strain and extent of the EDZi for the mesh size 0.067 m used for the mechanical model.

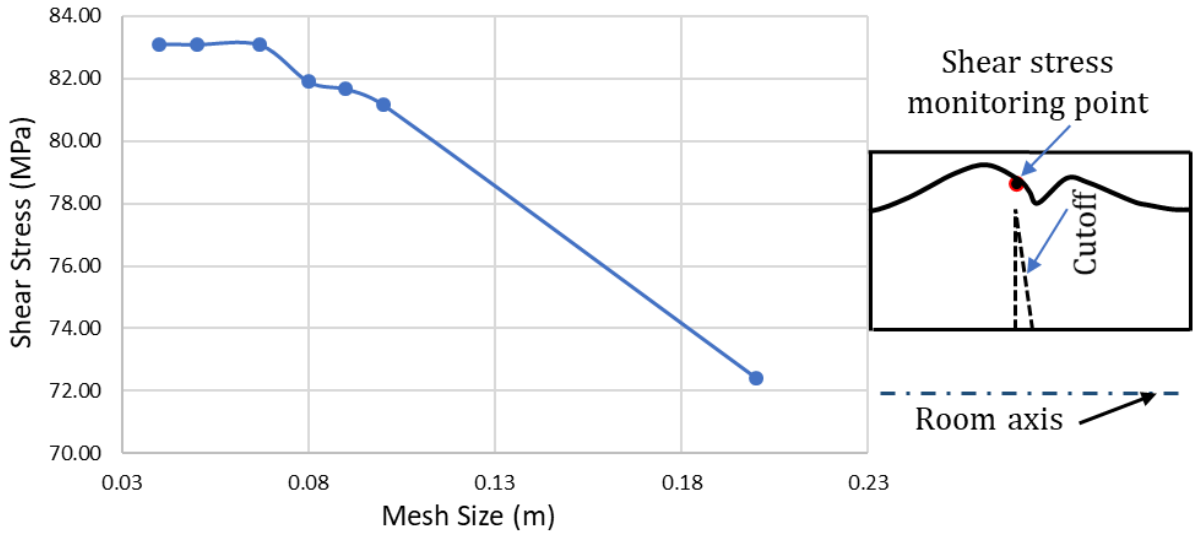

Fig. 6.3 Variation of shear stress with the size of the mesh around the tip of the cutoff for the mechanical model.

For the thermo-mechanical model, tetrahedral elements were used, the size of the mesh is 0.1 m in the surrounding of the cutoff and it increases moving away from the cutoff. The mesh size of 0.1 m was used for the thermo-mechanical model as opposed to the 0.067 m mesh size in the mechanical model. This is due to the large time (25 days) to solve the thermo-mechanical model. The fine mesh was used in the vicinity of the cutoff to improve the resolution of the EDZi measurement. The fine mesh was also used for the canisters in the placement room to accurately simulate the thermal gradients in the vicinity of the heat source (canister). The sensitivity analysis for the thermo-mechanical model was performed by solving the mechanical model at different sizes of a tetrahedral mesh. The contours of volumetric strain and dimension of EDZi for the model with a mesh size of 0.1 m are shown in Fig. 6.4.

The variation of shear stress as a function of mesh size is shown in Fig. 6.5. The value of shear stress increases with a decrease in the size of the mesh. A mesh size of 0.1 m was selected at the tip of the cutoff for the thermo-mechanical study. The size of the mesh increases on going away from the cutoff tip.

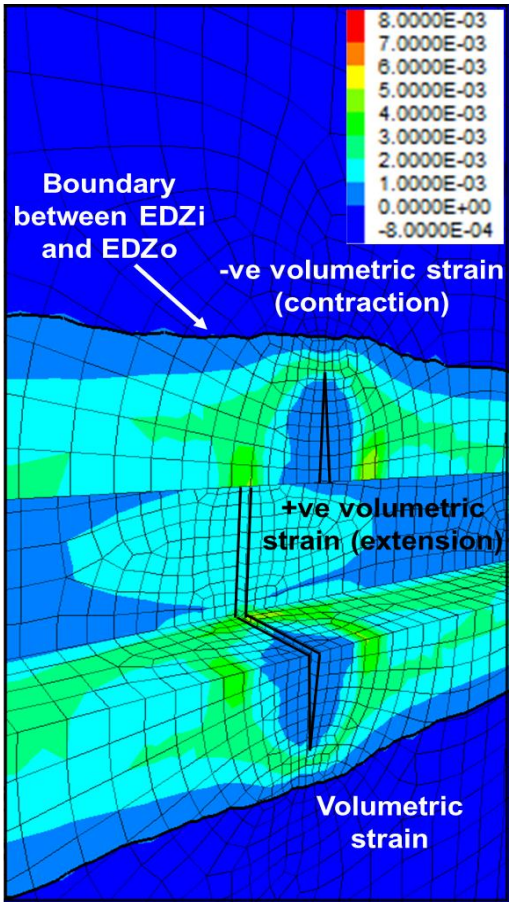

Fig. 6.4 Contours of volumetric strain and extent of the EDZi for the mesh size 0.1 m used for the thermo-mechanical model.

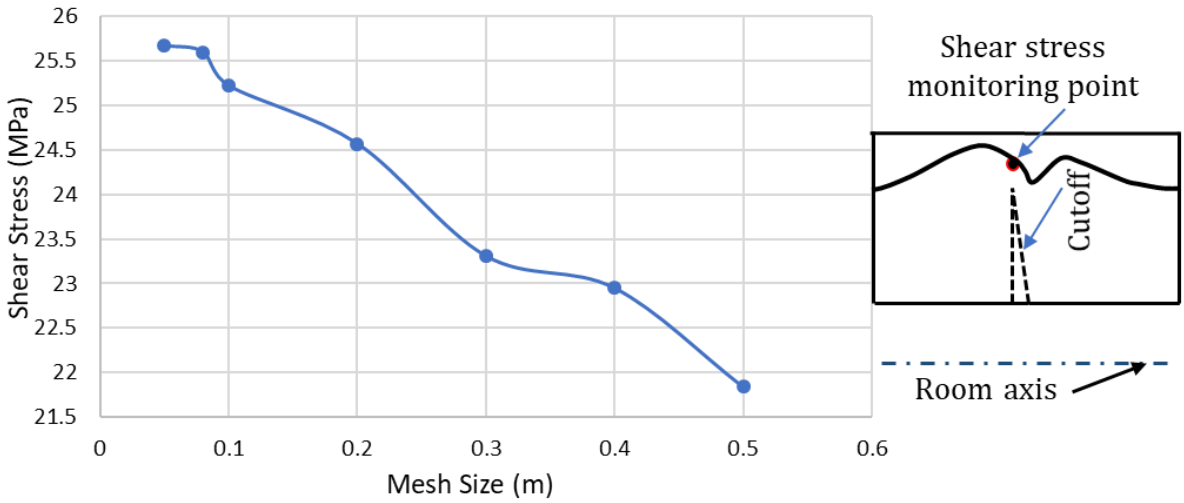

Fig. 6.5 Variation of shear stress with the size of the mesh around the tip of the cutoff for the thermo-mechanical model.

The results of thermal and thermo-mechanical modelling are analyzed in context with the previous studies in this chapter. The results from this study are compared with the results from the past empirical and numerical studies for both the thermal and thermo-mechanical behaviour of the underground excavations for the underground nuclear waste repositories. The limitations of the study are also discussed in this chapter. Finally, the sensitivity of mesh size on the results of the mechanical and thermo-mechanical models is presented here.

Chapter 7: Summary and Conclusions

7.1 Summary of Findings

According to the International Atomic Energy Commission, deep underground storage in a stable geological formation is a sustainable way to manage spent fuel and high-level waste (HLW) from nuclear power reactors (Dayal 2004). Typically, a deep geological repository (DGR) will contain several panels of rooms for nuclear fuel placement. When these placement rooms are constructed, different damage zones with connected and disconnected fractures are formed due to the excavation process and due to the in-situ stress redistribution around the excavation. The permeability of rock mass in EDZs is considerably increased due to an increase in the fracture density and hence EDZs can be potential pathways for radionuclide transport. Radionuclides such as radionuclides from the placement room can transport through HDZ and EDZi along the walls of the room. Engineered barriers such as cutoff seals are being considered to block the EDZs for the deep geological repository to minimize radionuclide transport. A cutoff is an excavation constructed perpendicular to the placement room axis that creates a cross-sectional enlargement of the excavation, which when filled with a sealing material such as bentonite, seals the EDZs. Cutoff seals are cutoff structures filled with a sealing material to prevent the potential migration of radionuclides within and around the room through EDZs. Conceptually, only the HDZ and EDZi need to be sealed using the cutoff structures, as beyond this region fractures are not connected to form a flow pathway. Therefore, the depth of the cutoff should be greater than or equal to the depth of EDZi before the cutoff construction.

This research developed a framework to help determine the dimension and shape of an optimum cutoff seal for underground excavations in DGRs for a wide range of geological scenarios based on the commercially available numerical modelling software. The framework consisted of three stages, first, determine the dimensions of EDZs induced due to the excavation of the placement room. Second, construct different shapes and dimensions of cutoff under different geological settings to seal the numerical dimensions of the EDZi and determine the optimum cutoff. Third, evaluate the effect of different variants such as shape and orientation of the placement room, rock mass properties, rock mass anisotropy, and temperature on the extent of EDZi and EDZo for the optimum cutoff (Sharma et al. 2019; Sharma et al. 2020). For the mechanical model analysis in

FLAC 3D, 140 models were solved in total and on average each model took 2 minutes to reach equilibrium. For the thermal model analysis in COMSOL, 4 models were solved and each model took approximately 5 hours to reach equilibrium. Similarly, for the thermo-mechanical model analysis in FLAC 3D, 4 models were solved and each model took approximately 25 days to reach equilibrium.

Results of the first stage of the study showed the extent of EDZs for a circular placement room located in granite at different depths. The depths of the numerical model were varied to induce different in-situ stresses around the placement room. The ratio between horizontal to vertical stress and between in-plane horizontal stresses was varied to analyze the damage zones in a wide range of in-situ stress conditions. The depth of different damage zones was predicted based on the magnitude of volumetric strain inside the plastic zone from the numerical model. The zone with positive volumetric strain within the plastic zone is termed as EDZi while the zone with negative volumetric strain within the plastic region is termed as EDZo. The positive volumetric strain shows a volumetric expansion of the rock while the negative volumetric strain shows volumetric contraction of the rock. From previous studies, it is evident that the positive volumetric strains are an indicator of the connected fractures (EDZi) (Perras and Diederichs, 2016). The extent of EDZi for the circular placement room is increased with the increase in the σ_{max} to CI ratio where σ_{max} is maximum stress along the placement room and CI is the crack initiation stress.

Based on the results of the EDZi from the first stage of the study, cutoffs with different shapes and dimensions were constructed in the second stage of the study. The depth of the cutoff was taken equal to the depth of EDZi and five widths of cutoffs were chosen such that to have an aspect ratio between 0.2 to 1. The pre-existing EDZi due to the excavation of the placement room is increased after the construction of the cutoff. The increase in EDZi is minimum for the trapezoid shape cutoff. Also, the increase in EDZi before and after the construction of the cutoff increases with an increase in the aspect ratio of the cutoff. The minimum increase in EDZi is found when the aspect ratio for the cutoff is minimum. Therefore, the optimum cutoff is considered with the minimum aspect ratio for each type of shape. For this study, the trapezoid shaped cutoff with an aspect ratio equal to 0.2 was considered optimum.

The results of the third stage of the study showed the effects of different variants such as shape and orientation of the placement room, rock mass properties, rock mass anisotropy, and temperature from the nuclear fuel on the extent of EDZo and EDZi for the optimum cutoff. For the given stress conditions in this study, the extent of EDZi before and after the construction of the optimum cutoff is approximately the same for the shaft and horizontal placement room. This is because the extent of EDZi depends on the ratio between the values of in-plane (xy) horizontal stresses. The in-plane ratio happens to induce approximately the same value of EDZi for the shaft and placement room for this study.

To understand the effect of rock mass anisotropy on the extent of EDZi and EDZo for the optimum cutoff, horizontal bedding planes were simulated in limestone and mudstone. The increase in EDZi before and after the construction of cutoff is more for the anisotropic rock mass as compared to the homogenous rocks. The presence of horizontal bedding planes causes failure along the weak plane in the rock mass which eventually causes a higher value of volumetric strain. The higher values of volumetric strain cause a higher extent of EDZi for the optimum cutoff located in anisotropic limestone and mudstone rock mass.

Three types of rocks, granite, limestone, and mudstone were used in the study to analyze the effect of rock mass properties on the extent of EDZo and EDZi for the optimum cutoff. Horizontal bedding planes were considered in mudstone and limestone while granite is considered intact to simulate the expected geological setting in DGR. The results showed that the increase in EDZi before and after the construction of the cutoff is highest for mudstone followed by limestone and granite. The presence of bedding planes causes shear failure along the weak planes in mudstone and limestone. The shear failure along the bedding planes induces higher values of dilatant volumetric strain and EDZi for mudstone followed by limestone and granite.

Interestingly, when the horizontal bedding planes were absent in limestone and mudstone the order of extent of EDZi before and after the construction of the cutoff is found the opposite to the latter case. The extent of EDZi is highest for granite followed by limestone and mudstone. This order is because of the difference in the values of strength and modulus of elasticity for the intact rocks. The extent of EDZi for intact rock depends on the ratio between the values of shear strength and

shear stress. The low value of the shear strength to shear stress ratio will induce a higher extent of the damage zone in the intact rock. The higher stiffness value for intact granite followed by intact limestone and mudstone induce higher values of shear stress in granite followed by limestone and mudstone. Although, the value of shear strength for intact granite is highest followed by intact limestone and mudstone, however, the higher values of shear stress in granite followed by limestone and mudstone cause a low value of the ratio between shear strength and shear stress for granite followed by limestone and mudstone. For the given strength and elastic properties for intact granite, limestone, and mudstone, the shear strength to shear stress ratio is lowest for granite followed by limestone and mudstone for this study. The lower values of strength to stress ratio induces higher values of EDZo and EDZi for intact granite as followed by limestone and mudstone.

In addition, to understand the effect of the shape of the placement room, the optimum cutoff with a rectangular placement room was simulated. The EDZi after the construction of the optimum cutoff is greater for the rectangular placement room as compared to the circular placement room. This happens because of the high stress concentration at the corners of the rectangular shape placement room. The high stress concentration causes a high value of dilatant volumetric strain and EDZi for the rectangular placement room even before the construction of the optimum cutoff as compared to the circular placement room with the optimum cutoff.

Finally, one important aspect of an underground nuclear waste repository is the heat generated from nuclear fuel which can influence the long-term safety requirements for the repository. In the domain of this study, the heat generated from nuclear fuel can induce the thermal stresses in the rock mass eventually influencing the values of EDZi. In order to understand the effect of heat from nuclear fuel, a thermo-mechanical model was used to simulate the response of the optimum cutoff. The results of the thermal model showed a maximum temperature of 72 ^{o}C in the rock mass surrounding the cutoff after 1000 years and a maximum temperature of 98 ^{o}C at the center of the repository panel for the crystalline rock mass setting. The increase in EDZi when the temperature of the rock mass around the cutoff is 64 ^{o}C was found to be 72 cm. The increase in temperature causes an increase in the shear stress due to additional thermal stress and eventually causing an increase in EDZi and EDZo.

7.2 Recommended Future Studies

In actual repository conditions, the cutoff will be filled with an impermeable backfill material such as bentonite. In this study, the placement room and cutoff were considered empty for the mechanical model. For the thermo-mechanical model, although the placement room and cutoff were considered empty in the mechanical model, they were present in the thermal model to simulate the representative temperature at the cutoff. The presence of backfill material, such as bentonite will provide support to the surface of the placement room and cutoff. When the groundwater will come in contact with bentonite, bentonite will swell and will provide additional normal traction due to the swelling pressure to the surface of the placement room and cutoff. The normal traction from swelling pressure to the placement room surface will help the rock mass sustain the tensile stresses induced from the excavation of the rock mass and heat from the nuclear fuel. This process will eventually cause a decrease in the extensile volumetric strain and hence the extent of EDZi, therefore, the dimension of EDZi was over predicted in this study. This study did not consider the effect of swelling pressure on the extent of EDZo and EDZi for the cutoff. The effect of swelling pressure on the extent of EDZo and EDZi for the cutoff can be one area of future research.

The safety requirements for a repository includes that it should be working for a time until nuclear fuel comes to a safe level of radioactivity. Given the long half-life period of some of the radionuclides, the repository is planned for a life period of 1 million years. The strength of the rock mass will decay with time and the magnitude of decay will be considerable for such a long life cycle of the repository. This study did not simulate the strength degradation of the rock mass with time. The decrease in rock mass strength with time will cause an increase in EDZo and EDZi for the placement room. Therefore, the effect of strength degradation with time on the extent of EDZo and EDZi for the cutoff can be one more area of future research.

The presence of groundwater is an important aspect of the design of underground nuclear waster repositories. The presence of groundwater provides a potential path for advective radionuclide transport. Furthermore, the pore water pressure from groundwater can induce fracturing in the rock mass due to induced tensile stresses from the water pressure, and these fractures can be a potential

path for radionuclides. From the cutoff design perspective, the groundwater pressure will aid in inducing the tensile failure in the rock mass surrounding the cutoff. The hydraulically induced tensile fractures in the rock mass can increase the pre-existing extent of EDZi. This study did not simulate the hydraulic behaviour of the rock mass where the cutoff is located. The effect of groundwater pressure on the extent of EDZo and EDZi for the cutoff can be one area of future research. Furthermore, the hydraulic modelling of the rock mass can be useful to understand the flow of water within the EDZi. This can be important to determine the quantity of water flow and radionuclide transport through the EDZi where connected fractures are present.

Given the long life cycle of the underground nuclear waste repository, it is important to consider the effect of a potential ice age in the future on the repository design. The thick ice sheet on the earth's surface will cause additional stress on the repository. Furthermore, the glaciation can cause induced seismic events affecting the safety requirements for the repository design. The additional stress from the weight of the ice sheet will cause an increase in the stress in the rock mass around the cutoff. The increase in stress can cause an increase in pre-existing EDZi. The effect of the glaciation cycle on the extent of EDZo and EDZi for the optimum cutoff can be a future area of research.

Although this study included the effect of horizontal bedding planes on the extent of EDZo and EDZi for the optimum cutoff, the effect of explicit joints such as major faults of any direction was not considered here. If the placement room will be located in a geological disturbed area, it is important to simulate joints and faults explicitly in order to understand the effect of the joint on the extent of EDZo and EDZi for the cutoff. The effect of a joint and fault and their orientation on the extent of EDZo and EDZi for the optimum cutoff can be a future area of research, as it will be important to cutoff sections of a repository which encounter such structures.

7.3 Conclusions

This study was aimed to understand the design of a cutoff for underground nuclear waste repositories based on the excavation damage zones using the continuum numerical modelling. Different shapes and dimensions of the cutoff were simulated to seal the numerically determined dimensions of the damage zones where connected fractures are present. Based on numerical

modelling results, the trapezoid shape cutoff with a minimum aspect ratio is found to have a minimum increase in the EDZi before and after the construction of the cutoff. For the same aspect ratio for the cutoffs, the trapezoid cutoff has the minimum increase in the EDZi before and after the construction of the cutoff. In general, all shapes of cutoffs, trapezoidal, triangular, and rectangular have a minimum increase in the EDZi before and after the construction of the cutoff for the minimum aspect ratio. Therefore, the trapezoidal shape cutoff with a minimum aspect ratio was selected optimum in this study for further analysis to understand the effect of different variants on the extent of EDZo and EDZi for the optimum cutoff.

The extent of EDZi for the optimum cutoff for the placement room and the shaft is approximately the same for the given stress conditions in this study. The extent of EDZi for the optimum cutoff when it is located in the homogenous rock mass is lower than the extent of EDZi for the cutoff for rock mass with horizontal bedding planes. Interestingly, the extent of EDZi for the optimum cutoff is found lower for the cutoff located in mudstone followed by limestone and granite when there are no bedding planes in mudstone and limestone. This is because of the difference in the physical and mechanical properties of the rock mass and the absence of the weak planes. However, the extent of EDZi for the optimum cutoff is found lower for the granite followed by limestone and mudstone when the bedding planes are present in limestone and mudstone rock mass. The presence of the bedding planes causes shear failure along the bedding planes causing an increase in the EDZi before and after the construction of the optimum cutoff. Furthermore, the extent of EDZi for the optimum cutoff is lower for the circular placement room as compared to the rectangular placement room because of the additional stress concentration along the corners in the rectangular shape placement room.

The finite element method was used to understand the effect of temperature from the spent nuclear fuel on the extent of EDZi and EDZo for the cutoff. The thermal modelling of the placement room showed that the maximum temperature at the cutoff is 71 ^{o}C after 1000 years of the placement of the nuclear fuel. A temperature of 64 ^{o}C from the spent nuclear fuel causes an increase in the EDZi by 72 cm for the optimum cutoff over the mechanical only model. The temperature from spent nuclear fuel causes an increase in the thermo-mechanical stress causing an increase in the EDZi.

This study developed a numerical modelling framework to understand the excavation damage zones around underground excavations, especially for the underground nuclear waste repositories. The study also outlined a numerical modelling framework to decide the optimum shape and dimensions of the cutoff based on the numerical dimensions of the excavation damage zones where connected fractures are present. Moreover, the study helped in understanding the effects of different variants, such as shape and orientation of placement room, rock mass properties, rock mass anisotropy, and heat from the nuclear fuel using numerical modelling. Finally, the study recommended areas such as the effect of groundwater, glaciation cycle, and rock mass strength degradation with time on the extent of EDZo and EDZi for the optimum cutoff for further investigation in the future.

References

Ababou, R., Valera, I.C. and Poutrel, A., 2011. Macro-permeability distribution and anisotropy in a 3D fissured and fractured clay rock:'Excavation Damaged Zone'around a cylindrical drift in Callovo-Oxfordian Argilite (Bure). Physics and Chemistry of the Earth, Parts A/B/C, 36(17-18), pp.1932-1948.

Akgün, H. and Daemen, J.J., 1999. Design implications of analytical and laboratory studies of permanent abandonment plugs. Canadian geotechnical journal, 36(1), pp.21-38.

Alejano, L.R., and Alonso, E., 2005. Considerations of the dilatancy angle in rocks and rock masses. International Journal of Rock Mechanics and Mining Sciences, 42(4), pp.481-507.

Alonso J, Becker DA, Storck R, Besnus F, Pellegrini D, Serres C, Vieno T, Norman H, Johnson L, Hart J, Marivoet J (2004) Bentonite barriers in integrated performance assessment (BENIPA). European Commission EC.

ANDRA, 2020. Project siting and facilities overview (https://international.andra.fr/projects/cigeo/cigeos-facilities-and-operation/project-siting-and-facilities-overview).

Mathers, W.G. and Atomic Energy of Canada Limited, 1985. HOTROK, A program for calculating the transient temperature field from an underground nuclear waste disposal vault. Whiteshell Nuclear Research Establishment.

Aubertin, M., Li, L. and Simon, R., 2000. A multiaxial stress criterion for short-and long-term strength of isotropic rock media. International Journal of Rock Mechanics and Mining Sciences, 37(8), pp.1169-1193.

Auld, F.A., 1996. Design of underground plugs. In Sealing of Boreholes and Underground Excavations in Rock (pp. 225-266). Springer, Dordrecht.

Avis, J., Suckling, P., Calder, N., Walsh, R., Humphreys, P. and King, F., 2014. T2GGM: a coupled gas generation model for deep geological disposal of radioactive waste. Nuclear Technology, 187(2), pp.175-187.

Bäckblom, G., 2008. Excavation damage and disturbance in crystalline rock-results from experiments and analyses (No. SKB-TR--08-08). Swedish Nuclear Fuel and Waste Management Co.

Barcena, I., Llamas, B., Bueno, J., Garcia-Sineriz, J.L., Suso, B.A. and Arduengo, B., 2005. Plug construction to isolate active zones of inactive zones in coal mine: WATERCHEM Project. In Proc. 9th International Mine Water Congress.

Barnichon, J.D. and Deleruyelle, F., 2009. Sealing experiments at the Tournemire URL. Towards convergence of technical nuclear safety practices in Europe, EUROSAFE.

Baumgartner, P., Tran, T.V. and Burgher, R., 1994. Sensitivity analyses for the thermal response of a nuclear fuel waste disposal vault. Atomic Energy of Canada Limited.

Bergh-Christensen, J., 1989. High pressure plugs for hydroelectric projects, Review and design and operational experiences in Norway. pp 463–470.

Blaheta, R., Byczanski, P., Čermák, M., Hrtus, R., Kohut, R., Kolcun, A., Malík, J. and Sysala, S., 2013. Analysis of Äspö Pillar Stability Experiment: Continuous thermo-mechanical model development and calibration. Journal of Rock Mechanics and Geotechnical Engineering, 5(2), pp.124-135.

Blümling, P., Bernier, F., Lebon, P. and Martin, C.D., 2007. The excavation damaged zone in clay formations time-dependent behaviour and influence on performance assessment. Physics and Chemistry of the Earth, Parts A/B/C, 32(8-14), pp.588-599.

Brawner, C.O., Bruce, D.A. and Littlejohn, G.S., 2005. Intruded Concrete Plugs in a Deep Gold Mine: An Exercise in Quality Control, Assurance, and Performance Verification. In Innovations in Grouting and Soil Improvement (pp. 1-15).

Bruce, D.A., Wells, M.F. and Venter, J., 2006. Construction of permanent intruded plugs at South Deep Gold Mine. Journal of the Southern African Institute of Mining and Metallurgy, 106(5), pp.343-350.

Carfora, D.J., 2012. Building a Sustainable Energy Future: Offering a Solution to the Nuclear Waste Disposal Problem through Processing and the Rebirth of Yucca Mountain. Tex. J. Oil Gas & Energy L., 8, p.143.

Carter, T.G., Diederichs, M.S. and Carvalho, J.L., 2008. Application of modified Hoek-Brown transition relationships for assessing strength and post yield behaviour at both ends of the rock competence scale. Journal of the Southern African Institute of Mining and Metallurgy, 108(6), pp.325-338.

Chandler, N.A., Martino, J., Dixon, D.A., 2002a. The Tunnel Sealing Experiment. In Trans. 6th International Workshop on Design and Construction of Final Repositories: Backfilling in Radioactive Waste Disposal. ONDRAF/NIRAS, Brussels, Belgium, 2002 March 11–13.

Chandler, N., Cournut, A., Dixon, D., Fairhurst, C., Hansen, F., Gray, M., Hara, K., Ishijima, Y., Kozak, E., Martino, J., Masumoto, K., McCrank, G., Sugita, Y., Thompson, P., Tillerson, J., Vignal, B., 2002b. The five year report of the Tunnel Sealing Experiment: an international project of AECL, JNC, ANDRA and WIPP. Atomic Energy of Canada Limited Report AECL-12127.

Chen, G., Wang, J., Li, J., Li, T. and Zhang, H., 2018. Influence of temperature on crack initiation and propagation in granite. International Journal of Geomechanics, 18(8), p.04018094.

COMSOL, (2015). Heat Transfer Module User's Guide. Version COMSOL 5.1.

Csullog, G.W., Bell, M.J., Pozdniakov, I., Petison, G. and Kostitsin, V., 2002. The IAEA's Net Enabled Waste Management Database: Overview and current status (No. IAEA-CN--90).

Dadashzadeh, N., 2020. Reliability of Stress Induced Damage Predictions in Hard Rocks With Continuum and Discontinuum Numerical Modelling Approaches. Phd thesis, Queens University. http://hdl.handle.net/1974/27630

Damjanac, B. and Fairhurst, C., 2010. Evidence for a long-term strength threshold in crystalline rock. Rock Mechanics and Rock Engineering, 43(5), pp.513-531.

Dayal, R., 2004. Disposal options for disused radioactive sources. Proc. WM, 4.

Diederichs, M.S., 2003. Manuel rocha medal recipient rock fracture and collapse under low confinement conditions. Rock Mechanics and Rock Engineering, 36(5), pp.339-381.

Diederichs, M.S., 2007. The 2003 Canadian Geotechnical Colloquium: Mechanistic interpretation and practical application of damage and spalling prediction criteria for deep tunnelling. Canadian Geotechnical Journal, 44(9), pp.1082-1116.

Diederichs, M.S., Kaiser, P.K. and Eberhardt, E., 2004. Damage initiation and propagation in hard rock during tunnelling and the influence of near-face stress rotation. International Journal of Rock Mechanics and Mining Sciences, 41(5), pp.785-812.

Dixon, D., Chandler, N., Graham, J. and Gray, M.N., 2002. Two large-scale sealing tests conducted at Atomic Energy of Canada's underground research laboratory: the buffer-container experiment and the isothermal test. Canadian Geotechnical Journal, 39(3), pp.503-518.

Dixon, D.A. and Martino, J.B., 2005. Testing of a bentonite-based tunnel seal for use in a deep geological repository: the tunnel sealing experiment (1998–2004). Proceedings of Waste Management, Decommissioning and Environmental Restoration for Canada's Nuclear Activities:"Current Practices and Future Needs", Ottawa, Ontario, Canada.

Dixon, D.A., Börgesson, L., Gunnarsson, D. and Hansen, J., 2009. Plugs for deposition tunnels in a deep geological repository in granitic rock. Concepts and experience (No. SKB-R--09-50). Swedish Nuclear Fuel and Waste Management Co.

Djahanaguiri, F. and Abel, J.F., 1997. Design and construction of a bulkhead for a simulated underground leaching stope. TRANSACTIONS-SOCIETY FOR MINING METALLURGY AND EXPLORATION INCORPORATED, 302, pp.1-57.

Durant, D., 2006. Managing expertise: performers, principals, and problems in Canadian nuclear waste management. Science and Public Policy, 33(3), pp.191-204.

Efremenkov, V.M., 2003. Chemistry and technology of radioactive waste management—the IAEA perspective. Czechoslovak Journal of Physics, 53(1), pp.A579-A587.

Eloranta, P., Simonen, A. and Johansson, E., 1992. Creep in crystalline rock with application to high level nuclear waste repository (No. YJT--92-10). Voimayhtioeiden Ydinjaetetoimikunta.

Enzell, J. and Malm, R., 2019. Full-scale test of the Dome Plug for KBS-3V deposition tunnels. Project summary and evaluation of the final results.

Fabian, D., Peter, C., Daniel, B. and Torsten, G., 2007. Evaluation of damage-induced permeability using a three-dimensional Adaptive Continuum/Discontinuum Code (AC/DC). Physics and Chemistry of the Earth, Parts A/B/C, 32(8-14), pp.681-690.

Fairhurst, C., Gera, F., Gnirk, P., Gray, M., Stillborg, B., 1993. OECD/NEA International Stripa Project Overview Volume I: Executive Summary. (SKB), ISBN 91-971906-2-4, Svensk Kärnbränslehantering AB.

Findlay, T., 2010. The future of nuclear energy to 2030 and its implications for safety, security and nonproliferation. Centre for International Governance Innovation.

Frank Garisto, 2018. Seventh Case Study: Features, Events and Processes. Nuclear Waste Management Organization, NWMO TR-2018-15.

Fuenkajorn, K. and Daemen, J.J., 2012. Sealing of boreholes and underground excavations in rock. Springer Science & Business Media.

Gens, A., Guimaraes, L.D.N., Garcia-Molina, A. and Alonso, E.E., 2002. Factors controlling rock–clay buffer interaction in a radioactive waste repository. Engineering geology, 64(2-3), pp.297-308.

Gnirk, P., 1993. OECD/NEA International Stripa Project Overview Volume II: Natural Barriers. (SKB), ISBN 91-971906-3-2, Svensk Kärnbränslehantering AB.

Grahm, P., Karlzén, R., 2015. System design of Dome Plug. Experiences from full-scale wire sawing of a slot abutment for the KBS-3V deposition tunnel plug. SKB R-14-24, Svensk Kärnbränslehantering AB.

Gray, M.N., 1993. OECD/NEA International Stripa Project Overview Volume III: Engineered Barriers. (SKB), ISBN 91-971906-4-0, Svensk Kärnbränslehantering AB.

Gunnarsson, D. and Borgesson, L., 2002. Development of a tunnel backfilling concept for nuclear waste disposal. In Clays in natural and engineered barriers for radioactive waste confinement. Experiments in underground laboratories.

Gunnarsson, D. and Borgesson, L., 2003. Development of a tunnel backfilling concept for nuclear waste disposal. In Clays in natural and engineered barriers for radioactive waste confinement. Experiments in underground laboratories.

Guo, R., 2011. Thermohydromechanical modelling of the buffer/container experiment. Engineering geology, 122(3-4), pp.303-315.

Guo, R., 2017. Thermal response of a Canadian conceptual deep geological repository in crystalline rock and a method to correct the influence of the near-field adiabatic boundary condition. Engineering Geology, 218, pp.50-62.

Hagros, A., Johansson, E. and Hudson, J.A., 2008. Time dependency in the mechanical properties of crystalline rocks. A literature survey (No. POSIVA-WR--08-68). Posiva Oy.

Hajiabdolmajid, V. and Kaiser, P., 2003. Brittleness of rock and stability assessment in hard rock tunneling. Tunnelling and Underground Space Technology, 18(1), pp.35-48.

Hajiabdolmajid, V., Kaiser, P. and Martin, C.D., 2003. Mobilised strength components in brittle failure of rock. Geotechnique, 53(3), pp.327-336.

Hajiabdolmajid, V., Kaiser, P.K. and Martin, C.D., 2002. Modelling brittle failure of rock. International Journal of Rock Mechanics and Mining Sciences, 39(6), pp.731-741.

Harrison, J.P., Hudson, J.A. and Popescu, M.E., 2002. Engineering rock mechanics: Part 2. Illustrative worked examples. Appl. Mech. Rev., 55(2), pp.B30-B31.

Harteis, S.P., Dolinar, D.R. and Taylor, T.M., 2008. Guidelines for permitting, construction, and monitoring of retention bulkheads in underground coal mines.

Hoek, E. and Brown, E.T., 1997. Practical estimates of rock mass strength. International journal of rock mechanics and mining sciences, 34(8), pp.1165-1186.

Hökmark, H., Ledesma, A., Lassabatere, T., Fälth, B., Börgesson, L., Robinet, J.C., Sellali, N. and Sémété, P., 2007. Modelling heat and moisture transport in the ANDRA/SKB temperature buffer test. Physics and Chemistry of the Earth, Parts A/B/C, 32(8-14), pp.753-766.

Hökmark, H., Lönnqvist, M. and Fälth, B., 2010. THM-issues in repository rock. Thermal, mechanical, thermo-mechanical and hydro-mechanical evolution of the rock at the Forsmark and Laxemar sites (No. SKB-TR--10-23). Swedish Nuclear Fuel and Waste Management Co.

Holt, E. and Koho, P., 2016. POPLU Experiment Summary Report. DOPAS Work Package, 4.

Hou, Z., 2003. Mechanical and hydraulic behavior of rock salt in the excavation disturbed zone around underground facilities. International Journal of Rock Mechanics and Mining Sciences, 40(5), pp.725-738.

Hudson, J.A., Bäckström, A., Rutqvist, J., Jing, L., Backers, T., Chijimatsu, M., Christiansson, R., Feng, X.T., Kobayashi, A., Koyama, T. and Lee, H.S., 2009. Characterising and modelling the excavation damaged zone in crystalline rock in the context of radioactive waste disposal. Environmental geology, 57(6), pp.1275-1297.

Hydrocarbons Technology, Haje Underground Gas Storage, 2020. Retrieved from https://www.hydrocarbonstechnology.com/projects/haje-underground-gas-storage/

IAEA, 1994. Classification of radioactive waste–A safety guide.

Itasca (2012) Fast Lagrangian analysis of continua in 3 dimensions, Version 5.0. Minneapolis, Minnesota, Itasca Consulting Group, 438.

Itasca Consulting Group Inc., 2014. User Manual, UDEC (Universal Distinct Element Code).

Itasca, 2003. PFC3D Manual – Theory and Background. Minneapolis.

Itasca. 2011. Long-Term Geomechanical Stability Analysis. Itasca report to the Nuclear Waste Management Organization NWMO DGR-TR-2011-17, Toronto, Canada.

Kaláb, Z., Šílený, J. and Lednická, M., 2017. Seismic stability of the survey areas of potential sites for the deep geological repository of the spent nuclear fuel. Open Physics, 15(1), pp.486-493.

King, F., 2013. Consequences of the general corrosion of carbon steel used fuel containers for gas generation in a DGR. Nuclear Waste Management Organization, NWMO TR-2013-16, Canada.

Kirkwood, D.T. and Wu, K.K., 1995. Technical considerations for the design and construction of mine seals to withstand hydraulic heads in underground mines. PREPRINTS-SOCIETY OF MINING ENGINEERS OF AIME.

Klemme, J., 1979. Conversion of the abandoned potash mine Wilhelmine--Carlsgluck in Hulsen--Verden, West Germany, to crude oil storage. In Situ;(United States), 3(2).

Kojo, M., Kari, M. and Litmanen, T., 2010. The socio-economic and communication challenges of spent nuclear fuel management in Finland: the post site selection phase of the repository project in Eurajoki. Progress in Nuclear Energy, 52(2), pp.168-176.

Koyama, T., Chijimatsu, M., Shimizu, H., Nakama, S., Fujita, T., Kobayashi, A. and Ohnishi, Y., 2013. Numerical modelling for the coupled thermo-mechanical processes and spalling phenomena in Äspö Pillar Stability Experiment (APSE). Journal of Rock Mechanics and Geotechnical Engineering, 5(1), pp.58-72.

Kwon, S., Min, K.B. and Stephansson, O., 2016. An Introduction to the Expansion Plan of the Underground Repository of Low-and Intermediate-level Radioactive Waste In Forsmark, Sweden. Tunnel and Underground Space, 26(5), pp.339-347.

Lanyon, G.W., 2011. Excavation damaged zones assessment. NWMO DGR-TR, 21.

Li, L., Aubertin, M., Simon, R. and Bussière, B., 2005. Formulation and application of a general inelastic locus for geomaterials with variable porosity. Canadian Geotechnical Journal, 42(2), pp.601-623.

Lidskog, R. and Sundqvist, G., 2004. On the right track? Technology, geology and society in Swedish nuclear waste management. Journal of risk research, 7(2), pp.251-268.

Lisjak, A., Garitte, B., Grasselli, G., Müller, H.R. and Vietor, T., 2015. The excavation of a circular tunnel in a bedded argillaceous rock (Opalinus Clay): short-term rock mass response and FDEM numerical analysis. Tunnelling and Underground Space Technology, 45, pp.227-248.

Lisjak, A., Tatone, B.S., Mahabadi, O.K., Grasselli, G., Marschall, P., Lanyon, G.W., De La Vaissière, R., Shao, H., Leung, H. and Nussbaum, C., 2016. Hybrid finite-discrete element

simulation of the EDZ formation and mechanical sealing process around a microtunnel in Opalinus Clay. Rock Mechanics and Rock Engineering, 49(5), pp.1849-1873.

Littlejohn, G.S. and Swart, A.H., 2006. Design of permanent intruded plugs at South Deep Gold Mine. Journal of the Southern African Institute of Mining and Metallurgy, 106(5), pp.331-341.

Lydmark, S., 2010. Aespoe Hard Rock Laboratory. Prototype Repository. Analyses of microorganisms, gases and water chemistry in buffer and backfill, 2009 (No. SKB-IPR--10-04). Swedish Nuclear Fuel and Waste Management Co.

Mahabadi, O.K., Lisjak, A., Munjiza, A. and Grasselli, G., 2012. Y-Geo: new combined finite-discrete element numerical code for geomechanical applications. International Journal of Geomechanics, 12(6), pp.676-688.

Martin, C.D. and Chandler, N.A., 1994, December. The progressive fracture of Lac du Bonnet granite. In International journal of rock mechanics and mining sciences & geomechanics abstracts (Vol. 31, No. 6, pp. 643-659). Pergamon.

Martin, C.D. and Christiansson, R., 2009. Estimating the potential for spalling around a deep nuclear waste repository in crystalline rock. International Journal of Rock Mechanics and Mining Sciences, 46(2), pp.219-228.

Martin, C.D., Kaiser, P.K. and McCreath, D.R., 1999. Hoek-Brown parameters for predicting the depth of brittle failure around tunnels. Canadian Geotechnical Journal, 36(1), pp.136-151.

Martino, J.B., Dixon, D.A., Keith, S.G., Chandler, N.A., Kjartanson, B.H., 2003. Sealing studies at the URL, Proceedings of the 56th Canadian Geotechnical Conference, Winnipeg, Canada, Sept. 29 – Oct. 1, 2003.

Martino, J.B. and Chandler, N.A., 2004. Excavation-induced damage studies at the underground research laboratory. International Journal of Rock Mechanics and Mining Sciences, 41(8), pp.1413-1426.

Masumoto, K., Sugita, Y., Fujita, T., Martino, J.B., Kozak, E.T. and Dixon, D.A., 2007. A clay grouting technique for granitic rock adjacent to clay bulkhead. Physics and Chemistry of the Earth, Parts A/B/C, 32(8-14), pp.691-700.

Meech, J.A., McPhie, M., Clausen, K., Simpson, Y., Lang, B., Campbell, E., Johnstone, S. and Condon, P., 2006. Transformation of a derelict mine site into a sustainable community: the Britannia project. Journal of Cleaner Production, 14(3-4), pp.349-365.

Müller-Hoeppe, N., Engelhardt, H.J., Lerch, C., Linkamp, M., Buhmann, D., Czaikowski, O., Herbert, H.J., Wieczorek, K., Xie, M., 2012. Integrität geotechnischer Barrieren Teil 1: Vorbemessung. Bericht zum Arbeitspaket 9, Vorläufige Sicherheitsanalyse.

Murray, R., 2006. ERPM still good for another 6 years thanks to water management program. Mining-technology.com.

Nicksiar, M. and Martin, C.D., 2013. Crack initiation stress in low porosity crystalline and sedimentary rocks. Engineering Geology, 154, pp.64-76.

Noiret, A., Bethmont, S., Bosgiraud, J.M. and Foin, R., 2013.DOPAS Work Package 4 Deliverable 4.8 FSS Experiment Summary Report.

Noronha, J. 2016. Deep Geological Repository Conceptual Design Report Crystalline/Sedimentary Rock Environment. Nuclear Waste Management Organization Report APM-REP-00440-0015 R001.

NWMO, 2018. Postclosure Safety Assessment of a Used Fuel Repository in Sedimentary Rock. NWMO TR-2018-08.

NWMO, 2019. Phase 2: Preliminary Environmental Studies: SUMMARY REPORT (APM-REP-07000-0208).

Orano, L.H., 2018. Orano Cycle-Annual environment monitoring report of the Orano la Hague site-2017 Edition.

Pacovský, J., 1999. Continuous measurements of stress and temperature during testing of a fibre shotcrete pressure plug. Geotechnical & Geological Engineering, 17(3-4), pp.335-349.

Park, J.H., Kuh, J.E., Kwon, S. and Kang, C.H., 2000. Thermal analysis of high level radioactive waste repository using a large model. JOURNAL-KOREAN NUCLEAR SOCIETY, 32(3), pp.244-253.

Perras, M.A. and Diederichs, M.S., 2016. Predicting excavation damage zone depths in brittle rocks. Journal of Rock Mechanics and Geotechnical Engineering, 8(1), pp.60-74.

Perras, M.A., Wannenmacher, H. and Diederichs, M.S., 2015a. Underground excavation behaviour of the queenston formation: tunnel back analysis for application to shaft damage dimension prediction. Rock Mechanics and Rock Engineering, 48(4), pp.1647-1671.

Perras, M.A., Loew, S., Diederichs, M.S., Lam, T. and Jensen, M., 2015b, January. Excavation damage zone cut-off dimension assessment using continuum mechanics. In ISRM Regional Symposium-EUROCK 2015. International Society for Rock Mechanics and Rock Engineering.

Pusch, R., Börgesson, L., Ramqvist, G., 1987a. Final Report of the borehole, shaft, and tunnel sealing test – Volume II: Shaft plugging, Stripa Project 87-02, Svensk Kärnbränslehantering AB.

Pusch, R., Börgesson, L., Ramqvist, G., 1987b. Final Report of the borehole, shaft, and tunnel sealing test – Volume III: Tunnel plugging, Stripa Project 87-03, Svensk Kärnbränslehantering AB.

Radakovic-Guzina, Z., Riahi, A., Damjanac, B., 2015. Long-Term Stability Analysis of APM Conceptual Repository Design in Sedimentary and Crystalline Rock Settings. Nuclear Waste Management Organization, NWMO-TR-2015-27.

Ranjith, P.G., Viete, D.R., Chen, B.J. and Perera, M.S.A., 2012. Transformation plasticity and the effect of temperature on the mechanical behaviour of Hawkesbury sandstone at atmospheric pressure. Engineering Geology, 151, pp.120-127.

Rinne, M., 2020. FRACOD Applications in Nuclear Waste Disposal. In: Shen B., Stephansson O., Rinne M. (eds) Modelling Rock Fracturing Processes. Springer, Cham.

Rutqvist, J., Börgesson, L., Chijimatsu, M., Hernelind, J., Jing, L., Kobayashi, A. and Nguyen, S., 2009. Modeling of damage, permeability changes and pressure responses during excavation of the TSX tunnel in granitic rock at URL, Canada. Environmental Geology, 57(6), pp.1263-1274.

Schmertmann, J.H. and Osterberg, J.O., 1960, June. An experimental study of the development of cohesion and friction with axial strain in saturated cohesive soils. In Research conference on shear strength of cohesive soils (pp. 643-694). ASCE.

Siren, T., Kantia, P. and Rinne, M., 2015. Considerations and observations of stress-induced and construction-induced excavation damage zone in crystalline rock. International Journal of Rock Mechanics and Mining Sciences, 73, pp.165-174.

Sitz, P., Koch, G. and Gruner, M., 2003. Results from the large scale in situ drift sealing experiment in the salt mine Sondershausen. In Clays in natural and engineered barriers for radioactive waste confinement. Experiments in underground laboratories.

Smith, P., Johnson, L., Snellman, M., Pastina, B. and Gribi, P., 2008. Safety assessment for a KBS-3H spent nuclear fuel repository at Olkiluoto. Evolution report (No. SKB-R--08-37). Swedish Nuclear Fuel and Waste Management Co.

Sharma, P., Perras, M., Sharma, J., Lam, T., Kasani, H. and Walton, G., 2019, August. Cutoff Modeling for Drift Sealing in Underground Nuclear Waste Repositories. In 53rd US Rock Mechanics/Geomechanics Symposium. American Rock Mechanics Association.

Sharma, P., Perras, M., Sharma, J., Lam, T., Kasani, H. and Walton, G., 2020, November. Influence of Thermo-Mechanical Loading on Cutoff Seals for Underground Nuclear Waste Repositories. In ISRM International Symposium-EUROCK 2020. International Society for Rock Mechanics and Rock Engineering.

Strandberg, U. and Andrén, M., 2009. Nuclear waste management in a globalised world.

Tsang, C.F., Bernier, F. and Davies, C., 2005. Geohydromechanical processes in the Excavation Damaged Zone in crystalline rock, rock salt, and indurated and plastic clays—in the context of radioactive waste disposal. International Journal of Rock Mechanics and Mining Sciences, 42(1), pp.109-125.

Tsui, K.K. and Tsai, A., 1985. Thermal analyses for different options of nuclear fuel waste emplacement. Pinawa, Man.: Whiteshell Nuclear Research Establishment.

Tuokko, T. 1990. The long-term strength and deformation properties of crystalline rock in a high level nuclear waste repository [in Finnish with an English abstract]. Helsinki, Finland: Nuclear Waste Commission of Finnish Power Companies. YJT-90-22.

Vandenbosch, R. and Vandenbosch, S.E., 2007. Nuclear waste stalemate: Political and scientific controversies. University of Utah Press.

Vira, J., 2017. Geological repository for high-level nuclear waste becoming reality in Finland. In Geological Repository Systems for Safe Disposal of Spent Nuclear Fuels and Radioactive Waste (pp. 645-666). Woodhead Publishing.

Voinis, S., Rabardy, M. and Griffault, L., 2016. Andra's Safety Options of French Underground Facility Cigeo–a Milestone towards the Licensing Application (No. IAEA-CN--242).

Walton, G. and Diederichs, M.S., 2015. A new model for the dilation of brittle rocks based on laboratory compression test data with separate treatment of dilatancy mobilization and decay. Geotechnical and Geological Engineering, 33(3), pp.661-679.

Walton, G. and Diederichs, M.S., 2015a. Dilation and post-peak behaviour inputs for practical engineering analysis. Geotechnical and Geological Engineering, 33(1), pp.15-34.

Walton, G., 2019. Initial guidelines for the selection of input parameters for cohesion-weakening-friction-strengthening (CWFS) analysis of excavations in brittle rock. Tunnelling and Underground Space Technology, 84, pp.189-200.

White, M.J. and Doudou, S. (2014). DOPAS Work Package 2, Deliverable D2.2: DOPAS Reference Designs Report, Version 1, October 2014.

Yates, Marshall., 1989. “DOE Waste Management Criticized: On-site Storage Urged.” Public Utilities Fortnightly 124 (July 6): 33.

Yuan, J., Vardon, P.J., Hicks, M.A., Hart, J. and Fokker, P.A., 2017. Technical feasibility of a Dutch radioactive waste repository in Boom Clay: Plugs and seals.

Zhao, X.G. and Cai, M., 2010. Influence of plastic shear strain and confinement-dependent rock dilation on rock failure and displacement near an excavation boundary. International Journal of Rock Mechanics and Mining Sciences, 47(5), pp.723-738.

Zhu, W.C. and Bruhns, O.T., 2008. Simulating excavation damaged zone around a circular opening under hydromechanical conditions. International journal of rock mechanics and mining sciences (1997), 45(5), pp.815-830.

Appendices

Appendix A: Code for Thermo-Mechanical Model

; Main FLAC 3D file to call other sub files for the thermo-mechanical model.

```
new
set fish safe off
set processor 9
def input_params ;define the required global input parameters for the model
modnum = 533
circle = 0
geomtype = 3
cutoffd = 0.2277
cutofft = 0.1139
rtype = 1
kH_rat = 3 ;horizontal to vertical stress ratio
k_inplane = 1.75 ;ratio between maximum to minimum horizontal stress
stress_CI = 2.75
shaft = 0
offset2 = 0.2500
radius = 1.0000
expansionfactor = 14
l_r = 12
r_ms = 15.00
xrat = 1.00
rrat = 0.72
orrat = 1.15
offset1 = 0.75
innerfactor = 6.00
idensrat = 1.25
ldens = 2000
lthick = 0.10
lE = 10000000000
lv = 0.20
rlength_rad = 1.00
bulkfactor = (1/r_ms)*32
end
input_params
```

```
call final_mesh ;call the mesh file for the thermo-mechanical model
call grouping ;change the name of the groups
call Assign_Props ;call the assign properties file to assign properties
call Initialize_Stresses ;call the stress file to initialize stresses and define boundary conditions
call Thermal_Analysis_stress_evolution_history ;couple the thermo-mechanical model

def name_comp
fname = 'Model'+string(modnum)+'_Complete'
end
name_comp
save fname

; Make the mesh (final_mesh.txt)

def parm
global rad=0.292 ; radius of spherical cavity
global len=0.422 ; length of outer box edge
global rad_size=4 ; number of zones in radial direction for outer shell of sphere and cylinder
global p0x=12.25 ; coordinated of p0
global p0y=0.978 ;
global p0z=0.5 ;
global s=2 ;define the object slot number number
global sxs1=4 ; number of y zones for sphere in layer 1
global sxc1=6 ; number of y zones for cylinder in layer 1
global sxbr1=2 ;number of x zones for bottom right DBF block in layer 1
global sybr1=4          ;number of y zones for bottom right DBF block in layer 1
global sybl1=6;number of y zones for bottom left DBF block in layer 1
global szbr1=8;number of z zones for bottom right DBF block in layer 1
global sxt1=2*5 ; number of x zones for top gap fill bentonite
global szt1=1 ; number of z zones for top gap fill bentonite
global sxr1=2*5 ; number of x zones for right side gap fill bentonite
global syr1=4/2 ; number of y zones for right side gap fill bentonite
global szr1=8*2 ; number of z zones for right side gap fill bentonite
global ratx1=1
global ratx2=1
global raty1=1.1
global raty2=1.1
global ratz1=1.1
global ratz2=1.1
```

```
global ratze=1.04
global sx11=11 ;first block first layer
global sx11m2=11 ;basically the far block in outer rock in right side
global sx21=20
global sx21m2=20 ;basically the far block in outer rock in right side
global sx31=20
global sx31m2=20 ;basically the far block in outer rock in right side
global sx12=sx11 ; first block second layer
global sx12m2=sx11 ;basically the far block in outer rock in right side
global sx13=6
global sx13m2=6
global sx14=sx13/2
global sx14m2=sx13m2/2
global sx22=sx21 ; second block second layer
global sx22m2=sx21
global sx23=sx22
global sx23m2=sx22m2
global sx24=sx23/2
global sx24m2=sx23m2/2
global sx32=sx31 ; third block second layer
global sx32m2=sx31
global sx33=sx32
global sx33m2=sx32m2
global sx34=sx33/2
global sx34m2=sx33m2/2
global sy11=12 ;first block first layer
global sy11m1=8 ; first block first layer with higher mesh size
global sy11m2=10 ;basically the far block in outer rock in right side
global sy21=sy11
global sy21m1=sy11m1
global sy21m2=sy11m2 ;basically the far block in outer rock in right side
global sy31=sy21
global sy31m1=sy21m1
global sy31m2=sy21m2
global sy12=sy11 ; first block second layer
global sy12m1=sy11m1 ; first block second layer with higher mesh size
global sy12m2=sy11m2 ;basically the far block in outer rock in right side
global sy13=sy12
global sy13m1=sy12m1
```

```
global sy13m2=sy12m2
global sy14=sy13/2
global sy14m1=sy13m1/2
global sy14m2=sy13m2 ;be careful!!
global sy22=12 ; second block second layer
global sy22m1=8
global sy22m2=10
global sy23=sy22/2
global sy23m1=sy22m1/2
global sy23m2=sy22m2
global sy24=sy23
global sy24m1=sy23m1
global sy24m2=sy23m2
global sy32=12 ; third block second layer
global sy32m1=8
global sy32m2=10
global sy33=sy32/2
global sy33m1=sy32m1/2
global sy33m2=sy32m2
global sy34=sy33
global sy34m1=sy33m1
global sy34m2=sy33m2
global sz11=9*2 ;first block first layer
global sz11m2=9 ;basically the far block in outer rock in right side
global sz21=sz11/2
global szh21=9 ;right part of the cutoff in block2 layer 1 half of sz21
global sz21m2=sz21 ;basically the far block in outer rock in right side
global sz31=sz21
global sz31m2=sz31
global szh31=9 ;be careful!! ;right part of the cutoff in block 3 layer 1 half of sz21
global sz12=8 ; first block second layer
global sz12m2=sz12 ;basically the far block in outer rock in right side
global sz13=sz12
global sz13m2=sz13
global sz14=100
global sz14m2=sz14
global sz22=8 ; second block second layer
global sz22m2=8
global sz23=sz22
```

```
global sz23m2=sz23
global sz24=100
global sz24m2=sz24
global sz32=8 ; third block second layer
global sz32m2=sz32
global sz33=sz32
global sz33m2=sz33
global sz34=100
global sz34m2=sz34
;mesh sizes 0.05,0.1,0.2 0.1,0.1,0.2, 0.2,0.2,0.6 0.3,0.3 0.4
global m1 = 0.1
global m2 = 0.1
global m3 = 0.2
end
@parm
;make spherical shell
gen zone radbrick p0 @p0x, @p0y, @p0z  p1 12.25, 1.4, 0.5 p2 11.75, 0.978, 0.5 p3 12.25, 0.978,
1 size @sxs1 @sxs1 @sxs1 @rad_size &
rat 1.0 1.0 1.0 1 dim @rad @rad @rad fill group UFCi slot @s
group block slot @s range group UFCi slot @s not
group gp gp_sphere slot @s range group UFCi slot @s
group gp gp_block slot @s range group block slot @s
def make_sphere ;make the spherical cap of canister
local p_gp = gp_head
loop while p_gp # null
; Get gp coordinate: P=(px,py,pz)
local px = gp_xpos(p_gp)
local py = gp_ypos(p_gp)
local pz = gp_zpos(p_gp)
local group_str=gp_group(p_gp,s)
px=px-p0x ;take the point in local coordinate system
py=py-p0y
pz=pz-p0z
local dist = sqrt(px*px+py*py+pz*pz)
if group_str='gp_sphere' ;if, to make the fill brick a sphere
if dist>0
local k = max(abs(px),max(abs(py),abs(pz)))/dist ;calculat the radius of cube and divide it with
distance
local ax = px*k ;calculate the point on the sphere of radius k*dist
```

```
local ay = py*k
local az = pz*k
gp_xpos(p_gp)=ax+p0x ; take back the coordinates to global coordinate system
gp_ypos(p_gp)=ay+p0y
gp_zpos(p_gp)=az+p0z
end_if
end_if
if group_str='gp_block' ; if to make the outside block as spherical mesh
if dist>0
if abs(px)<len
if abs(py)<len
if abs(pz)<len
local l=rad/dist ; calculate a point radially below r on the sphere
local cx = px*l
local cy = py*l
local cz = pz*l
local maxp=max(abs(px),max(abs(py),abs(pz))) ; calculate a point radially above r on the sphere
local m = len/maxp
local bx = px*m
local by = py*m
local bz = pz*m
local u = (maxp-rad)/(len-rad)
gp_xpos(p_gp)=cx+u*(bx-cx)+p0x ;interpolate the point p
gp_ypos(p_gp)=cy+u*(by-cy)+p0y
gp_zpos(p_gp)=cz+u*(bz-cz)+p0z
else
gp_xpos(p_gp)=px+p0x ;interpolate the point p
gp_ypos(p_gp)=py+p0y
gp_zpos(p_gp)=pz+p0z
end_if
end_if
end_if
end_if
end_if
p_gp=gp_next(p_gp)
end_loop
end
@make_sphere
set @s=3
```

```
gen zone radtunn p0 @p0x, @p0y, @p0z  p1 11.75, 0.978, 0.5 p2 12.25, 0 , 0.5 p3 12.25, 0.978,
1 size @sxs1 @sxc1 @sxs1 @rad_size &
rat 1.0 1.0 1.0 1 dim @rad @rad @rad fill group UFCi slot @s
group block slot @s range group UFCi slot @s not group UFCi slot 2 not group block slot 2 not
group gp gp_sphere slot @s range group UFCi slot @s
group gp gp_block slot @s range group block slot @s

def make_cylinder ;make the cylindrical part of the canister
local p_gp = gp_head
loop while p_gp # null
; Get gp coordinate: P=(px,py,pz)
local px = gp_xpos(p_gp)
local pz = gp_zpos(p_gp)
local group_str=gp_group(p_gp,s)
px=px-p0x ;take the point in local coordinate system
pz=pz-p0z
local dist = sqrt(px*px+pz*pz)
if group_str='gp_sphere' ;if to make the fill brick sphere
if dist>0
local k = max(abs(px),abs(pz))/dist ;calculat the rasius of cube and divide it with distance
local ax = px*k ;calculate the point on the sphere of radius k*dist
local az = pz*k
gp_xpos(p_gp)=ax+p0x ; take back the coordinates to glaobal coordinate system
gp_zpos(p_gp)=az+p0z
end_if
end_if
if group_str='gp_block' ; if to make the outside block as spherical mesh
if dist>r
if abs(px)<len
if abs(pz)<len
local l=rad/dist ; calculate a point radially below r on the sphere
local cx = px*l
local cz = pz*l
local maxp=max(abs(px),abs(pz))
local m = len/maxp ; calculate a point radially above r on the box
local bx = px*m
local bz = pz*m
local u = (maxp-rad)/(len-rad)
gp_xpos(p_gp)=cx+u*(bx-cx)+p0x ;interpolate the point p
```

```
gp_zpos(p_gp)=cz+u*(bz-cz)+p0z
else
gp_xpos(p_gp)=px+p0x ;interpolate the point p
gp_zpos(p_gp)=pz+p0z
end_if
end_if
end_if
end_if
p_gp=gp_next(p_gp)
end_loop
end
@make_cylinder

gen zone reflect origin 12.25,0.978,0.5 normal 0, 0,1 range union group UFCi  group block
gen zone copy -0.75,0,-1
gen zone reflect origin 11.5,1.4,0 normal 1,0,0 range x 10.9 11.6 y -0.1 1.5 z -1.1 0.1
gen zone brick p0 12.25,0.978,0 p1 12.25,1.4,0 p2 12.25,0.978,-1 p3 12,0.978,0 size @sybr1, @szbr1, @sxbr1 group DBF
gen zone brick p0 12.25,0.978,0 p1 12.25,0,0 p2 12,0.978,0 p3 12.25,0.978,-1 size @sybl1, @sxbr1, @szbr1 group DBF
gen zone copy -0.5,0,1 range group DBF
gen zone copy -0.75,0,1 range x 11.99 12.26 y -0.01 1.41 z -1.01 0.01
gen zone copy -1,0,1 range x 11.99 12.26 y -0.01 1.41 z -1.01 0.01
group gp_bentonite range x 10.99 11.26 y -0.01 1.41 z -0.01 1.01
gen zone brick p0 12.25 1.4 1 p1 11 1.4 1 p2 12.25 0.978 1 p3 12.25 1.4 1.1 size @sxt1, @sybr1, @szt1 group gp_bentonite ;top right gap fill bentonite
gen zone brick p0 12.25 0.978 1 p1 11 0.978 1 p2 12.25 0.0 1 p3 12.25 0.978 1.1 size @sxt1, @sybl1, @szt1 group gp_bentonite ;top left gap fill bentonite
gen zone brick p0 12.25 1.4 1.0 p1 11.0 1.4 1.0 p2 12.25 1.6 1.0 p3 12.25 1.4 -1.0 size @sxr1 @syr1 @szr1 group gp_bentonite ;right gap fill bentonite
gen zone brick p0 12.25 1.4 1.1 p1 11.0 1.4 1.1 p2 12.25 1.6 1.1 p3 12.25 1.4 1.0 size @sxr1 @syr1 @szt1 group gp_bentonite ;corner gap fill bentonite
gen zone reflect origin 12.25,0,0 normal 0, 0,1 range x 10.96 12.26 y -0.1 1.7 z 1 1.2
gen zone brick p0 11 0 -1.1 p1 11 1.6 -1.1 p2 10.875 0 -1.1 p3 11 0 1.1 size 12, 1, 18 group gp_bentonite
gen zone brick p0 12.25,0,1.1 p1 12.25,1.6,1.1 p2 10.875,0,1.1 p3 12.25,0,2.58 size @sy12, @sx12, @sz12 group shield slot 10 ;top shield
gen zone brick p0 12.25,1.6,1.1 p1 12.25,3.08,1.1 p2 10.875,1.6,1.1 p3 12.25,1.6,2.58 size @sy12m1, @sx12, @sz12  group shield slot 10 ;corner
```

```
gen zone brick p0 12.25,1.6,-1.1 p1 12.25,3.08,-1.1 p2 10.875,1.6,-1.1 p3 12.25,1.6,1.1 size @sy11m1, @sx11, @sz11  group shield ;right side
gen zone reflect origin 12.25,0.978,0 normal 0, 0,1 range group shield slot 10
group gp gp_shtobo range group shield x 10.93 12.3 y -0.01 1.52 z 1.06 1.15
group gp gp_shtobo range group shield x 10.93 12.3 y -0.01 1.52 z -1.15 -1.06
group gp gp_shtobo range group gp_bentonite x 10.93 11.03 y -0.01 1.62 z -1.15 1.15
group gp gp_shtobo range group shield x 10.93 12.3 y 1.55 1.62 z -1.15 1.15

def gp_arrange
local p_gp = gp_head
loop while p_gp # null
local group_str = gp_group(p_gp)
local px = gp_xpos(p_gp)
local py = gp_ypos(p_gp)
local pz = gp_zpos(p_gp)
local dz = 0.001
local z = 0.122222
local z0 = 0.125
local x = 0.133333
local x0 = 0.163
local x01 = 0.105
local x02 = 0.1
if group_str = 'gp_shtobo'
if pz > -0.99
if pz < -0.96
gp_zpos(p_gp)=-1
end_if
end_if
if pz < 0.99
if pz > 0.96
gp_zpos(p_gp)=1
end_if
end_if
loop i(0,15)
if pz < -0.856+i*z+dz
if pz > -0.856+i*z-dz
gp_zpos(p_gp)=-0.875+i*z0
end_if
end_if
```

```
end_loop
loop i(0,2)
if py < 1.6-i*x+dz
if py > 1.6-i*x-dz
gp_ypos(p_gp)= 1.6-i*x02
end_if
end_if
end_loop
loop i(0,3)
if py < 1.2-i*x+dz
if py > 1.2-i*x-dz
gp_ypos(p_gp)= 1.2945-i*x01
end_if
end_if
end_loop
loop i(0,6)
if py < 0+i*x+dz
if py > 0+i*x-dz
gp_ypos(p_gp)= 0+i*x0
end_if
end_if
end_loop
end_if
p_gp=gp_next(p_gp)
end_loop
end
@gp_arrange
;;fill the tunnel with backfill material
gen zone brick p0 10.875 1.6 1.1 p1 10.875 0.0 1.1 p2 4 1.6 1.1 p3 10.875 1.6 -1.1 size @sy21,@sx21,@sz21 rat 1 @ratx1 1 group gp_bentonite
gen zone brick p0 4.0 1.6 1.1 p1 4.0 0.0 1.1 p2 3.85 1.6 1.1 p3 4.0 1.6 -1.1 size @sy21,1,@sz21 group block ;part of HCB
gen zone brick p0 3.85 1.6 1.1 p1 3.85 0.0 1.1 p2 -8.0 1.6 1.1 p3 3.85 1.6 -1.1 size @sy31,@sx31,@sz31 rat 1 @ratx2 1 group concrete
group block range x 6.97 3.87 y -0.02 1.62 z -1.12 1.12
group block range x 1.08 3.83 y -0.02 1.62 z -1.12 1.12

; Make the cutoff
call cutoff_final
```

gen zone wedge p0 (3.85,0,1.1) p1 (4,0,1.1) p2 (3.85,1.6,1.1) p3 (3.85,0,2.58) size 1, @sy21, @sz12 group cutoff
gen zone wedge p0 (4,0,2.58) p1 (3.85,0,2.58) p2 (4,1.6,2.58) p3 (4,0,1.1) size 1, @sy21, @sz12 group mirror
gen zone wedge p0 (4,3.08,1.1) p1 (3.85,3.08,1.1) p2 (4,3.08,0) p3 (4,1.6,1.1) size 1, @szh21, @sy21m1 group mirror
gen zone wedge p1 (4,1.6,1.1) p0 (3.85,1.6,1.1) p2 (3.85,1.6,0) p3 (3.85,3.08,1.1) size 1, @szh21, @sy21m1 group cutoff
gen zone reflect origin 12.25,0,0 normal 0, 0,1 range union group cutoff group mirror
;;make rock above the tunnel
gen zone brick p0 10.875 0 1.1 p1 10.875 1.6 1.1 p2 4 0 1.1 p3 10.875 0 2.58 size @sy22,@sx22,@sz22 rat 1 @ratx1 1 group rock
gen zone brick p0 3.85 0 1.1 p1 3.85 1.6 1.1 p2 -8 0 1.1 p3 3.85 0 2.58 size @sy32,@sx32,@sz32 rat 1 @ratx2 1 group rock
;;make rock right of tunnel
gen zone brick p0 10.875 1.6 0 p1 10.875 3.08 0 p2 4 1.6 0 p3 10.875 1.6 1.1 size @sy21m1,@sx21,@szh21 rat 1 @ratx1 1 group rock
gen zone brick p0 3.85 1.6 0 p1 3.85 3.08 0 p2 -8 1.6 0 p3 3.85 1.6 1.1 size @sy31m1,@sx31,@szh31 rat 1 @ratx2 1 group rock ; here 2 should be three but assumed equal
;;make corner rock for above and right of tunnel rock
gen zone brick p0 10.875 1.6 1.1 p1 10.875 3.08 1.1 p2 4 1.6 1.1 p3 10.875 1.6 2.58 size @sy22m1,@sx22,@sz22 rat 1 @ratx1 1 group rock
gen zone brick p0 3.85 1.6 1.1 p1 3.85 3.08 1.1 p2 -8 1.6 1.1 p3 3.85 1.6 2.58 size @sy32m1,@sx32,@sz32 rat 1 @ratx2 1 group rock
gen zone reflect origin 12.25,0,0 normal 0, 0,1 range group rock
;;;make outer of rock located right of tunnel
gen zone brick p0 12.375,3.08,0 p1 12.375,10,0 p2 10.875,3.08,0 p3 12.375,3.08,1.1 size @sy11m2, @sx11m2, @sz11m2 group orock
gen zone brick p0 12.375,3.08,1.1 p1 12.375,10,1.1 p2 10.875,3.08,1.1 p3 12.375,3.08,2.58 size @sy12m2, @sx12m2, @sz12m2 group orock
;;two commands for two blocks 0-1.1 and 1.1 2.58
gen zone brick p0 10.875,3.08,0 p1 10.875,10,0 p2 4,3.08,0 p3 10.875,3.08,1.1 size @sy21m2, @sx21m2, @sz21m2 rat 1 @ratx1 1 group orock
gen zone brick p0 10.875,3.08,1.1 p1 10.875,10,1.1 p2 4,3.08,1.1 p3 10.875,3.08,2.58 size @sy22m2, @sx22m2, @sz22m2 rat 1 @ratx1 1 group orock
gen zone brick p0 4,3.08,0 p1 4,10,0 p2 3.85,3.08,0 p3 4,3.08,1.1 size @sy21m2, 1, @sz21m2 group orock

gen zone brick p0 4,3.08,1.1 p1 4,10,1.1 p2 3.85,3.08,1.1 p3 4,3.08,2.58 size @sy22m2, 1, @sz22m2 group orock
gen zone brick p0 3.85,3.08,0 p1 3.85,10,0 p2 -8,3.08,0 p3 3.85,3.08,1.1 size @sy31m2, @sx31m2, @sz31m2 rat 1 @ratx2 1 group orock
gen zone brick p0 3.85,3.08,1.1 p1 3.85,10,1.1 p2 -8,3.08,1.1 p3 3.85,3.08,2.58 size @sy32m2, @sx32m2, @sz32m2 rat 1 @ratx2 1 group orock
;;;make the outer of rock above tunnel
gen zone brick p0 12.375,0,2.58 p1 12.375,1.6,2.58 p2 10.875,0,2.58 p3 12.375,0,6 size @sy13, @sx13, @sz13 group orock ;need to shift
gen zone brick p0 12.375,1.6,2.58 p1 12.375,3.08,2.58 p2 10.875,1.6,2.58 p3 12.375,1.6,6 size @sy13m1, @sx13, @sz13 group orock
;;two commands for two blocks in z direction 0-1.6 and 1.6-3.08
gen zone brick p0 10.875,0,2.58 p1 10.875,1.6,2.58 p2 4,0,2.58 p3 10.875,0,6 size @sy23, @sx23, @sz23 rat 1 @ratx1 1 group orock
gen zone brick p0 10.875,1.6,2.58 p1 10.875,3.08,2.58 p2 4,1.6,2.58 p3 10.875,1.6,6 size @sy23m1, @sx23, @sz23 rat 1 @ratx1 1 group orock
gen zone brick p0 4,0,2.58 p1 4,1.6,2.58 p2 3.85,0,2.58 p3 4,0,6 size @sy23, 1, @sz23 group orock
gen zone brick p0 4,1.6,2.58 p1 4,3.08,2.58 p2 3.85,1.6,2.58 p3 4,1.6,6 size @sy23m1, 1, @sz23 group orock
gen zone brick p0 3.85,0,2.58 p1 3.85,1.6,2.58 p2 -8,0,2.58 p3 3.85,0,6 size @sy33, @sx33, @sz33 rat 1 @ratx2 1 group orock
gen zone brick p0 3.85,1.6,2.58 p1 3.85,3.08,2.58 p2 -8,1.6,2.58 p3 3.85,1.6,6 size @sy33m1, @sx33, @sz33 rat 1 @ratx2 1 group orock
;;;make the corner outer rock for above and right of rock
gen zone brick p0 12.375,3.08,2.58 p1 12.375,10,2.58 p2 10.875,3.08,2.58 p3 12.375,3.08,6 size @sy13m2, @sx13m2, @sz13m2 group orock
gen zone brick p0 10.875,3.08,2.58 p1 10.875,10,2.58 p2 4,3.08,2.58 p3 10.875,3.08,6 size @sy23m2, @sx23m2, @sz23m2 rat 1 @ratx1 1 group orock
gen zone brick p0 4,3.08,2.58 p1 4,10,2.58 p2 3.85,3.08,2.58 p3 4,3.08,6 size @sy23m2, 1, @sz23m2 group orock
gen zone brick p0 3.85,3.08,2.58 p1 3.85,10,2.58 p2 -8,3.08,2.58 p3 3.85,3.08,6 size @sy33m2, @sx33m2, @sz33m2 rat 1 @ratx2 1 group orock
;;;;make the elastic rock
;;;make the top elastic rock on the top of outer rock mass
gen zone brick p0 12.375,0,6 p1 12.375,1.6,6 p2 10.875,0,6 p3 12.375,0,500 size @sy14, @sx14, @sz14 rat 1 1 @ratze group outer_elastic
gen zone brick p0 12.375,1.6,6 p1 12.375,3.08,6 p2 10.875,1.6,6 p3 12.375,1.6,500 size @sy14m1, @sx14, @sz14 rat 1 1 @ratze group outer_elastic

```
gen zone brick p0 10.875,0,6 p1 10.875,1.6,6 p2 4,0,6 p3 10.875,0,500 size @sy24, @sx24, @sz24 rat 1 1 @ratze group outer_elastic
gen zone brick p0 10.875,1.6,6 p1 10.875,3.08,6 p2 4,1.6,6 p3 10.875,1.6,500 size @sy24m1, @sx24, @sz24 rat 1 1 @ratze group outer_elastic
gen zone brick p0 4,0,6 p1 4,1.6,6 p2 3.85,0,6 p3 4,0,500 size @sy24, 1, @sz24 rat 1 1 @ratze group outer_elastic
gen zone brick p0 4,1.6,6 p1 4,3.08,6 p2 3.85,1.6,6 p3 4,1.6,500 size @sy24m1, 1, @sz24 rat 1 1 @ratze group outer_elastic
gen zone brick p0 3.85,0,6 p1 3.85,1.6,6 p2 -8,0,6 p3 3.85,0,500 size @sy34, @sx34, @sz34 rat 1 1 @ratze group outer_elastic
gen zone brick p0 3.85,1.6,6 p1 3.85,3.08,6 p2 -8,1.6,6 p3 3.85,1.6,500 size @sy34m1, @sx34, @sz34 rat 1 1 @ratze group outer_elastic
;;;make the top elastic rock on the corner outer rock mass
gen zone brick p0 12.375,3.08,6 p1 12.375,10,6 p2 10.875,3.08,6 p3 12.375,3.08,500 size @sy14m2, @sx14m2, @sz14m2 rat 1 1 @ratze group outer_elastic
gen zone brick p0 10.875,3.08,6 p1 10.875,10,6 p2 4,3.08,6 p3 10.875,3.08,500 size @sy24m2, @sx24m2, @sz24m2 rat 1 1 @ratze group outer_elastic
gen zone brick p0 4,3.08,6 p1 4,10,6 p2 3.85,3.08,6 p3 4,3.08,500 size @sy24m2, 1, @sz24m2 rat 1 1 @ratze group outer_elastic
gen zone brick p0 3.85,3.08,6 p1 3.85,10,6 p2 -8,3.08,6 p3 3.85,3.08,500 size @sy34m2, @sx34m2, @sz34m2 rat 1 1 @ratze group outer_elastic

def orarrange
local p_gp = gp_head
loop while p_gp # null
local px = gp_xpos(p_gp)
local py = gp_ypos(p_gp)
local pz = gp_zpos(p_gp)
if px<12.4
if px>12.26
gp_xpos(p_gp)=12.25
end_if
end_if
p_gp=gp_next(p_gp)
end_loop
end
@orarrange

gen zone reflect origin 12.25,0,0 normal 0, 0,1 range union group orock group outer_elastic
```

```
group mesh range group cutoff not group mirror not x 3.258 4.688 y -0.1 4.08 z 1.09 3.435
group mesh range group cutoff not group mirror not x 3.258 4.688 y -0.1 4.08 z -3.435  -1.09
gen zone densify maxlength @m1 @m1 @m1 range group mesh
;zone 1
gen zone densify maxlength @m2 range x 4.688 5.688 y -0.1 5.08 z 1.09 4.435
gen zone densify maxlength @m2 range x 2.258 3.258 y -0.1 5.08 z 1.09 4.435
gen zone densify maxlength @m2 range x 3.258 4.688 y -0.1 5.08 z 3.435 4.435 ;miidle z
gen zone densify maxlength @m2 range x 4.688 5.688 y -0.1 5.08 z -4.435 -1.09
gen zone densify maxlength @m2 range x 2.258 3.258 y -0.1 5.08 z -4.435 -1.09  ;middle z
gen zone densify maxlength @m2 range x 3.258 4.688 y -0.1 5.08 z -4.435 -3.435
gen zone densify maxlength @m2 range x 2.258 3.258 y 4.08 5.08 z 1.09 4.435 ;middle y
gen zone densify maxlength @m2 range x 2.258 3.258 y 4.08 5.08 z -4.435 -1.09 ;middle y
;zone 2
gen zone densify maxlength @m3 range x 5.688 6.688 y -0.1 6.08 z 1.09 5.435
gen zone densify maxlength @m3 range x 1.258 2.258 y -0.1 6.08 z 1.09 5.435
gen zone densify maxlength @m3 range x 2.258 5.688 y -0.1 6.08 z 4.435 5.435 ;miidle z
gen zone densify maxlength @m3 range x 5.688 6.688 y -0.1 6.08 z -5.435 -1.09
gen zone densify maxlength @m3 range x 1.258 2.258 y -0.1 6.08 z -5.435 -1.09
gen zone densify maxlength @m3 range x 2.258 5.688 y -0.1 6.08 z -5.435 -4.435 ;middle z
gen zone densify maxlength @m3 range x 2.258 5.688 y 5.08 6.08 z 1.09 5.435 ;middle y
gen zone densify maxlength @m3 range x 2.258 5.688 y 5.08 6.08 z -5.435 -1.09 ;middle y

def mesden
ms = 0.5
inc = 1
xil = 3.258
xir = 4.688
yil = 3.08
yir = 4.08
zib = -3.435
zit = 3.435
loop i(0,2)
ts = ms+0.2
xl1 = xil - inc*i/2
xl2 = xil - inc*(i+1)/2
xr1 = xir + inc*i/2
xr2 = xir + inc*(i+1)/2
yl1 = yil + inc*i/2
yl2 = yil + inc*(i+1)/2
```

```
yr1 = yir
yr2 = yir
zb1 = zib - inc*i/2
zb2 = zib - inc*(i+1)/2
zt1 = zit + inc*i/2
zt2 = zit + inc*(i+1)/2
command
gen zone densify maxlength @ts @ts @ts range @xl1 @xl2 @yl1 @yl2 @zb1 @zb2
gen zone densify maxlength @ts @ts @ts range @xr1 @xr2 @yl1 @yl2 @zb1 @zb2
end_command
end_loop
end
attach face
call grouping_flac_mesh

; Make the cutoff (cutoff_final.txt)

gen zone wedge  p0 (3.85,1.6,1.1) p1 (4,1.6,1.1) p2 (3.85,3.08,1.1) p3 (3.85,1.6,2.58) size 1, 8, 8
group cutoff
group gp gp_cutoff range group cutoff
def delp
local pnt=zone_head
loop while pnt#null
local group_str1=z_group(pnt)
if group_str1='cutoff'
local point=z_cen(pnt)
local val= 0*xcomp(point)- 1110000*ycomp(point) + 1110000*zcomp(point) + 543900
if val<0
z_group(pnt)='me'
end_if
end_if
pnt=z_next(pnt)
end_loop
end
@delp
del zone range group me
;gen zone wedge p0 (3.85,1.6,1.285) p1 (3.85,1.785,1.285) p2 (3.981,1.6,1.285) p3 (3.85,1.6,1.1)
p4 (3.981,1.785,1.285) p5 (4,1.6,1.1) size 1, 1, 1 group cutoff
```

```
def points
n_zones=8
c1=vector(3.85,3.08,2.58)
c2=vector(3.85,1.6,1.1)
c3=vector(4,1.6,1.1)
l_digonal12=sqrt(dot((c1-c2),(c1-c2)))
l_digonal13=sqrt(dot((c1-c3),(c1-c3)))
l_12 = l_digonal12/8
l_13 = l_digonal13/8
uv_12 = (c1-c2)/l_digonal12
uv_13 = (c1-c3)/l_digonal13
p0m = vector(3.85,1.6,1.285)
p1m = vector(3.85,1.785,1.285)
p2m = vector(3.981,1.6,1.285)
p3m = vector(3.85,1.6,1.1)
p4m = vector(3.981,1.785,1.285)
p5m = vector(4,1.6,1.1)
loop i(1,8)
if i#8
command
gen zone wedge p0 @p0m p1 @p1m p2 @p2m p3 @p3m p4 @p4m p5 @p5m size 1, 1, 1 group
cutoff
end_command
else
command
gen zone tet p0 @p0m p1 @p5m p2 @p3m p3 @p1m size 1, 1, 1 group cutoff
end_command
end_if
p0m = p0m + l_12*uv_12
p1m = p1m + l_12*uv_12
p3m = p3m + l_12*uv_12
p2m = p2m + l_13*uv_13
p4m = p4m + l_13*uv_13
p5m = p5m + l_13*uv_13
end_loop
end
@points
```

```
gen zone wedge  p0 (4,1.6,2.58) p1 (3.85,1.6,2.58) p2 (4,3.08,2.58) p3 (4,1.6,1.1) size 1, 8, 8 group
mirror

def delpm
local pnt=zone_head
loop while pnt#null
local group_str1=z_group(pnt)
if group_str1='mirror'
local point=z_cen(pnt)
local val= 0*xcomp(point)- 1110250*ycomp(point) + 1110000*zcomp(point) + 520800
if val<0
z_group(pnt)='mem'
end_if
end_if
pnt=z_next(pnt)
end_loop
end
@delpm
del zone range group mem
def points
n_zones=8
c1=vector(4,1.6,1.1)
c2=vector(4,3.08,2.58)
c3=vector(3.85,3.08,2.58)
l_digonal12=sqrt(dot((c1-c2),(c1-c2)))
l_digonal13=sqrt(dot((c1-c3),(c1-c3)))
l_12 = l_digonal12/8
l_13 = l_digonal13/8
uv_12 = (c1-c2)/l_digonal12
uv_13 = (c1-c3)/l_digonal13
p0m = vector(4,2.895,2.58)
p1m = vector(4,2.895,2.395)
p2m = vector(3.85,2.895,2.58)
p3m = vector(4,3.08,2.58)
p4m = vector(3.869,2.895,2.395)
p5m = vector(3.85,3.08,2.58)
loop i(1,8)
if i#8
command
```

```
gen zone wedge p0 @p0m p1 @p1m p2 @p2m p3 @p3m p4 @p4m p5 @p5m size 1, 1, 1 group
mirror
end_command
else
command
gen zone tet p0 @p0m p1 @p1m p2 @p2m p3 @p3m size 1, 1, 1 group mirror
end_command
end_if
p0m = p0m + l_12*uv_12
p1m = p1m + l_12*uv_12
p3m = p3m + l_12*uv_12
p2m = p2m + l_13*uv_13
p4m = p4m + l_13*uv_13
p5m = p5m + l_13*uv_13
end_loop
end
@points
gen zone reflect origin 4,1.6,1.1 normal 0, 0.707107,-0.707107 range union group cutoff group
mirror
```

; Grouping different zones (grouping.txt)

```
group HCB range group cutoff
group host_rock range union group rock group mirror group shield group orock group mesh
group buffer_block range group block
```

; Assigning the properties (Assign_Props.txt)

```
def rock_select
if rtype = 1
graniteflag = 1
command
call Limestone
end_command
else
if rtype = 2
command
call mudstone
end_command
```

```
else
graniteflag = 1
command
call Granite
end_command
end_if
end_if
end
rock_select
def calc_elastic
bulkval = E/(3*(1-2*v))
shearval = E/(2*(1+v))
end
calc_elastic
def calcdil
dilval = (1/stress_CI-0.1)*fr_mob
end
calcdil
def joint_props
if graniteflag = 0
command
model mech subi
prop bimatrix 0
prop density densval
prop ttable 2
prop bulk bulkval
prop shear shearval
prop dilation dilval
prop cohesion coh_peak
prop friction fr_init
prop tension tval
table 2 0 tval t_str t_res
prop ctable 3
prop ftable 4
table 3 0 coh_peak coh_str coh_res
table 4 0 fr_init fr_str fr_mob
prop bijoint 0
prop jtension jtval
prop tjtable 1
```

```
table 1 0 jtval jt_str jt_res
prop jcohesion jcoh_peak
prop jfriction jfr_init
prop jdilation jdilval
prop cjtable 7
prop fjtable 8
table 7 0 jcoh_peak jcoh_str jcoh_res
table 8 0 jfr_init jfr_str jfr_mob

end_command
if shaft = 0
command
prop jddirection = 0
prop jdip = 0
prop jnx = 0
prop jny = 0
prop jnz = 1
end_command
else
command
prop jddirection = 90
prop jdip = 90
prop jnx = 1
prop jny = 0
prop jnz = 0
end_command
end_if
else
command
model mech strainsoftening range group host_rock
prop density densval range group host_rock
prop ttable 2 range group host_rock
prop bulk bulkval range group host_rock
prop shear shearval range group host_rock
prop dilation dilval range group host_rock
prop cohesion coh_peak range group host_rock
prop friction fr_init range group host_rock
prop tension tval range group host_rock
table 2 0 tval t_str t_res
```

prop ctable 3 range group host_rock
prop ftable 4 range group host_rock
table 3 0 coh_peak coh_str coh_res
table 4 0 fr_init fr_str fr_mob
end_command
end_if
end
joint_props
model mech elastic range group outer_elastic
prop density densval range group outer_elastic
prop bulk bulkval shear shearval range group outer_elastic
ini density densval range group outer_elastic
ini density densval range group host_rock
ini density densval_UFCi range group UFCi
ini density densval_concrete range group concrete
ini density densval_HCB range group HCB
ini density densval_DBF range group DBF
ini density densval_gp_bentonite range group gp_bentonite
ini density densval_buffer_block range group buffer_block
model mech elastic range union group concrete group HCB group gp_bentonite group buffer_block group DBF group UFCi
prop density densval_UFCi bulk bulkval_UFCi shear shearval_UFCi range group UFCi
prop density densval_concrete bulk bulkval_concrete shear shearval_concrete range group concrete
prop density densval_HCB bulk bulkval_HCB shear shearval_HCB range group HCB
prop density densval_DBF bulk bulkval_DBF shear shearval_DBF range group DBF
prop density densval_gp_bentonite bulk bulkval_gp_bentonite shear shearval_gp_bentonite range group gp_bentonite
prop density densval_buffer_block bulk bulkval_buffer_block shear shearval_buffer_block range group buffer_block

; Assign the material parameters (Limestone.txt)

define propvals
; INTACT PARAMETERS
; Elastic Parameters
densval = 2660
E = 40000e6
v = 0.25

```
;parameters for engineered barrier
densval_HCB = 1955
densval_DBF = 2120
densval_concrete = 2400
densval_gp_bentonite = 1410
densval_buffer_block = 1880
densval_UFCi = 5345
bulkval_UFCi = 140e9
bulkval_concrete = 22.22e9
bulkval_HCB = 41.7e6
bulkval_DBF = 83.3e6
bulkval_gp_bentonite = 41.7e6
bulkval_buffer_block = 41.7e6
shearval_UFCi = 80e9
shearval_concrete = 16.67e9
shearval_HCB = 45.4e6
shearval_DBF = 91e6
shearval_gp_bentonite = 45.4e6
shearval_buffer_block = 45.4e6

; Peak Parameters
coh_peak = 15.5e6
fr_init = 15
tval = 6.5e6
; Tension table parameters
t_str = 0.002
t_res = 1e5
; Cohesion table parameters
coh_str = 0.002
coh_res = 1.2e6
; Friction table parameters
fr_str = 0.003
fr_mob = 50
; thermal properties of limestone
therm_cond_host_rock = 2.5
therm_cond_outer_elastic = 2.5
therm_cond_HCB = 1
therm_cond_DBF = 2
therm_cond_concrete = 1.0
```

```
therm_cond_gp_bentonite = 0.4
therm_cond_buffer_block = 0.5
therm_cond_UFCi = 45
specific_heat_host_rock = 845
specific_heat_outer_elastic = 845
specific_heat_HCB = 1280
specific_heat_DBF = 1110
specific_heat_concrete = 880
specific_heat_buffer_block = 1440
specific_heat_gp_bentonite = 870
specific_heat_UFCi = 434
therm_exp = 5.4e-6
; JOINT PARAMETERS
; Basic Joint parameters
jnxval = 0
jnyval = 0
jnzval = 1
jtval = 0.66e6
jdilval = 5
; Joint tension table parameters
jt_str = 0.003
jt_res = 1e5
; Joint strength parameters

jcoh_peak = 3.3e6
jfr_init = 38
; Joint cohesion table parameters
jcoh_str = 0.003
jcoh_res = 1e4
; Joint friction table parameters
jfr_str = 0.003
jfr_mob = 30
end
propvals

; Initialize the stresses and fix the boundaries (Initialize_stresses.txt)

def stress_calcs
```

```
CI = 2*coh_peak*cos(fr_init*pi/180)/(1-sin(fr_init*pi/180)) ; Determine the peak unconfined strength
maxstress = stress_CI*CI ; Calculate the maximum stress value
if shaft = 0 ; If the excavation is not aligned with the gravity vector
sigz = -maxstress/(3*kH_rat-1) ; Vertical stress at the surface of excavation
sigzs = sigz-(0.027*1.1e6) ; Vertical stress at origin
sigy = kH_rat*sigzs ; Maximum horizontal stress
sigx = sigy/k_inplane ; Minimum horizontal stress along tunnel axis
ygrad = (kH_rat*0.027)*1e6 ; y stress gradient
xgrad = (kH_rat/k_inplane)*0.027*1e6
command
set gravity 0, 0, -10 ; Gravity was vertical (excavation was horizontal)
ini sxx sigx gradient 0, 0, xgrad
ini syy sigy gradient 0, 0, ygrad
ini szz sigzs gradient 0, 0, 0.027e6
end_command
else ; If the excavation WAS aligned with the gravity vector
sigz = -maxstress/(3*k_inplane-1) ; Minimum horizontal stress
sigy = k_inplane*sigz ; Maximum horziontal stress
sigx = sigy/kH_rat ; Vertical stress
command
set gravity (-9.81,0,0) ; Gravity was along the x-axis (excavation-parallel)
ini sxx sigx
ini syy sigy
ini szz sigz
end_command
end_if
end
stress_calcs

fix x range x -8.1 -7.9
fix x range x 12.2 12.27
fix y range y -0.1 0.1
fix y range y 9.9 10.1
fix z range z -500.1 -499.9
```

: Couple the thermal and mechanical model (Thermal_Analysis_stress_evolution_history.txt)

```
;set fish autocreate off
```

config thermal
model therm th_iso
prop conducti therm_cond_outer_elastic thexp therm_exp spec_heat specific_heat_outer_elastic range group outer_elastic
prop conducti therm_cond_host_rock thexp therm_exp spec_heat specific_heat_host_rock range group host_rock
prop conducti therm_cond_concrete thexp therm_exp spec_heat specific_heat_concrete range group concrete
prop conducti therm_cond_HCB thexp therm_exp spec_heat specific_heat_HCB range group HCB
prop conducti therm_cond_DBF thexp therm_exp spec_heat specific_heat_DBF range group DBF
prop conducti therm_cond_gp_bentonite thexp therm_exp spec_heat specific_heat_gp_bentonite range group gp_bentonite
prop conducti therm_cond_buffer_block thexp therm_exp spec_heat specific_heat_buffer_block range group buffer_block
prop conducti therm_cond_UFCi thexp therm_exp spec_heat specific_heat_UFCi range group UFCi
ini density densval range group outer_elastic
call heatvstimeif18 ; call the variation of heat load with time
apply vsource=1 hist=table 1 range group UFCi
apply flux=0 range x 12.2 12.27
apply flux=0 range x -8.1 -7.9
apply flux=0 range y -0.1 0.1
apply flux=0 range y 9.9 10.1
fix t 17 range z -500.1 -499.9
fix t 5 range z 499.9 500.1
set mech on thermal off
solve ;bring model to the equlilibruim under gravity
call reassignmat ;excavate and then put backfill material
history nstep 1300 id 2 thtime
history nstep 1300 add id 3 zone vsi 7.2 0.001 1.7
history nstep 1300 add id 4 zone vsi 7.2 0.001 3.04
history nstep 1300 add id 5 zone vsi 7.2 0.001 4.56
history nstep 1300 add id 6 zone smax 7.2 0.001 1.7
history nstep 1300 add id 7 zone smax 7.2 0.001 3.04
history nstep 1300 add id 8 zone smax 7.2 0.001 4.56
history nstep 1300 add id 9 zone smin 7.2 0.001 1.7
history nstep 1300 add id 10 zone smin 7.2 0.001 3.04
history nstep 1300 add id 11 zone smin 7.2 0.001 4.56

```
history nstep 1300 add id 12 gp temperature 7.2 0.001 1.7
history nstep 1300 add id 13 gp temperature 7.2 0.001 3.04
history nstep 1300 add id 14 gp temperature 7.2 0.001 4.56
set mech off thermal on
set thermal implicit on
set thermal dt 2000
set thermal ratio 1e-5
call solvec

; Variation of heat load with time (heatvstimeif18.txt)
def mtable
xtable(1,1)= 0
ytable(1,1)= 5.217839e+03
xtable(1,2)= 157680000
ytable(1,2)= 4.785592e+03
…….
xtable(1,23)= 314413920000
ytable(1,23)= 2.050086e+02
xtable(1,24)= 629773920000
ytable(1,24)= 1.185592e+02
end
@mtable

; Excavation of the material ;(reassignment.txt)
model mech null range union group concrete group HCB group gp_bentonite group buffer_block
group DBF group UFCi
solve

; Call the solvec file for solving the model (solvec.txt)

set thermal age 31536000
solve
set thermal off mechanical on
solve
set thermal on mechanical off
set thermal age 63072000
……
solve
set thermal on mechanical off
```

```
set thermal age 30621456000
solve
set thermal off mechanical on
solve
set thermal on mechanical off
```